San Jose State University

SJSU ScholarWorks

2008

Self-assembled layer-by-layer star polymers by electrostatic interactions

Cecile Semana Bonifacio
San Jose State University

SELF-ASSEMBLED LAYER-BY-LAYER STAR POLYMERS
BY ELECTROSTATIC INTERACTIONS

A Thesis

Presented to

The Faculty of the Department of Chemical and Materials Engineering

San Jose State University

In Partial Fulfillment of

the Requirements for the Degree

Master of Science

by

Cecile Semana Bonifacio

May 2008

UMI Number: 1458171

INFORMATION TO USERS

The quality of this reproduction is dependent upon the quality of the copy submitted. Broken or indistinct print, colored or poor quality illustrations and photographs, print bleed-through, substandard margins, and improper alignment can adversely affect reproduction.

In the unlikely event that the author did not send a complete manuscript and there are missing pages, these will be noted. Also, if unauthorized copyright material had to be removed, a note will indicate the deletion.

UMI®
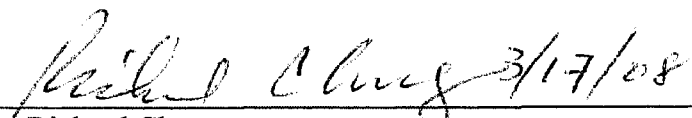
APPROVED FOR THE DEPARTMENT OF
CHEMICAL AND MATERIALS ENGINEERING

Dr.Melanie McNeil

Dr. Richard Chung

Dr. Roger Terrill

Dr. Joseph Sly, IBM Almaden Research Center

Dr. Robert Miller, IBM Almaden Research Center

APPROVED FOR THE UNIVERSITY

ABSTRACT

SELF-ASSEMBLED LAYER-BY-LAYER STAR POLYMERS BY ELECTROSTATIC INTERACTIONS

by Cecile S. Bonifacio

A technique for building multilayer polymeric nano-structures by electrostatic layer-by-layer (LBL) self-assembly using functionalized star polymers is presented. Film formation was studied using Surface Plasmon Reso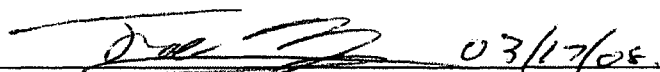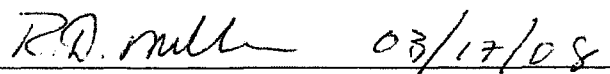nance (SPR) spectroscopy, Quartz Crystal Microgravimetry (QCM), Atomic Force Microscopy (AFM), and Infrared Absorption Spectroscopy (IR).

The effectiveness of the LBL self-assembly of the PS-NH$_2$ and PS-COOH star polymers in dichloromethane and tetrahydrofuran was demonstrated using SPR with the uniform angular shifts observed indicating that sequential monolayers of molecularly thin films were deposited. This uniformity of LBL deposition was verified by QCM. Kinetics analysis showed both a rapid film formation of 16-18 seconds and the subsequent stability of the films once formed. By AFM characterization, the self-assembled star polymer thin films produced contiguous, uniform, and smooth surfaces which remained intact over two weeks after deposition. Finally, the carboxylate anion formation relevant to the confirmation of the electrostatic interaction was identified through IR analysis.

ACKNOWLEDGEMENTS

me in as a peer researcher at IBM. Dr. Kanazawa and Bill Hinsberg, I am grateful for the knowledge and expertise you all willingly offered. To Victor, thank you for the guidance, supervision, and expertise during my stay at IBM. To Bill Risk, thank you for sharing your expertise in data analysis which was vital to this research. To Mike, thank you for your support and unwavering belief in my abilities. I will bring with me all your words of advice in my years at grad school. Miss Jane Frommer, my source of wisdom throughout this journey. Thank you for sharing your experiences, expertise, and taking care of me at IBM. Your passion for science is tremendously inspiring. I appreciate everything you've done for me and I am hopeful that one day I can be of help to you. May this be just a start of fruitful things to come.

My friends and family: Lilian Chang, Fatima and Glenda. Glenda and Fatima are great friends that I always cherish. Both of you helped me during the toughest times for the last two years. Lilian, my partner, thank you for bringing sense to me during times of confusion, doubt, and antagonism. I appreciate all the experiences we've shared. I am looking forward to more years of friendship in grad school. My family: Semana, Benito, Ocaya and Bonifacio families. Thank you to Papa, Mama, and all my aunts/uncles, who've supported me through the last five years of my stay here in the US. I found a new home here in the US. To my sisters, Christine and Charmaine, my brother, JR, Mommy and Daddy: I am proud to have great sisters and brother, most especially, the best parents. All of you have been my inspiration in all my endeavors.

I owe and share all my successes to my dear family. I dedicate my thesis manuscript to all of you.

TABLE OF CONTENTS

LIST OF FIGURES

LIST OF TABLES

CHAPTER ONE
INTRODUCTION

Nanotechnology is a field of engineering that deals with manufacturing, designing, and characterizing materials at the 1-100 nm length scale [1]. The principle of nanotechnology to fabricate at the nano-scale is not a new concept of science. It goes back to Richard Feynman's talk in 1959 when he introduced the idea of manipulating atoms from the bottom-up to build new nanosized materials that can change the magnitude of physical phenomena available [2]. He thought that one can manipulate and control components at a small scale leading to improved applications such as denser circuitry and better electron microscopes [2]. Eventually, better electron microscopes, atomic force microscopes (AFM), scanning tunneling microscopes (STM), and probe storage systems (*e.g.*, the Millipede of IBM) were developed based on the ideas he proposed [2].

Although the concept of nanotechnology has been around for a while, the process of creating new materials at the nano-scale is not trivial. The challenge is to build materials that utilize quantum mechanical effects that are distinct and prominent at this small scale [1]. The different nano-scale dimensions of materials: zero dimensional nanoparticles, 1D nanowires, nanotubes, 2D nano particle arrays, and 3D dimensional super lattices, can be obtained by two techniques. These techniques are the top-down and bottom-up approaches. The top-down approach starts from a large segment of bulk material that is reduced in size and thus, does not allow atomic control while the bottom-up approach builds materials from molecular components that chemically interact to form

the final structure [1]. Self-assembly is one process which allows for a bottom-up approach and which can be manipulated for processes such as multilayer thin film formation.

Multilayer thin film formation is an area of nanotechnology that has great potential. Through the bottom-up approach, the effective and efficient self-assembly technique can be employed for the layer-by-layer deposition of complementary polymers. In this study, the novel technique of using surface plasmon resonance, SPR, is introduced to study the *in situ* layer-by-layer self-assembly of star polymers. These star polymer multilayers can be functionalized to create versatile macromolecular structures that could one day be used for promising applications in such areas as catalysis and drug delivery.

1.1   Background

1.1.1   Film Formation by Self-assembly

Self-assembly is a major process that occurs in nature. An example of such a process is when cells divide, develop, and organize to become an organism. Self-assembly is the process of spontaneous organization in systems of components [3]. At the molecular level, self-assembly is defined as the spontaneous formation of ordered aggregates by non-covalent interactions through supramolecular chemistry [3, 4]. Supramolecular chemistry is the concept of exploiting non-covalent (electrostatic, Van der Waals, hydrogen bonding, and dipole-dipole) interactions [4]. By utilizing

supramolecular chemistry, manipulation of non-covalent interactions of molecules can be attained [4].

Self-assembly is predicted to have a great potential in providing new techniques for making new materials such as thin films of heterogeneous nanoporous and optical materials [3]. The ability to manipulate interactions within molecular components through supramolecular self-assembly makes it possible to create multilayer thin films from compatible polymers. Self-assembly provides the flexibility of creating two and three dimensions of polymolecular assemblies such as layers, films, membranes, micelles, gels, and liquid crystals [4]. According to Boncheva and Whitesides [3], self-assembly has the following advantages in developing new materials: it allows formation of small components into an ordered structure in either two or three dimensions, it allows hybrid materials to be easily formed that would be difficult to make by traditional means, and it has the ability to accurately position small components. Today, the concept of self-assembly is still under development. More research is necessary in order to determine if self-assembly will live up to its promise for man-made processes.

Another concept applied with supramolecular chemistry is the concept of polyvalency which is a concept common to biological systems. Polyvalency pertains to a type of interaction common to ligand and receptor biological entities where multiple simultaneous interactions exist [5]. An example of this biological polyvalent interaction is the adhesion of influenza virus on bronchial epithelial cells where multiple interactions occur due to ligand-receptor or antigen-antibody recognition [5]. This concept has been modeled in non-biological systems and is found to be an effective technique of building

3

supramolecular complexes. For building polymeric architectures, the ability of a molecule to interact with three or more molecules by polyvalent interactions allow spontaneous ordered assemblies of different architectures of filaments, cages or ordered arrays [6]. The great number of non-covalent interactions makes it possible to create an overall stronger bond compared to the initial single weak interaction. According to Yeatts and Padilla [6], self-assembly of proteins by polyvalency has great potential in protein-based nanomaterial applications.

1.1.2   Layer-by-layer by Electrostatic Self-assembly

Thin polymer films with nano-scale components can be produced by layer-by-layer self-assembly. The layer-by-layer (LBL) technique is a process of sequential thin film depositions that exploits chemical or physical adsorption between the complementary layers [7]. There are different techniques of LBL self-assembly of thin polymer films including spin coating and solution casting, thermal deposition, chemical assembly, free-standing films, Langmuir-Blodgett (LB) techniques and electrostatic or polyelectrolyte LBL interactions [8].

The choice of LBL technique is dependent on the properties of the films being assembled. A common example would be when the thin films are charged as shown in Figure 1. In this case, electrostatic or polyelectrolyte LBL is a promising approach of self-assembly. Figure 1 shows the method of electrostatic or polyelectrolyte LBL self-assembly by dipping. In this procedure, solutions of polycation (positively functionalized polymer) and polyanion (negatively functionalized polymer) are prepared in separate

4

beakers. The substrate surface is appropriately charged to attract one of the polyion

molecules which is dipped into that solution first, shown in blue in Figure 1. After a

washing step to remove unattached polyion and prevent cross-contamination, the sample

is then dipped in the complementary polyion solution shown in red below. This process

is repeated until the desired number of layers has been deposited.

polycation solution   wash   polyanion solution   wash
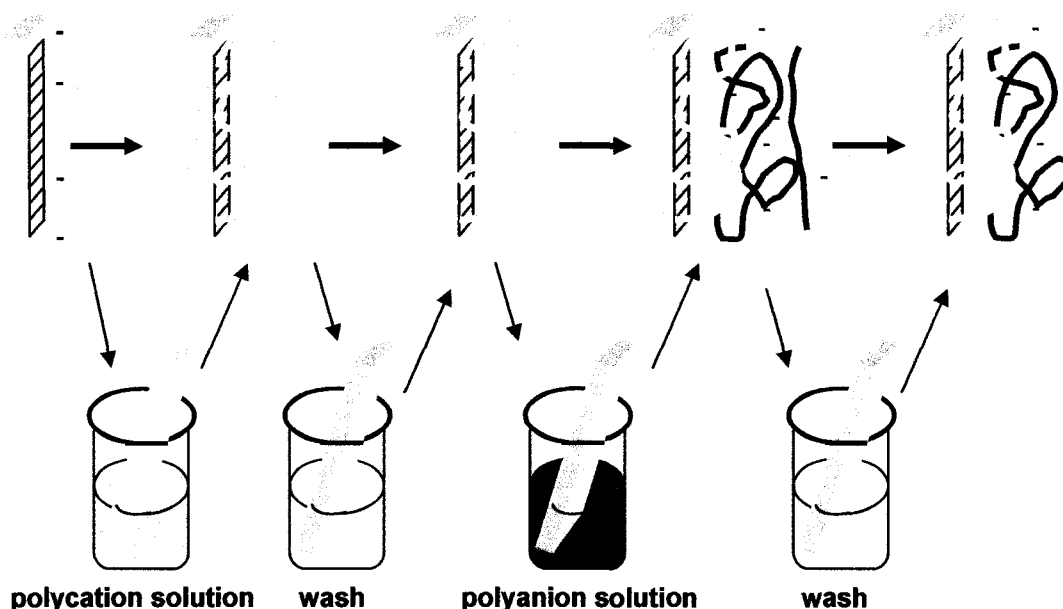
Figure 1. Electrostatic LBL self-assembly by alternating adsorption of oppositely
charged polymers on a negatively charged substrate.

Electrostatic or polyelectrolyte self-assembly is a technique where alternate

deposition of oppositely charged macromolecules (polymers, nanoparticles, and proteins)

is used to produce the thin film layers [7]. By using electrostatic interactions for

assembly, molecular components of the films can be controlled as they self-organize.

The film charge is not the only factor controlling electrostatic or polyelectrolyte LBL. It

is also dependent on the following factors: the molecular weight of the polymer, linear

5

charge density, the chain's linear charge distribution, ionic strength of solution, charge of substrate and non-electrostatic affinity between the substrate and the polyion [7].

Because the layers have multiple ionic bond properties, electrostatic LBL self-assembled films can have comparable strength to that of covalent bonding [10]. As a result, the polyionic interaction in electrostatic self-assembly can easily make a stable surface. Thin films prepared by self-assembly using electrostatic interactions have no defects or pinholes which are often inherent in other techniques [9]. Aside from these advantages, electrostatic self-assembly allows incorporation of electrically charged molecules such as organic macromolecules, proteins, and inorganic nanoparticles into the polymer matrix which makes it useful for various applications such as catalysis or drug diffusion [11].

1.1.3 Star Polymers

The efficacy of polymers is differentiated by their chemical composition which determines their thermal, chemical, and physical properties. Polymers are categorized based on the unique structures they possess. According to Tomalia and Frechet [12], the different polymers are classified as such: Class I are linear polymers, Class II are cross-linked polymers, Class III are the branched polymers and Class IV are the dendritic polymers.

The star polymers shown in Figure 2 fall under the Class IV polymer type. Class IV polymers are comprised of random hyperbranched, dendigrafts, dendrons, and dendrimers. As shown in Figure 2, both dendrimer and star polymers, have a "star-like"

shape. Different types of polymers under Class IV are distinguished based on the synthesis steps they undergo. According to Kim [13], star polymers are prepared by a single step synthesis of the highly branched polymer while a second order synthesis of highly branched polymer produces dendrites.

(a). Star Polymer   (b). Dendrimer
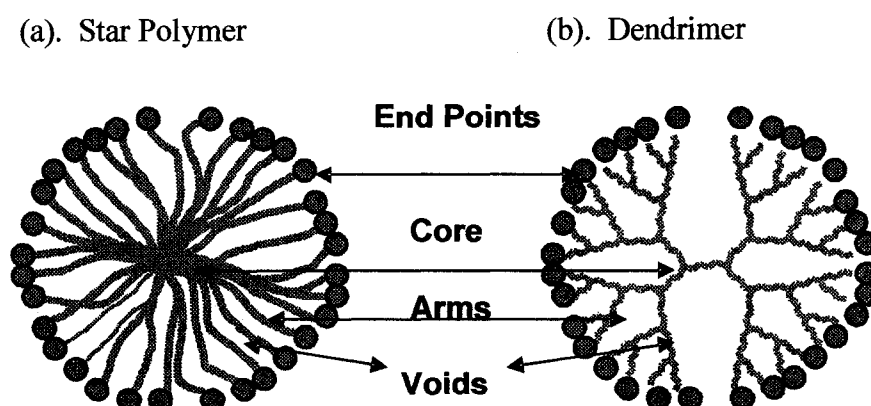
Figure 2. Example of a) a star polymer and b) a dendrimer counterpart [14] (reprinted with permission from J. Sly *et al.*).

The structures of the two molecular architectures of dendrimers and star polymers are similar each with a focal point or "core" in the center, branching peripheral end chains or "arms" and void spaces between branches [14]. The different parts of the macromolecule are identified in Figure 2. The core, arms, and chain ends are composed of polymer chains that can be tailored by the addition of functional groups or elements. This can be done by occluding substances inside the void spaces or by synthesizing functional groups at the chain ends or core. Because of the close similarity between the star polymers and dendrimers, their synthesis steps are similar, creating core and arms of the macromolecules [12]. The method of synthesis is distinguished by the order growth,

7

the periphery or the focal point/core. The method of synthesizing the arms of the macromolecule first is the convergent method for dendrimers. The other synthetic techniques for the star polymer such as coupling of living polymer chains (core initially synthesized) are synonymous with the divergent methods for dendrimers [12, 14]. The applications of these two types of macromolecules are based on the resulting characteristics and functionalities of their topological features such as the end chains and void spaces in the branches [14].

Although both macromolecules have the same features, dendrimers have been studied more than star polymers. The detailed properties and structure of star polymers are still unknown since their development was stunted by studies concentrating on dendrimers. Dendrimers are well studied even though they require a costly multi-step synthesis and have structural limitations of surface density [14]. Initially, star polymers were difficult to control and functionalize compared to the dendrimers. This was originally due to difficulties encountered in reproducibly synthesizing star polymers. Due to the common features of the two macromolecules, star polymers can often be used for the same applications as dendrimers. Now that the synthesis is better understood, star polymers can be prepared cost-effectively and rapidly for large scale and bulk applications [15].

Some applications of the dendrimers are in drug delivery, catalysis, light and energy harvesting, molecular imaging technologies and optoelectronic materials [15]. The topographical parts of the dendrimers are utilized for these various applications. The ends of the peripheral chains are functionalized with dyes that act as contrast agents and

the void spaces used to localize the contrast agents or hosts serve as for drugs such as anti-cancer agents [15]. It is expected the same will be true for star polymers due to the close similarities in the two macromolecular structures.

1.1.4   Detection by Surface Plasmon Resonance (SPR)

The surface plasmon resonance (SPR) detector is an optical detector that has been widely used for biological studies and is a sensitive, tag-less and real-time method of detection. Some of the most common applications of SPR include studying protein binding, association/dissociation kinetic studies and affinity constant investigations which are utilized in the fields of molecular engineering, food analysis, clinical diagnosis, proteomics, environmental monitoring, bacteriology, virology, cell biology, drug discovery and warfare agent detection [16].

The concept of total internal reflection is important in understanding the theory of surface plasmon resonance (SPR). When light goes through a material of high refractive index to a material of low refractive index, some light is reflected from the interface [17]. However, when light hits an interface at a greater angle than the critical angle, the light is completely reflected causing total internal reflection [17]. As light passes through an interface of two media with dielectric constants of opposite signs, for instance a metal and a dielectric, charge-density oscillations occur, also known as surface plasmons resonance [18]. As shown in Figure 3, the SPR apparatus consists of the prism, noble metal interface, light source, detector, and flow cell. From a light source, an incident light of specific angle or wavelength goes through the prism and through the metal film at

9

total internal reflection. The plane polarized light wave incident upon the metal surface

causes a displacement of free electrons in the metal which move across the metal surface

and are called plasmons. The oscillation or separation of the free electrons creates an

evanescent electromagnetic field that decays exponentially with distance away from the

gold film and the sample. A typical evanescent field decay length of 300 nm is observed

depending on the materials and wavelength. Also shown in Figure 3 is surface plasmon

wave moving across the evanescent field. At a particular angle of incidence, this wave

vector of surface plasmons and the component of the wave vector of the incident light

tangential to the surface will match, causing the electrons to resonate (hence called

surface plasmon resonance) [17]. When this happens, energy is lost, reducing the

intensity of the light reflected out of the prism to the detector. Hence, at this angle, the

intensity of the light reaches a minimum or "dip" which is known as the surface plasmon

resonance angle [17].
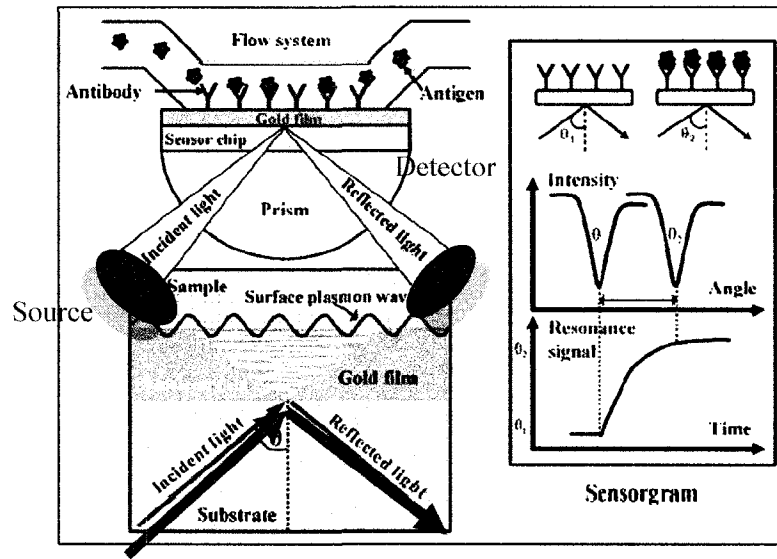
Figure 3. Surface plasmon resonance (SPR) set-up and real-time data of time and angle of reflectance (sensogram) [16] (reprinted with permission from Elsevier Limited).

Surface plasmon resonance detectors measure the change in resonance angle caused by a change in refractive index adjacent to the surface caused by materials immobilized on the metal surface. In the case of Figure 3, antigen and antibody binding interactions are being studied by measuring the change in angle of reflectance for the antibody binding and antigen-antibody binding. As the antibody binds on the metal surface, a change in angle or wavelength is detected by SPR. As observed in Figure 3, a specific angle of reflectance, θ_1 is measured for the antibody and a new angle, θ_2 is measured as the antigen binds to the antibody as an antigen solution flows through the detector cell (flow cell). The change in the angle indicates that binding has occurred between the antibody and antigen.

The plasmon curves from SPR experiments are fit to theoretical curves to check the validity of the results. Data fitting is done by mathematical curve fitting techniques to

11

find the minima of the inverted bell-shaped curve. Based on this change, a specific

thickness of the layer formed on the surface can be calculated based on the following

three layer Fresnel equations [19].

$$R = |r_{pms}|^2$$

Equation 1

with

$$r_{pms} = \frac{r_{pm} + r_{ms}\exp(2ik_{mz}d)}{1 + r_{pm}r_{ms}\exp(2ik_{mz}d)}$$

Equation 2

$$r_{pm} = \frac{k_{pz}\varepsilon_m - k_{mz}\varepsilon_p}{k_{pz}\varepsilon_m + k_{mz}\varepsilon_p}$$

Equation 3

$$r_{ms} = \frac{k_{mz}\varepsilon_s - k_{sz}\varepsilon_m}{k_{mz}\varepsilon_s + k_{sz}\varepsilon_m}$$

Equation 4

and

$$k_{jz} = \left(\varepsilon_j\frac{\omega^2}{c^2} - k_x^2\right)^{1/2} \quad \text{for } j = p, m, s$$

Equation 5

$$k_x = \sqrt{\varepsilon_p}\frac{\omega}{c}\sin\theta$$

Equation 6

$$\omega = \frac{2\pi c}{\lambda}$$

Equation 7

where: r_{pm} and r_{ms} = amplitude reflectance by Fresnel equation
ε_j and k_{jz} = dielectric constant, wave vector perpendicular to the interface j
k_x = component of wave-vector parallel to the interface
ω = angular frequency
λ = wavelength
d = thickness of layers

1.2   Significance

As part of the on-going developments in polymer thin film assembly, a versatile technique of thin film fabrication using novel polymeric materials are proposed in this study. The potential of electrostatic LBL self-assembly is predicted to be an efficient thin film fabrication technique for industrial applications. Electrostatic LBL polyvalent self-assembly offers a time efficient, labor effective, clean process that produces quality films. Aside from this, the industry strives to produce new products from novel raw materials of low costs. As such, different types of polymers are being used because of their thermal, chemical, and physical properties. Dendrimers have been well studied compared to the star polymers. The possibility of star polymers as novel materials for electrostatic LBL self-assembly is based on their similarity with dendrimers.

The market of catalysis-based industries is relevant to the electrostatic LBL self-assembly of star polymers. With the use of the multilayer star polymers, catalysts are protected and can remain intact for multiple cycles since the arms attached in the core of the star polymers maintain the integrity of the catalyst. Also, the multilayer star polymers can easily be removed and recycled from the reaction. This capability of the star polymers is significant in processes where the catalysts are difficult to eliminate.

Also, the potential of star polymers for pharmaceutical industry is enormous. One significant advantage of star polymers is its scalable synthesis. Application of dendrimers is relevant to star polymer because of the close similarities of the two. The use of dendrimers as raw materials is still in its infancy. The costly ($1500 per 1 kg of a

13

7th Generation) and lengthy synthesis (a month to yield) of dendrimers hinder the potential of these macromolecules in applications at the industrial scale.

Although still in the early stage of research, some dendrimers have been found to be viable pharmaceutical products. Dendrimers in multilayer polymer structures can be used for applications in drug delivery. With the multilayer dendrimer structure, the time for the drug to be released in the body can be controlled by the thickness of the multilayer structure. One recent application of dendrimers (still under FDA testing) is the Starpharma Vivagel. This dendrimer gel has functionalized end points that target the HIV virus blocking it from targeting the T cells of the body.

Polyvalent self-assembled LBL polymers can be economically feasible because of the high efficiency and stability of film produced. As such, it is predicted to bring great revenue in different industries. The costly synthesis of dendrimers makes star polymers excellent alternatives because of the structural similarities with dendrimers and economical synthesis. This study serves to provide materials and techniques that can be further developed for applications in for drug delivery and catalysis.

CHAPTER TWO
LITERATURE REVIEW

2.1   Development of Self-assembly: Electrostatic LBL

Through the years, fabrication techniques for polymer multilayers have been

found to have process limitations. Processes such as spin coating and thermal deposition

of macromolecules on substrates had limited applications due to the uncontrollable

molecular order of the fabricated films [8]. Molecular order describes how molecules of

thin films align to build the multilayer thin film structure. Multilayer fabrication of

macromolecules requires that the molecular order in films to be controlled and stable in

order to be useful [8]. It was in the 1930s when the first controlled process of fabricating

layers of polymers on solid substrates was discovered, the Langmuir Blodgett (LB)

technique [20]. Langmuir Blodgett (LB) deposition is a method of self-assembly that

fabricates a compressed monolayer polymer on a water surface which is then transferred

to a flat substrate [20]. Figure 4 shows the LBL technique using the LB technique.
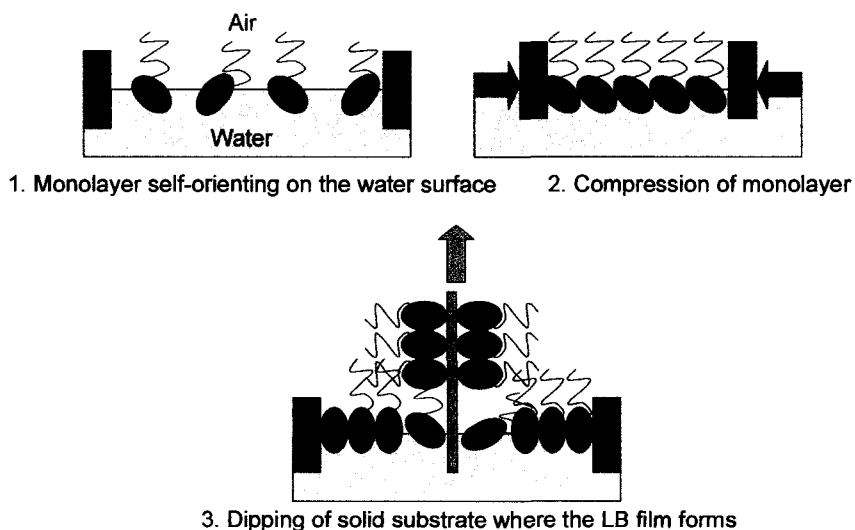
Figure 4. Steps of film formation by Langmuir Blodgett method.

In Figure 4, the first monolayer is formed on the water surface. The layer of polymer is then compressed to produce a cohesive layer [21]. Then, a solid substrate of high surface pressure is then dipped up and down into the water solution. The whole process is repeated to buildup the desired number of layers. Polymer multilayers fabricated using this technique are 5 to 500 nm thick [8]. Industrially, the LB technique is not a feasible method; the quality of films produced from the process could not be accurately controlled due to size, and topology issues resulting from the film formation and transferring technique [20]. It was not until the 1960s that Kuhn and co-workers used the LB technique to produce nano-scale heterogeneous structures of organic molecules [20].

Self-assembly via chemical interactions such as ionic attraction started in the early of the 1980s. The new technique improved multilayer polymer fabrication by eliminating the size and topology issues of the LB technique. Such improvements were observed by Kuhn and Mobius in the self-assembly of monomers on silicon and silicon dioxide (SiO_2) by being able to manipulate individual molecular layers. By using different donor and acceptor dyes, they found that Forster energy transfer is dependent electronic structure and the distance between the donors and acceptors. By the energy transfer method, the formation of multilayer of films was confirmed [22].

According to Nalwa [8], it was in the 1980s when polymers 2-5 nm thick were first fabricated on silicon and gold surfaces through multilayer film self-assembly. This was the beginning of nano-scale fabrication of polymer multilayers. Decher [20] demonstrated self-assembly by chemical interactions by using covalent or coordination chemistry. However problems such as steric effects due to covalent bonding and limited

reactivity of the organic reactants were encountered. Electrostatic interactions were first

utilized for the self-assembly by Iler in 1965 to form films on glass using alternating

films of oppositely charged colloids [23]. Iler's study was not successful since there was

destruction of layer uniformity due to flocculation after only a few deposition cycles [20].

It was not until the 1990s that electrostatic LBL self-assembly of polymers was achieved.

In 1991, Decher and colleagues described the deposition of oppositely charged

polymers by electrostatic interactions [8]. This method of electrostatic interactions

reduced steric limitations observed for self-assembly by covalent or coordination

chemistry [20]. At the same time, several studies on adsorption of oppositely charged

molecules such as linear polymers, proteins, or nanoparticles on a charged substrate in

solution were reported by different groups [8]. One of the first successful studies on the

electrostatic LBL of polymers was conducted by Keller *et al.* [24], who showed that

multilayers of polymers can be built through electrostatic interactions. In their

experiment, they found that the deposition is self-regulating or self-limiting. They

indicated that an immersion step can only produce one type of layer (polycation or

polyanion) and any additional species of the same polymer type was repelled. Keller *et

al.* [24] described the polymer films as self-regulating. With this study, self-assembly by

electrostatic LBL became a fast and precisely controlled technique that can produce

multilayers of structurally well defined films as shown in Figure 5. Ellipsometry

techniques were used to measure film thickness and provided good fits with the

theoretical thicknesses. Theoretical thicknesses of the polycations and polyanions were

assumed based on their crystallographic diameters which were used to fit the data. Keller

and colleagues [24] results showed four layers of alternating structures of anionic films of

á-ZrP (á-Zr $(HPO_4)_2$) /PAH (poly (allylamine) hydrochloride) /$K_6Nb_6O_{17}$ $^{2-}$/PAH and

polycation films of á-ZrP /Al_{13} $^{7+}$/ á-ZrP /PAH could be formed.
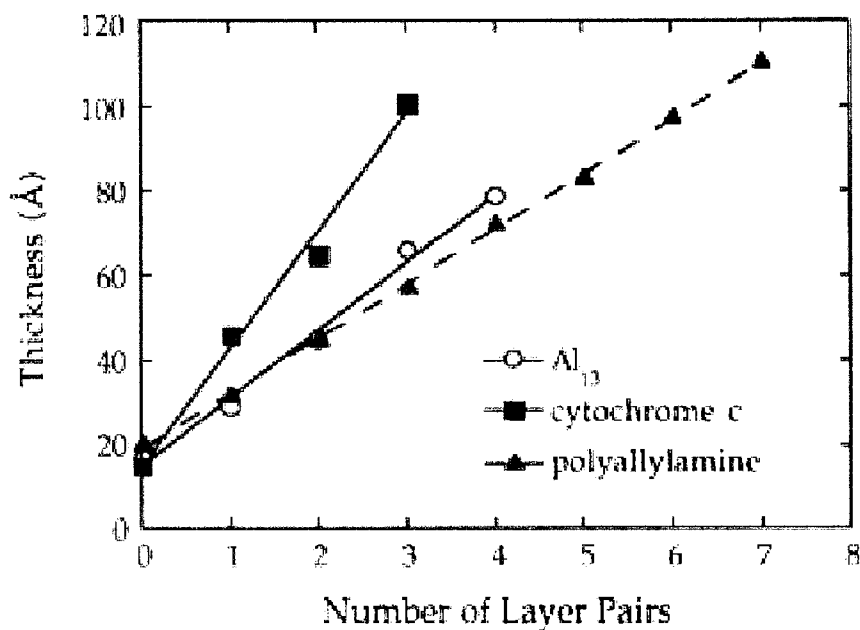
Figure 5. Linear deposition behavior of electrostatic LBL fit with the theoretical film thickness (Straight lines) [24] (reprinted with permission from American Chemical Society).

The ease in building layers of polymers without any limitation in size, topology

and flocculation effects makes electrostatic self-assembly viable to various applications.

Nalwa described some of the applications of self-assembly by electrostatic LBL

including fabrication of ultra thin films from charged polymers to modify surfaces to

make "smart" biocompatible films, catalytic nanoreactors, sensor layers, and bioreactors

[8]. For making new materials as mentioned, other film characteristics in addition to

polymer charge can be manipulated. Rubner et al. [25] studied the effect of manipulating

linear charge density in LBL self-assembly of linear polymers. They looked at the layer

thickness and surface properties of multilayer films of bilayer weak polyelectrolytes

(weak polyacid, polyacrylic and polyallylamine). In this study, a dipping technique

(dipping time of 15 min. for polymer solutions and 2 min. for water rinse) was used for

electrostatic LBL self-assembly. With pHs varying between 2.5 and 4.5, a linear

relationship between thickness as a function of the number of bilayers was observed as

shown in Figure 6.
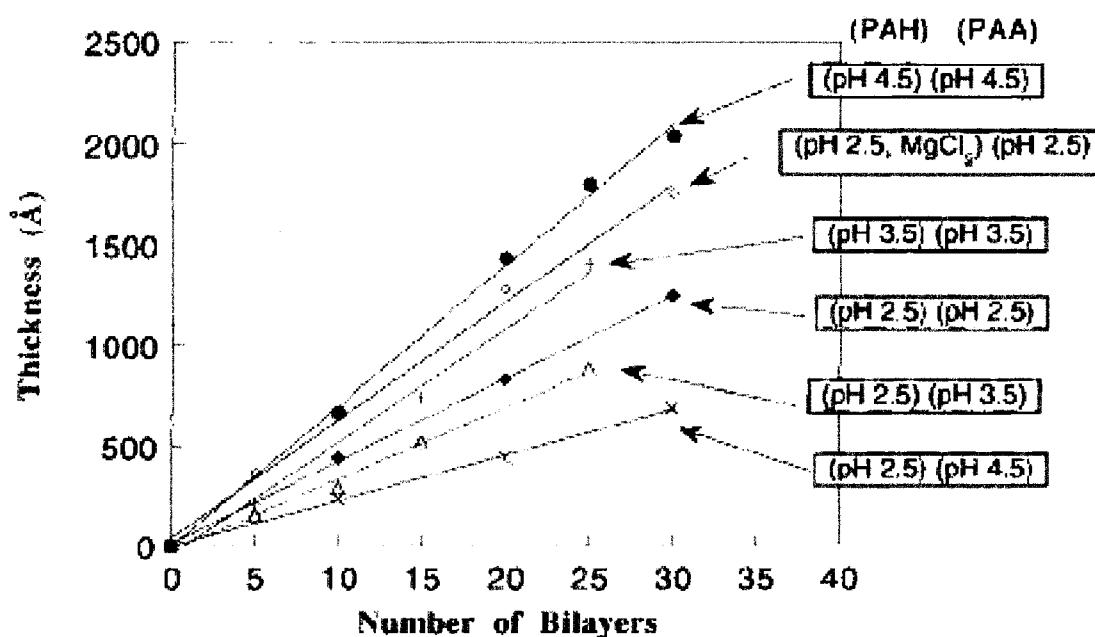
Figure 6. Thickness versus bilayers deposited at varying pH of PAA (poly (aspartic acid)) and PAH (poly (allylamine) hydrochloride) dipping solutions [25] (reprinted with permission from American Chemical Society).

As shown in Figure 7, the thickness of the layers was found to be dependent on

the pH of the polymer solutions and was also affected by the thickness of the previously

deposited polymer layer [25]. The thickness of PAA in PAH over a pH range from 2.5 to

4.5 increased and was almost constant for PAH. They concluded that the surface charge

density of the absorbing layer and of the previously absorbed layer affected the thickness

of polymers.
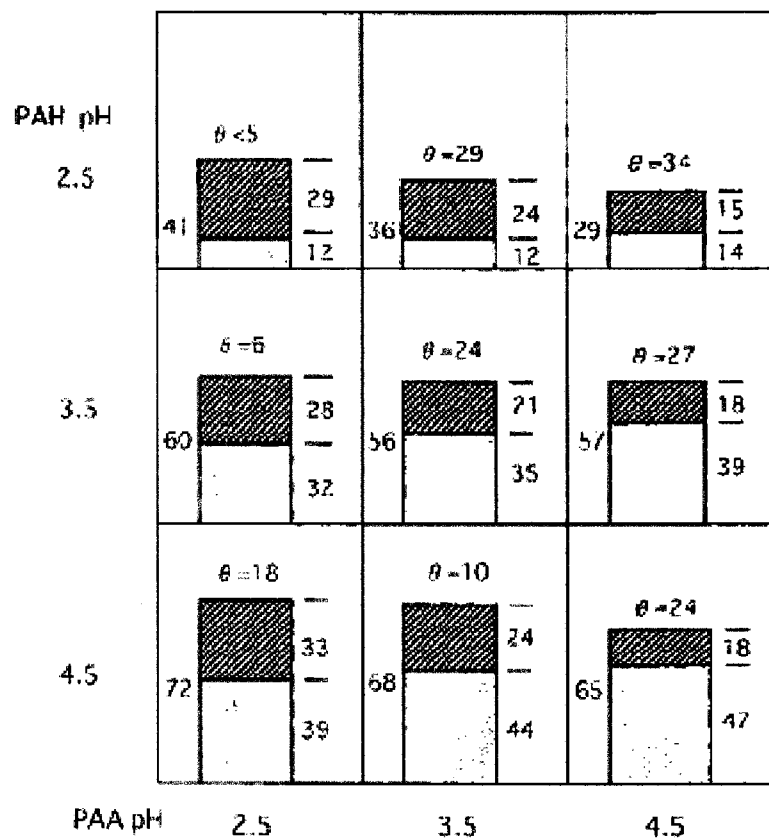
Figure 7. Thickness distribution of PAA (poly (aspartic acid)), dark regions, and PAH (poly (allylamine) hydrochloride), light regions, in dipping solutions of different pH [25] (reprinted with permission from American Chemical Society).

By manipulation of linear charge densities of linear polymers, Rubner *et al.* [26]

were able to apply electrostatic LBL self-assembly in porous linear polymers for

application in controlled drug release. The weak polyelectrolytes of PAA and PAH

bilayers were fabricated by electrostatic LBL through the dipping method. By using

porous polymers, they were able to control the release rate of the drug by the number of

layers and porosity of the polymers [26]. The rate of drug release was related to the

number of layers and varied pore sizes [26]. The pores in the film were formed by

dipping the multilayer films for 5 minutes in water of different pH (2.0, 2.2, and 2.3)

followed by treatment in pH 5.5 deionized water or pH 10.0 NaOH solution. The size of

pores was determined through AFM characterization. Characterization of the films was

done using AFM imaging as shown in Figure 8. The non-porous films were smooth and

had good coverage based on the AFM imaging. It was found that at an average nanosize

pores of approximately 100 nm (10 nm to 150 nm range), a zero order rate of release

occurs compared to the Fickian diffusion mechanism in micropores of 1 micron (300 nm

to 2 micron range) [26].
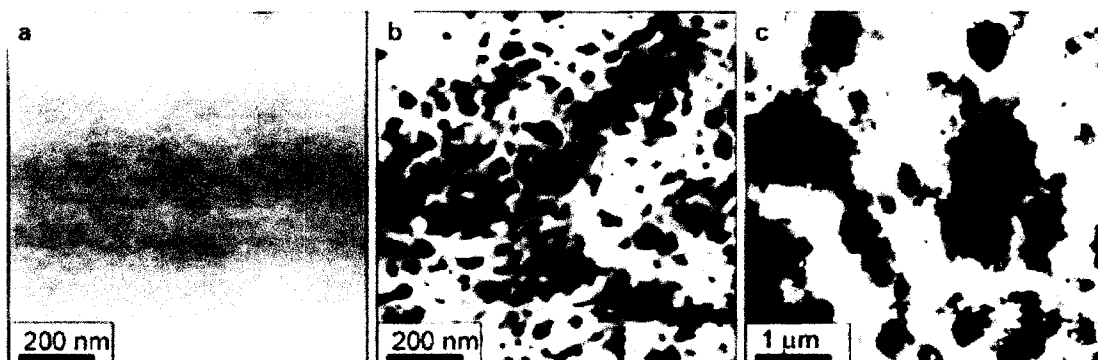
Figure 8. a. Non-porous film (1 x 1 micron image size), b. nanoporous (1 x 1 micron image size) and c. microporous (5 x 5 micron image size) 20 bilayers of PAH/PAA multilayer films [26] (reprinted with permission from American Chemical Society).

2.2   Development of Self-Assembled Star Polymer Multilayers

The development of star polymers coincides with that of their dendrimer

counterpart. The development of star polymers was diverted by the discovery of

dendrimers. Although both macromolecules are part of the same architectural class of polymers, many more studies have been done using dendrimers for various applications. The development and applications of star polymers along with their dendrimer counterparts will be discussed in this section.

In the 1950s, Flory studied polymerization steps that produced monodispersed synthetic macromoloecules [12]. At that time, the hyperbranched or star polymers were classified under the dendritically structured or Class IV type of polymers. The first branched macromolecule was synthesized by Vogtle in 1978 [27]. Before that, there had been earlier attempts to synthesize the star polymers. In 1968, Zilliox and colleagues attempted to make star polymers but large polydispersities resulted causing a decrease in the number of branches of the star polymers [28]. There was no distinction drawn between the two types macromolecules until the Tomalia et al synthesized the first "true" dendrimer in 1984 [12]. DuPont classified the other type of Class IV polymers as "hyperbranched polymers" until 1987 when the synthesis of a true hyperbranched polymer was patented by Kim [13]. Kim used multifunctional initiators in the ring-opening polymerization of propiolactone and anionic polymerization of methyl methacrylate [13]. Characterization of star polymers was difficult due to the unusual solubility of the macromolecules compared to other types of polymers. Since the results of the first experiments on star polymers were uncharacterizable, there was a temporary decline in studies of the star polymers. According to Tomalia and Frechet [12], there were only three research studies presented for the star polymers compared to a dozen for

dendrimers through 1991. From a rate of one to two publications per year from 1987 to 1991, there was an increase to 170 publications in 1997 [13].

As years passed, interest in the star polymers increased as the synthesis of dendrimers proved to be time consuming and costly. Interesting properties of the star polymers were eventually recognized including unimolecular micelle-like properties [13] and surfactant properties. Important comparative studies between linear polymers, dendrimers, and star polymers were done by Wooley and colleagues in 1994. In this study, star polymers were found to have different thermal properties compared to dendrimers but have similar solubilities which are greater than those of the linear polymers [13]. In the opinion of Yates and Hayes [27], Wooley and colleagues rejuvenated the interest in star polymer by identifying unique thermal and mechanical properties of star polymers including modulus, tensile strength and compressive moduli. The study star polymers might be used in the various applications generally reserved for linear polymers and dendrimers. The similar topological characteristics of both dendrimer and star polymers indicate that potential applications for dendrimers might apply to star polymers as well [13]. As a result, many studies using dendrimers are being duplicated using star polymers. Recently, various studies have been reported using star polymers as unimolecular nanoreactors for applications in catalysis [29]. In the review by Vriezema and colleagues [29], the authors were presented in detail various applications of dendrimers for catalysis. In this review, it was suggested that star polymers are preferred as a nanoreactors because of the time consuming synthetic reactions required to produce dendrimers. Star polymers became an alternative structure

that can capture an active metal complex in the core due tothe micelle properties of the structures studied [27]. Such examples of catalytic applications of star polymers that have been studied are: hydrogenation of cyclohexene by Mecking *et al.* [30], double Michael addition by Slagt *et al.* [31], Heck reaction by Bosman *et al.* [32], and oxidation of alcohols to ketones by Terashima *et al.* [33].

Because of the similarities of the two macromolecular architectures of dendrimers and star polymers, researchers have tried using star polymers for the same applications of self-assembled LBL as studied for dendrimers. Dendrimers are currently used in applications of drug delivery using biomolecular imaging such as the Gadomer17- MRI probe which is available and drug delivery by recombinant DNA technology according to Helms and Meijer's review [34]. The multilayer film applications of dendrimers were first studied by Regen and Watanabe in 1994. They used coordination technique to form 100 nm thick multilayers of PAMAM dendrimers [35]. After which more studies such as Bergbreiter's group, Crook's group and Klein's group and Frechet's group followed [35].

In one study by Tsukruk and colleagues [36], the self-assembly of multilayer dendrimers was investigated. The behavior of the macromolecules at interfaces is not known because of the limited data on the dendrimer structure [36]. The results from the study showed a compact composite type multilayer of dendrimers with oblate shaped layers after self-assembly. In their experiment, different generations of dendrimers (Starburst, G 3.5 and G4 from two sources and G 5.5, G 6, G 9.5 and G 10) were fabricated to 20 molecular layers by electrostatic LBL self-assembly. Thickness measurements of the films were done by scanning probe microscopy (SPM) and X-ray

reflectivity measurements. The occasional holes found near the film end in Figure 9 were measured using the SPM by height comparisons to the silicon substrate. The thickness measurements from the SPM were verified using X-ray reflectivity results.
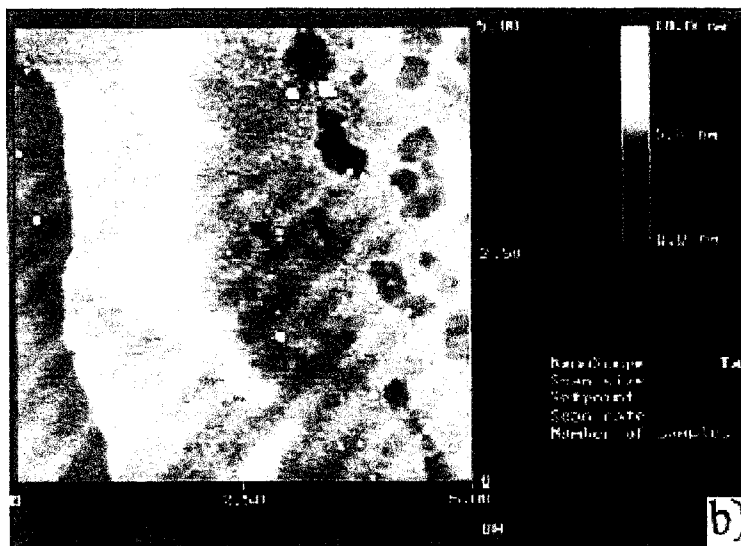
Figure 9. SPM micrograph (scan size 5 micron) of G6 monolayer at the dipping edge of the film. Measurements were done using random holes by the height difference from the bare silicon substrate (left) compared to the height of the film [36] (reprinted with permission from American Chemical Society).

Different compression states of the dendrimer on a dendrimer and within a LBL multilayer film as shown in Figure 10 were assumed in the study to estimate layer thickness. The estimated thickness was based on the known average density of the dendrimer monolayers, molecular mass, and cubic packing within layers. They concluded that the highly compressed layers of dendrimers observed in this study were due to the behavior of the dendrimers to spread on a normal surface. The dendrimers formed a compressed oblate shape with axial ratio in the range from 1:3 to 1:6 [36].
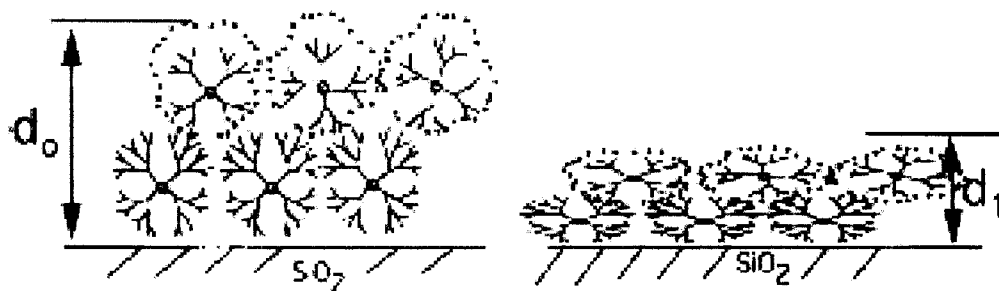
Figure 10. LBL of dendrimers with d_0 as assumed model of dendrimer on dendrimer while d_1 is compressed state within the LBL multilayer film [36] (reprinted with permission from American Chemical Society).

2.3   Solvents Effects in Self-Assembly

Even though self-assembly has been well studied, the mechanism of film formation is critical. As mentioned earlier, there are different factors to be considered in multilayer self-assembly. An important factor is solvent choice and its effects. As defined by Hirst and Smith [37], solvent effects refer to solvent polarity in terms of both macroscopic (*i.e.* refractive index, density etc.) and microscopic (*i.e.* intermolecular forces, solvation etc.) properties. Solvent polarity can be measured by studying both equilibrium kinetic rate constants, and the spectroscopic properties of both the solvent and solute [37].

Previous studies show that the choice of solvent systems for self-assembly is crucial for the success in fabricating multilayer LBL self assemblies. In a study fabricating LBL multilayer of polyelectrolytes, it was found that water-insoluble polyelectrolytes undergo intermolecular association and intramolecular aggregation due to hydrophobic effects when dissolved in aqueous media [38]. By choosing anhydrous N, N-dimethylformamide (DMF), the formation of a LBL multilayer film of insoluble

azo-containing polyelectrolytes was successful [38]. The LBL self-assembly of PEPB6P-

AC (azo polyelectrolyte) /PDAC (poly (diallyldimethylammonium chloride))was tested

using THF, and DMF. They found that the carboxyl groups of the THF miscible

PEPB6P-AC (azo polyelectrolyte) can only be ionized in DMF and not in THF. Using

DMF as solvent, the hydrophobic aggregation of the azo polymer was eliminated forming

smooth multilayer polymer surfaces [38]. In this study, the aggregation of the films

during self-assembly was investigated by UV-vis spectroscopy and the film morphology

was probed using AFM (atomic force microscopy) as shown in Figure 11.
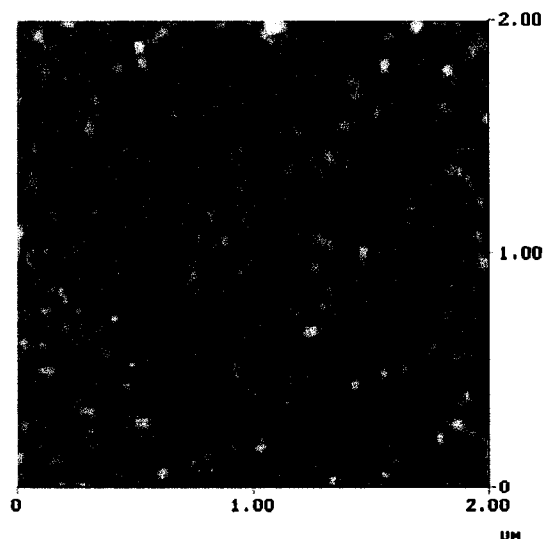
Figure 11. The AFM surface morphology, 2 μm x 2 μm height image, of the PEAPB6P-AC/PDAC multilayers with 12 Bilayers [38] (reprinted with permission from Springer).

The discovery that THF is an ineffective solvent for self-assembly of water

insoluble polyelectrolytes has other implications. In a study by Barron *et al.* [39],

preferential solvation in THF-water system was studied by looking at the dissociation

constants (pKa) of acidic components. They looked at the pKas of different types of pH

reference materials at different THF-water ratios and observed variations in the pKa

values of the acidic components in the THF-water mixture. The pKa values of the acid

components were lower than expected compared to values in dry THF in (*e.g.,* acetic

acid, pKa = 24.42 from the literature). This observation was explained by the differences

in structural features of the acid components where that preferential solvation by water

exists. Preferential water solvation was described to be the tendency of water molecules

to be found in the vicinity of hydrogen ions of the acid compared to THF [39]. As an

example, for the case of acetic acid as shown in Figure 12, the increase in the measured

pK_a values compared to the ideal dependence of pK_a values on the mixture composition

was smaller in the water-rich region. The small increase in pK_a at higher mole fraction of

water was explained as the continuous increase in preferential solvation by water in the

THF-water mixture [39].
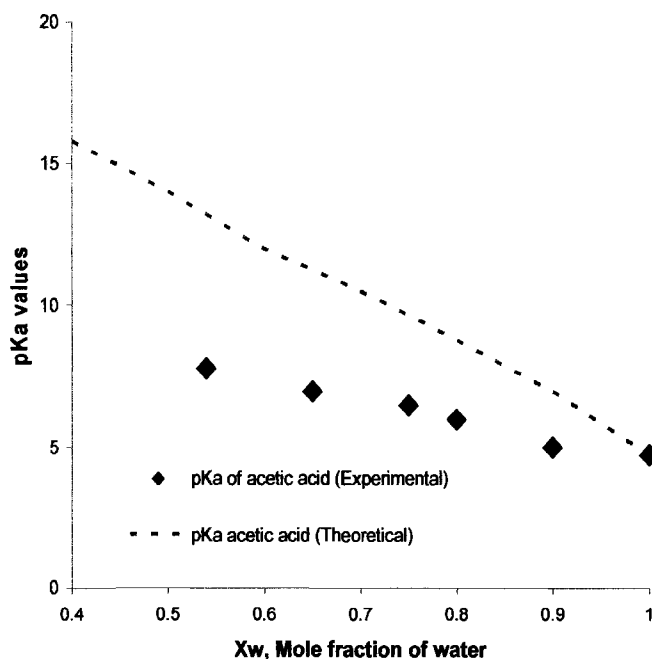
Figure 12. Plot of acetic acid's pKa values versus mole fraction of water, X_w, in THF-water mixtures with the dashed line as the ideal variation of pKa values acetic acid.

Dubas and Schelenoff [40] studied factors such salt concentration, salt type, solvent quality, deposition time, and polymer concentration. In their study, they proposed that salt concentration had the strongest influence in layer thickness and found that the solvent system for self-assembly can actually provide a degree of control of film formation [40]. The solvent quality was investigated by looking at the variation of ethanol in water for self-assembly of the linear polymers. At higher fraction of the organic solvent (ethanol) in solution, the polyelectrolytes were found near the interface and precipitated at ethanol concentrations more than 40 wt % [40]. This behavior was due to a decrease in dielectric constant making the solvation of the hydrophobic polyelectrolyte favorable.

2.4 Development of SPR and its Role in Self-Assembly of Polymers

Surface plasmon resonance or SPR is a widely used optical sensor for various applications, many of which are biological. Today, SPR is an important tool for quantifying changes within a system that are accompanied by a change in refractive index, as reported by shifts in the plasmon resonance. The evolution of SPR from an optical detector to a biodetector, and current studies on the self-assembly of polymer multilayers will be discussed.

According to Homola et al. [17], optical sensors emerged in the 1970s for measurement of CO_2 and O_2 concentrations. Several optical methods were discovered for chemical and biological detection such as ellipsometry, spectroscopy (phosphorescence, fluorescence, Raman), interferometry (white light, modal in

waveguide structures), spectroscopy of guided modes in optical waveguide structures (grating coupler, resonant mirror) and surface plasmon resonance [17]. These methods measure intrinsic properties such as refractive index, absorbance, and fluorescence of the material [17]. For SPR as an optical sensor, the intrinsic property measured is the refractive index.

An SPR detector was first used to detect formation of organic mono and multilayer on metal surfaces by Pockard et al. in 1978 [41] and Swalen et al. in 1980 [41]. Surface plasmon resonance was originally used as a sensing tool for gas adsorption studies. Similarly in 1982 and 1983 Kindlund and Lundstrum [41] successfully detected anesthetic gases based on silicone oil as the sensing layer using the quartz microbalance (QCM) sensor. Results from other studies such as ellipsometry for adsorption studies of organic molecules on gold, macromolecular surface interaction studies, and the results from Kindlum and Lunstrum helped advance SPR as a biosensor [41]. By 1983, the study of biosensor applications of SPR using the Kretchmann configuration for immunosensing purposes was published by Liedberg et al. [41]. Because of these endeavors, a Swedish company showed interest in the capabilities of the SPR for biomolecule detection. In 1984 that Pharmacia of Sweden developed the biosensor technology and by 1986 Pharmacia Biosensor was formed [41]. In the 90's, new biosensors companies as BIAcore (1990) and BIAlite in 1994 were introduced into the market. By 1997, SPR has been validated as useful for biological sensing studies. Most of the relevant publications were on biomolecular interactions [17].

As a biosensor, SPR offers "real-time interaction analysis" not only for biological purposes but for other purposes as well [41]. Because of this capability, SPR as a detection tool is valuable in studies chemical binding, reactions and interactions studies. SPR is capable of detecting organo monolayers and multilayers on metal surfaces [41]. Upon the realization of the value of electrostatic self-assembly of polymers, SPR became an important characterization tool for such purposes. In 1998, Beketov *et al.* studied the polyelectrolyte self-assembled films of PAA (poly acrylic acid) and PSS (poly (styrenesulfonate)) linear polymers and immobilized urease [11]. The layers of polymers were immobilized and real-time SPR data were gathered as shown in Figure 13. The shift in the SPR curve for the polymer layer provided the thickness for each layer and surface topology of the films. It was observed that the SPR curve for the layers had a broader plasmon curve and suggesting a rough surface of the polymer compared to the gold substrate [11]. The thickness of the layers was calculated by iterating the dielectric film thickness and dielectric permitivities [11].
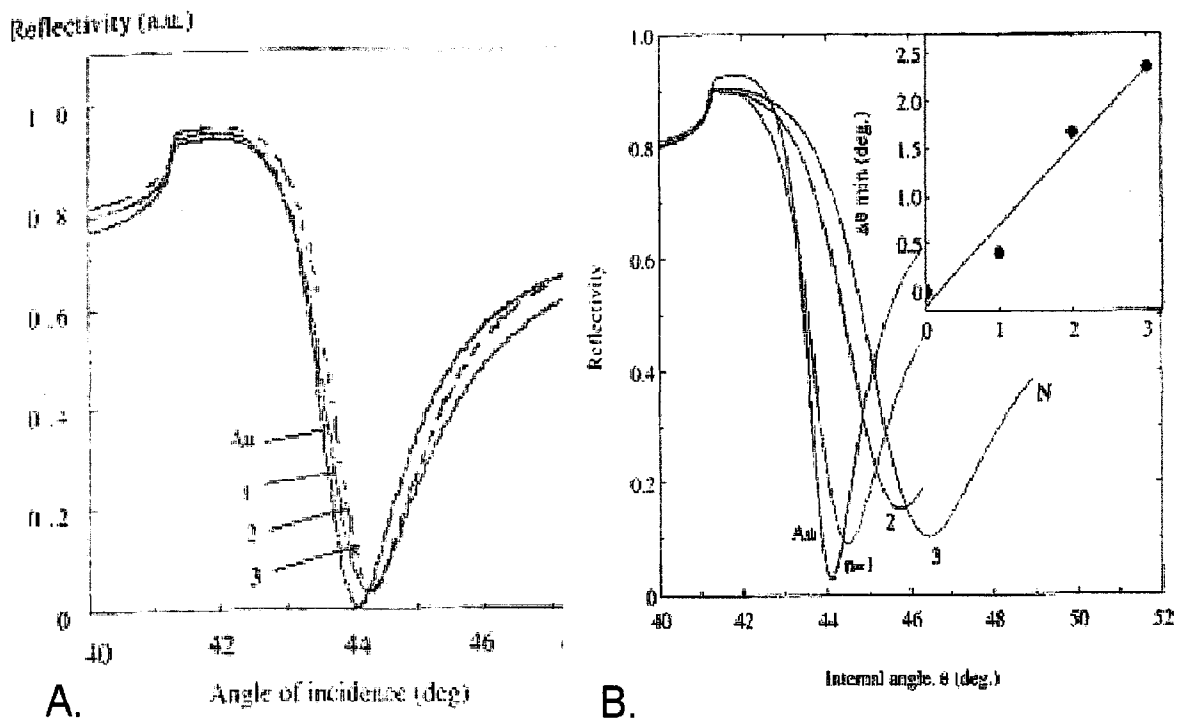
Figure 13. A) SPR curves of Au with three layers fabricated by electrostatic self-assembly LBL technique. Layer 1, Layer 2 and Layer 3 are PAA, PSS, and PAA, respectively. B) SPR curves of the same experiment as A but urease is immobilized instead of PSS, alternating layer of Au, PAA and urease [11] (reprinted with permission from American Scientific Publishers).

2.5   Summary

From this literature review, it can be inferred that electrostatic LBL self-assembly of macromolecules (dendrimers and star polymers) is still in the early stages of development. Electrostatic LBL self-assembly is a promising technique for building multilayer structures for various applications. The studies reviewed showed that the details of the LBL technique are dependent on the type of polymer and its characteristics. Because of the unique properties of macromolecules such as dendrimers and star polymers, they have the potential to be used as starting materials for this multilayer polymer structure. Optimization of methodology (dipping, flowcell etc.) and analysis technique of electrostatic LBL self-assembly will be required. This will facilitate the development of further studies on the promising applications of electrostatic LBL self-assembly technique using novel materials. This study therefore presents star polymers as novel materials for the electrostatic LBL self-assembly.

CHAPTER THREE
HYPOTHESIS AND OBJECTIVES

The overall hypothesis of this study was that layer-by-layer functionalized star

polymers structure can be formed on silicon dioxide by electrostatic self-assembly. The

layer-by-layer deposition of alternating layers of PS-NH$_2$ and PS-COOH on a silicon

dioxide substrates were characterized by Surface Plasmon Resonance (SPR)

spectroscopy, Quartz Crystal Microgravimetry (QCM), Atomic Force Microscopy

(AFM), and Infrared Absorption Spectroscopy (IR).

The specific objectives of the study were:

- To investigate the electrostatic self-assembly of PS-NH$_2$ and PS-COOH and their relative thickness by SPR
- To investigate the uniformity of the films by QCM
- To characterize PS-NH$_2$ and PS-COOH polymers' morphology by AFM
- To characterize PS-NH$_2$ and PS-COOH polymers' stability in terms of dewetting by AFM
- To investigate the interactions of PS-NH$_2$ and PS-COOH by IR

3.1   Justification

The electrostatic self-assembly of LBL polymers is economically appealing

because of it is a time efficient, labor effective, clean process that produces stable films.

The emerging applications of macromolecules for catalysis provide a tremendous

motivation for this research. Currently, dendrimers are mostly used for multilayer

assemblies but have not been successful at the industrial level due to costly and extensive synthetic steps. Star polymers are an excellent alternative for feasible industrial applications because of their structural similarities to dendrimers and economical and scalable synthesis.

CHAPTER FOUR
MATERIALS AND METHODS

The proposed technique of electrostatic self-assembly of LBL deposition of star

polymers is a time efficient technique of producing multilayer thin films. This study

investigated self-assembly of thin films star polymers on silicon dioxide substrates. The

resulting films were examined for coverage, stability in terms of dewetting, layer

uniformity, interactions formed, and relative thickness. The experimental matrices in and

Table 1 and Table 2 summarize the experiments, output, and analysis techniques of this

study.

Table 1. Experimental matrix for self-assembled LBL star polymers on silicon dioxide
surface.

Surface on substrate	Expt. #	Combination of layers	Number of layers	Number of runs	Output
• SiO$_2$ (substrate)	1	• Alternating PS-NH$_2$ followed by PS-COOH	10	3	• Relative film thickness (SPR)** • Uniformity of films by mass (QCM)
	2	• PS-NH$_2$ followed by PS-NH$_2$	2	3	• Relative film thickness (SPR) • Specific electrostatic interactions of the star polymers (SPR)
	3	• PS-NH$_2$ followed by two consecutive depositions of PS-COOH	3	3	

Note: **Samples were imaged under the AFM
  • Experimental conditions: (ambient temperature and pressure conditions)
        - constant concentrations of PS-NH$_2$ and PS-COOH solutions 1:1 ratio
            (weight in mg of star polymer/volume in mL of solvent) prepared at ambient
            temperature and pressure conditions

- constant volume and pH of dichloromethane wash and polymer solutions
- constant flow rate of polymer solutions and solvent wash

Table 2. Additional experiments to verify initial results from Table 1.

Surface on substrate	Expt. #	Combination of layers	Number of layers	Number of runs	Output
• SiO₂ (silicon)	4	• PS-COOH on surface • PS-NH₂ on surface followed by deposition of PS-COOH	3	3	• Confirmation of film interactions (IR) *
• SiO₂ (silicon)	5 6	• PS-COOH and PS-NH₂ on surface • Alternating PS-NH₂ followed by PS-COOH	1 4	1 1	• Film coverage (AFM) * • Stability in terms of dewetting (AFM) *

Note: * Dipping method was employed
       **Samples were imaged under the AFM
   • Experimental conditions: (ambient temperature and pressure conditions)
       - constant concentrations of PS-NH₂ and PS-COOH solutions 1:1 ratio
         (weight in mg of star polymer/volume in mL of solvent) prepared at ambient
         temperature and pressure conditions
       - constant volume and pH of dichloromethane wash and polymer solutions
       - constant flow rate of polymer solutions and solvent wash

4.1   Materials

4.1.1   Star Polymers

Two types of star polymers were used in this study. They were amino (PS-NH$_2$) and carboxylic acid terminated (PS-COOH) as shown in Figure 14. The star polymers used in this study were synthesized by an "arm-first" approach based on the Sly *et al.* recipe [14]. For this synthetic procedure [14], solvents from the Aldrich Chemical Co. were used either as received or purified by standard literature procedures.
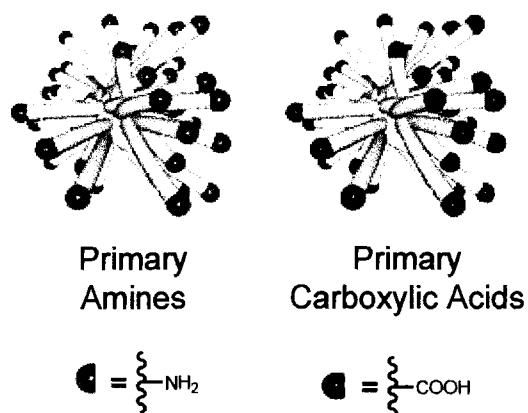
Figure 14. Amino functionalized and carboxylic acid star polymer as polycation and polyanion for the electrostatic LBL self-assembly [42].

According to Sly *et al.* [14], *p*-toluenesulfonyl oxy terminated polystyrene (PS) was used as the functionalized but unreactive/"non-functionalized" star-polymer. These star polymers contained approximately 23 arms with 30 repeat units/arms[14]. The same base polystyrene polymers were further functionalized to produce both the amino and carboxylic acid star polymers.

4.1.2 Substrates

Table 3. Summary of the substrate information and the appropriate surfaces for the purpose of this study.

Surface on substrate	Substrates	Surface	Description	Manufacturer
• SiO_2 (substrate) **	SF-11*	SiO_2 (4 nm sputtered) on Au (50 nm) and Cr (3 nm)	• One inch diameter, 0.020 inch thick with surface roughness less than 10 A	Stefan Sydor Optics
• SiO_2 (substrate) **	QCM crystal	SiO_2 on Ti/Au/ Ti adhesion layers	• Part Number: (149277-1)	Maxtex Inc.
• SiO_2 (silicon)	Silicon wafers	Inherent SiO_2 from oxidation of Si	• One inch diameter, research grade silicon wafers Part Number: (T05120)	Virginia Semiconductor Inc.

NOTE: ** The SPR and QCM substrates were exclusively for the use of the analytical tool

* SF-11 substrates were specific for SPR experiment to have a uniform refractive index transition from the prism and substrate.

- All SiO_2 surfaces have intrinsic silanols (acidic SiOH groups) which were utilized for the electrostatic self-assembled LBL star polymers.

4.2   Procedure

4.2.1   Substrate and Star Polymer Solution Preparation

The substrates were used as received except for SF 11. SF 11 wafers were

cleaned by wiping with acetone-soaked lens paper. All the substrates were subjected to

UV ozone cleaning for 20 minutes to remove organic material, flushed with Millipore

water and dried under a low nitrogen gas flow. The grazing attenuated total reflectance infrared (GATR IR) analysis indicated the surface was free of oils after this length of time.

The sensing layers of the SPR substrate consist of gold on chromium as an adhesion layer, followed by a silicon dioxide layer. The metal layers of gold and chromium were thermally evaporated while SiO_2 was sputtered. Using the public evaporator, 3 nm of chromium was deposited. Using the same equipment after chromium deposition, a layer of 50 nm of Au was deposited. The 4 nm SiO_2 layer was sputtered onto the gold using a separate sputtering tool.

Because the thermal evaporator is a common used tool at IBM where different samples are processed, the inside of the evaporator was cleaned before the depositions. Using a vacuum source, small particles were picked up and removed. Surfaces inside the evaporator were cleaned by wiping with *iso*-propyl alcohol-soaked Kimwipes.

The solutions of the amino and carboxylic acid terminated star polymers for the electrostatic LBL self-assembly were prepared with a 1:1 (weight per volume) ratio of the star polymer and the solvent (*e.g.,* dichloromethane). A weighed mass (mg) of the star polymer was mixed into a measured volume (mL) of solvent. Amino (PS-NH_2) and carboxylic acid (PS-COOH) terminated star polymers were filtered through a 0.20 micron syringe filter. Several solvents such as dry THF, dichloromethane, chloroform, and toluene, were used during the course of this study. All solvents were obtained from Pure Solv solvent dispenser from Innovative Technology Inc.

4.2.2 Dipping and Flow Experiments

Dipping is a common method of electrostatic LBL self-assembly of multilayer thin films. The discrete steps used in the dipping experiments employed in this study were conducted with three dichloromethane and one tetrahydrofuran (THF) wash steps after the deposition of each polymer layer. Each substrate was dipped for 2 minutes in each polymer solution and 2 minutes in each wash solution. As shown in Figure 15, a substrate with silanol surface (pKa = 4) was dipped for 2 minutes in a solution of PS-NH$_2$ polymer (shown in blue); subjected to the series of washes (three separate beakers of dichloromethane wash and one beaker of THF wash); redipped into PS-COOH polymer solution (shown in red) and again treated with a series of washes (three separate beakers of dichloromethane wash and one beaker of THF wash). This cycle was repeated based on the number of layers desired and the substrates were air-dried at room temperature for characterization. Samples for AFM and IR analysis were obtained through the dipping experiment.
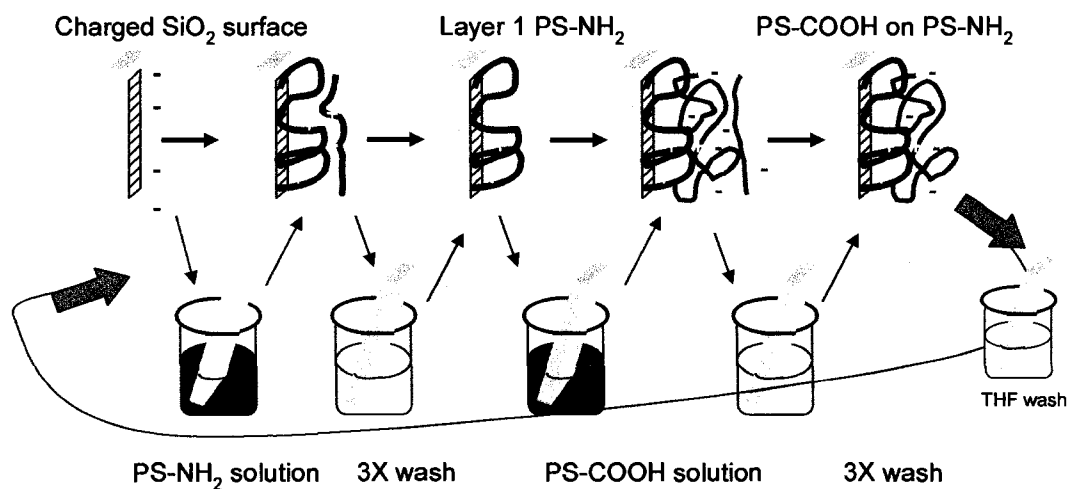
Figure 15. Dipping experiment where oxide surface was sequentially exposed to PS-NH$_2$ and PS-COOH star polymers with dichloromethane-THF washes in between. The cycle was repeated to accumulate the desired number of layers.

Due to the difficulty of obtaining pristine surfaces by the dipping technique, a flow technique was designed. This method of deposition was achieved using a flow cell as described in the SPR *in situ* experimental set-up. Using this procedure, the excess polymers and non-adsorbed materials which were ubiquitous using the dipping method were eliminated. The deposition involved flowing the polymer solutions and wash solvents through the flow cell using a syringe pump. The flow system consists of a single flow cell that has inlet and outlet ports and a plate that holds a wafer under vacuum as shown in Figure 16. Using a syringe pump, the solutions were pumped through a 0.2 micron syringe filter connected to the solvents lines. Each solvent syringe had an individual filter to prevent the cross contamination of solvents.
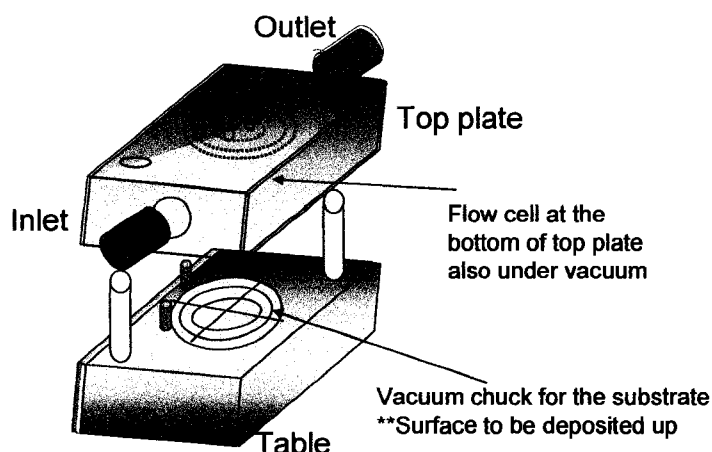
Figure 16. Flow experiment set-up with flow-cell derived from the SPR flow cell design.

The substrate to be coated was placed with the desired side for deposition upward since the flow cell is engraved under the top plate of the set-up. The top and bottom plates were both placed under a vacuum to provide good contact and to hold the substrate in place during the deposition. Once the substrate was secured, the deposition steps could begin. One cycle of deposition included dichloromethane surface preparation, polymer deposition, and wash cycles of dichloromethane followed by THF wash. The surface equilibration was achieved by flowing 3 mL of dichloromethane at 2 mL/min. After this, the polymer solution in dichloromethane was injected at 1 mL/min for 1 min. The layer formation was conducted for 2 minutes followed by wash steps of dichloromethane and THF. The non-adsorbed materials and excess polymer were removed by injecting 9 mL of dichloromethane at 2 mL/min followed by 1 mL of THF at 2 mL/min. The film surface was then primed for the next deposition layer with 3 mL of dichloromethane at 2 mL/min. The deposition cycle was repeated until the desired number of star polymer layers was obtained.

4.2.3 *In situ* SPR LBL Self-assembly
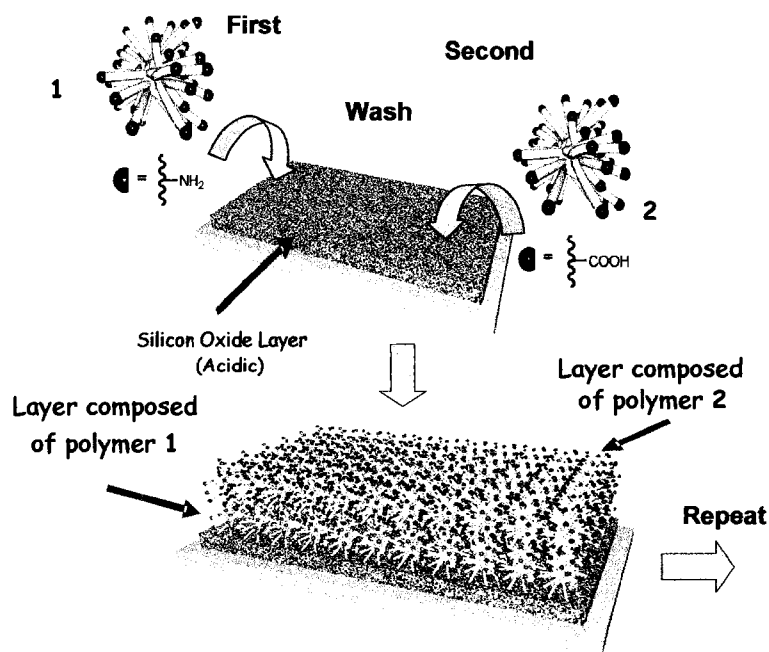
Figure 17. Schematic for the LBL surface deposition of functional star-polymers films *in situ* electrostatic LBL self-assembly [42].

The *in situ* electrostatic LBL self-assembly of star polymers on a silanol surface, as depicted in Figure 17, was conducted by alternate adsorption of PS-NH₂ and PS-COOH on the silicon dioxide layer coated on the SF 11 substrate by controlled injection using the fluidic SPR attachment.

To accomplish this, the SF11 substrate with sensing layers of silicon dioxide, gold, and chromium was placed on the flow cell. The uncoated side of the substrate was in contact with the SF 11 prism using an index matching fluid (Cargille, methylene iodide solution) with the same refractive as SF 11 (refractive index = 1.76). The flow cell was flushed with THF at 1 mL/min until a volume of 1.5 mL was injected in the flow cell.

Then, the SPR data for pure THF were gathered and plotted as the baseline comparison as subsequent resonance angle shifts that occurred as layers were deposited.

The *in situ* deposition cycle in the SPR involved preparation of the surface with dichloromethane, deposition of the polymer from dichloromethane solution, and wash cycles using dichloromethane and THF. The *in situ* LBL began with the surface preparation and solvent exchange of dichloromethane with THF at 1 mL/min until a volume of 1.5 mL had been dispensed. Then, the PS-NH$_2$ star polymer dissolved in dichloromethane was injected in the flow cell at 1.0 mL/min for 1 min. The wash cycles followed by injecting 3.0 mL dichloromethane at 1.0 mL/min then the same volume and rate of 3.0 mL of THF at 1.0 mL/min. The SPR data was taken in the scan mode. The layer of PS-COOH deposition followed with the standard sequence of dichloromethane surface preparation, PS-COOH in dichloromethane injection, and dichloromethane-THF wash. These steps were repeated until the desired number of polymer layers was obtained. SPR data were recorded in real-time using the Labview program kinetics mode during each stage of the process.

4.2.4   *In situ* QCM LBL Self-assembly

The studies of *in situ* LBL self-assembly monitored by QCM recorded the change in crystal resonance frequency due to the material adsorbed on the surface of the quartz crystal over time. An LBL self-assembly protocol similar to that for the SPR was designed to allow comparison of the results from the two analytical techniques.

45

A vacuum chuck is used to hold the quartz crystal in place on the flow cell of the apparatus with the electrodes making good contact with the crystal. At the start of the experiment, a frequency baseline was obtained from the oscillation of the crystal in air. Then, a THF frequency baseline was obtained by injecting a total volume of 1.5 mL of THF at 1.0 mL/min. During the run, the oscillation frequency was allowed to stabilize after each solution or solvent injection until a straight baseline was obtained. The deposition cycle began with the dichloromethane solvent introduced at 1.0 mL/min until a volume of 1.5 mL was reached in order to prepare the surface for the polymer deposition. The first polymer solution of PS-NH$_2$ in dichloromethane was injected (1 mL/min, total volume of 1.5 mL) and the frequency was allowed to stabilize before the wash steps were initiated. The first step of the wash was the injection of dichloromethane at a volume of 3 mL and rate of 1 mL/min followed by THF at the same volume and rate. Another surface preparation with dichloromethane followed after which the PS-COOH in dichloromethane solution was deposited. The polymer deposition cycle was repeated until the desired number of layers was obtained.

4.3   Instrumentation

4.3.1   Surface Plasmon Resonance (SPR)
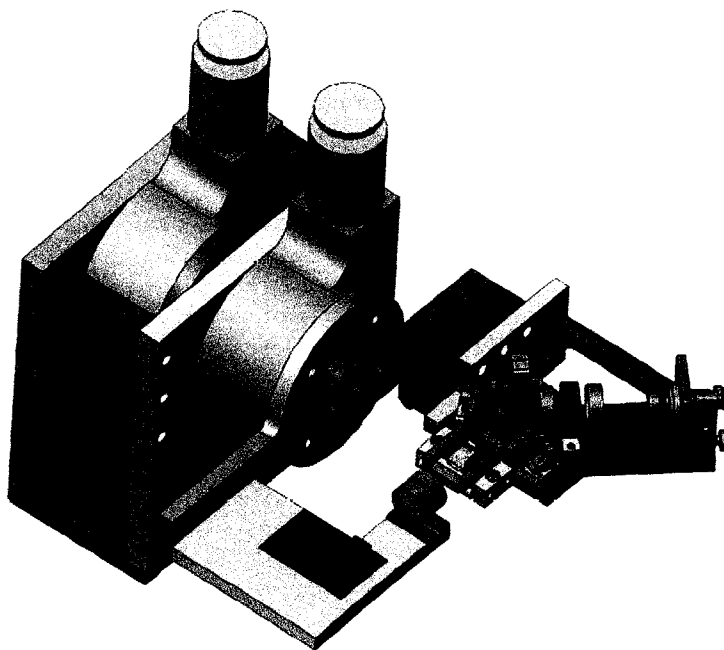
Figure 18. Schematic of the variable angle SPR system operating at 854 nm wavelength located at IBM Almaden Research Center used in this study [43] (reprinted with permission from C.M. Jefferson).

Surface plasmon resonance measurements were performed using a variable angle, single wavelength (854 nm) SPR system housed at the IBM Almaden Research Center. Fluids were transferred in a specially designed Kel-F flow cell (0.5 mm deep with axes 7.0 by 2.1 mm, volume of 40.8 µL) through a fluidic system. The flow cell (dual channel) as shown in Figure 18 was maintained under vacuum to hold the substrate in place on the cell. O-rings around the two flow cells and the outer diameter were used to seal the cell to vacuum. The flow cell of the SPR instrument as shown in Figure 19 was

designed by Shyama Shrinivas of San Jose State University as part of her Master's

Degree research [43].

Inlet Port (F2)
Outlet Port (F2)

Hemi-cylindrical prism

SF-11 substrate

O-ring grooves

Vacuum Source

Flow cell 2 (F2)
Flow cell 1 (F1)

Inlet Port (F1)
Outlet Port (F1)
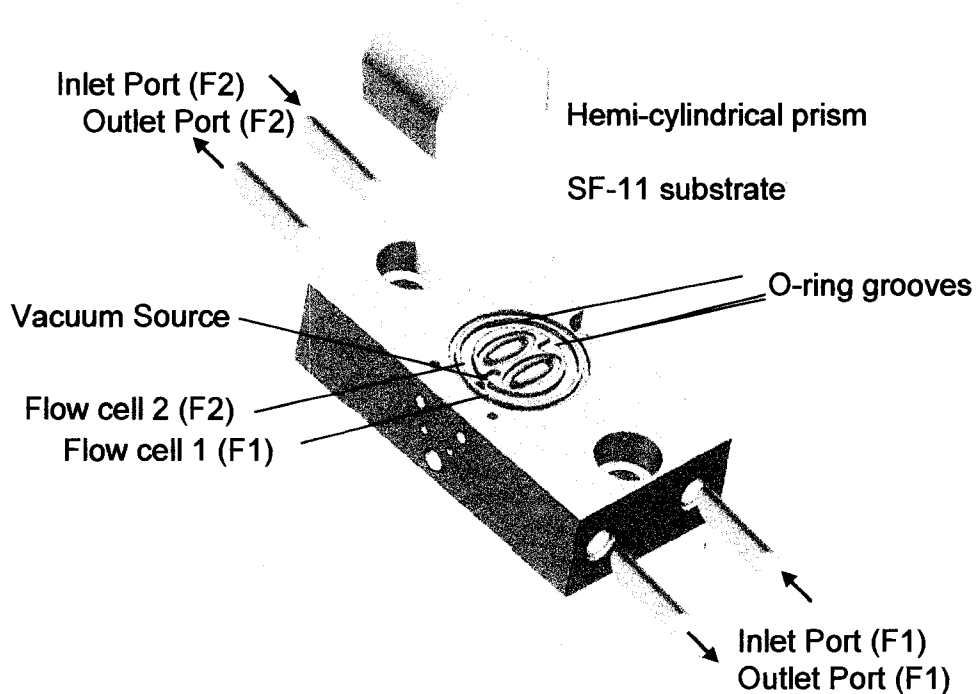
Figure 19. The designed Kel-F flow cell and its parts.

Two sets of inlet and outlet ports are included in the flow cell (F1 and F2) as

shown in Figure 19. One of the inlet ports was connected to a six port injection valve for

the fluidic system while the outlet port was connected to a waste reservoir. The fluidic

handling system was added to the SPR set-up to dispense and control the solvents and

polymer for the *in situ* LBL procedure. The fluidic system shown in Figure 20 consisted

of two syringe pumps that dispense the solvents and polymer solution at a constant flow

rate and a six port liquid valve that controls the fluids entering in the flow cell of the SPR

system.
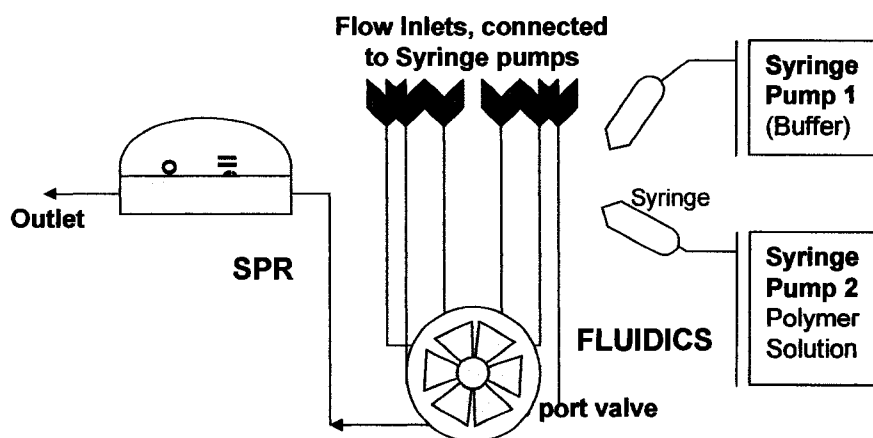
Figure 20. Fluidic system of SPR set-up.

The Upchurch six-port valve is made of ceramic and has no dead volume, thus

preventing any mixing of fluids. Most of the parts of the fluidic set-up had solvent

resistant tubing and connectors. Six chemically resistant Teflon tubes (ID = 0.032

inches) leading to separate ports of the 6 port valve have the same length (65 cm). A

common tube of the same diameter and 30.5 cm in length transferred the fluids to the

SPR system. Each line was connected to the valve by a PEEK flangeless nut with a

Teflon ferrule that seals the tube and is in contact with the fluid. Each solution of

polymer in either dichloromethane or THF solvent had a specific port that was exclusive

for that solution to prevent any cross-contamination of solutions. Because of its high

affinity with water, THF solvent has its own Syringe Pump 1 as shown in Figure 20 to

prevent its exposure to moisture. Due to the limited availability of syringe pumps, the

dichloromethane solvent, PS-NH_2 and PS-COOH solutions, in their own syringes, were

pumped interchangeably using Syringe Pump 2. Individual syringes were rotated as

required for delivery.

The residence time of polymer solutions and solvent were calculated for the fluidics system. This was done to ensure that the polymer solutions and solvents had enough contact time in the flow cell for polymer deposition or removal of surface artifacts. The residence time of the polymer solution through the fluidic system and SPR set-up was calculated to be 56.3 seconds. The calculated residence time of the wash solvent (dichloromethane or THF) for two consecutive washes in the system was 112.5 seconds.

The variable angle SPR set-up was designed to optically probe the substrate fixed at the center of rotation with 0.001 angular resolution. The source optical system consists of a laser diode, a polarizer and compensation optics that focus light from the source onto the hemi-cylindrical SF 11 glass prism. The SF 11 substrate and the hemi-cylindrical prism with similar refractive index of 1.76 were held in contact using a liquid matching fluid in between. The SPR setup was operated with the source and collection arms of the SPR system counter-rotating at equal and opposite angles so that the reflected beam was captured for any angle of incidence, which could be scanned over a range of 10 to 60 degrees. Because a hemi-cylindrical prism is used, the laser light impinges on the prism surface at normal incidence for any angle of incidence. The light reflected out of the hemi-cylindrical prism was imaged onto a solar blind silicon detector, which produced an electrical signal proportional to the optical intensity. This electrical signal was digitized and recorded using the Labview program.

Labview software was used to control the SPR apparatus and to make measurements in either of two modes: "scan mode," in which the angle of incidence was

scanned over a selected the range, or "kinetics mode," in which the reflected intensity was recorded at a constant angle of incidence. The specific location of the plasmon angle of a material (solvent and/or deposited layer) was obtained through the scan mode of the SPR. The SPR THF baseline was gathered initially before running an *in situ* LBL experiment. This baseline was required for SPR curve comparisons to find the relative thickness of the deposited star polymers. A shift in the SPR curve indicated an adsorption interaction of the layer build-up of which was monitored by the kinetics mode of the SPR instrument.

During an *in situ* LBL self-assembly run, a standardized procedure of obtaining a THF baseline in scan mode, monitoring the adsorption interactions in the kinetics mode, and obtaining the SPR curve for the deposited layer was followed. Although the real-time adsorption was observed in the kinetics mode only, the corresponding adsorption event can be related to a resulting SPR curve measured in the scan mode. An example of the relationship between the scan and kinetics mode measurements is shown in Figure 21.

a.)   b.)
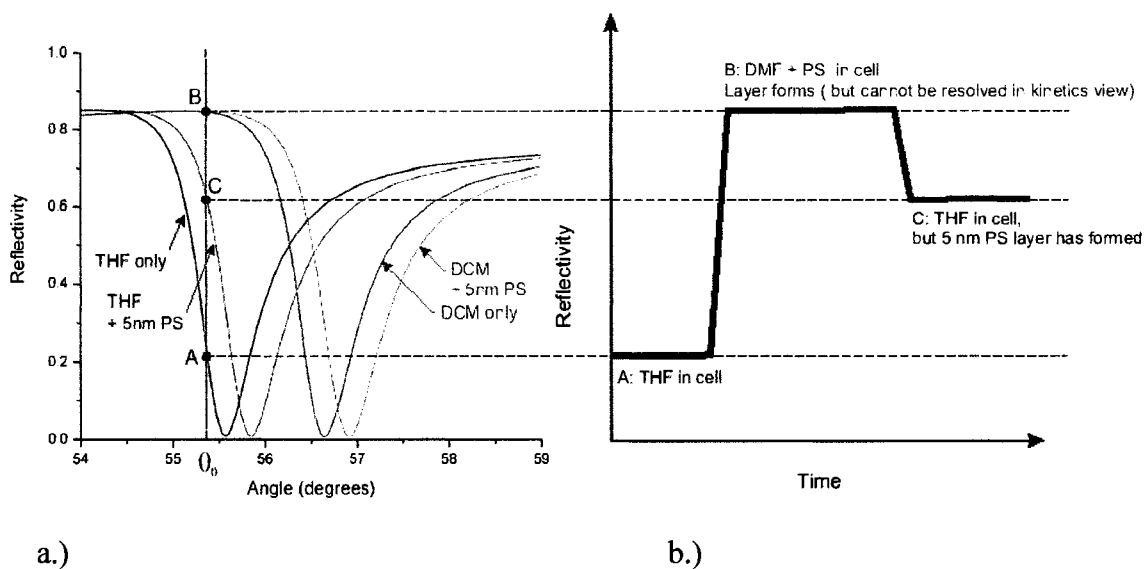
Figure 21. Relationship of SPR curves obtained in a) scan mode to b) the fixed angle measurement in the kinetics mode (DCM as dichloromethane, PS as polystyrene and THF as tetrahydrofuran) [44] (reprinted with permission from W. Risk).

In the SPR scan mode, an output curve of reflectivity versus angle was obtained for the THF baseline as shown as the blue SPR curve A in Figure 21a. To switch to kinetics mode, the angle of the optics and detector arms were fixed at an angle, equal to θ_0 as the point of inflection of the SPR curve as shown in Figure 21a, which was 0.05 degrees less than the THF SPR minimum reflectance angle. In the kinetics mode, the reflectivity versus time was plotted as shown in Figure 21b. Initially, a THF reflectivity baseline of 0.2 was obtained and as the dichloromethane filled the flow cell, an immediate increase in the reflectivity was observed to 0.8. According to theory, the dichloromethane SPR curve angle, shown in Figure 21a (curve B), is greater than the THF angle due to the larger refractive index of dichloromethane. Then as the polymer in dichloromethane solution was injected, an increase in reflectivity was observed but is not

52

shown in Figure 21b. This again had a corresponding SPR shift (red SPR curve labeled DCM + 5 nm PS) equivalent to the thickness of the layer deposited. For the wash cycle of the dichloromethane and the polymer injection, the change in intensity was too small to be observed at the rate of data collection. But as the THF was injected for the wash step, a decrease in reflectivity to 0.6 was obtained as shown in Figure 21b. Only this SPR curve after the THF wash was plotted during the adsorption interaction process. Since it should correspond to the stable new layer, the difference in the starting and final THF reflectivity levels and an angular shift greater than the starting THF SPR angle as shown in Figure 21 indicated that a layer had been deposited.

4.3.2 Quartz Crystal Microgravimetry (QCM)

Quartz Crystal Microgravimetry (QCM) is an analytical technique that measures the changes in crystal resonance frequency and resistance (or impedance) that occur in response to changes in the environment or amount of material applied to the crystal face [45]. As previously demonstrated by Reikert [45], QCM can be used for quantitative studies measuring mass changes in the electrostatic LBL self-assembly process. Here the QCM results provided the relative mass of the star polymer layers in a multilayer polymer system by the measured frequency change defined by the Saurbrey equation as shown in Equation 8 [46].

$$\Delta F = -\frac{2F_0^2}{\sqrt{\rho_Q \mu_Q}} m'$$

Where: ΔF is the change in resonant frequency

F_0 is the resonant frequency of the unloaded resonator

m' is the mass density of the film

ρ_Q is the density of the quartz crystal,

μ_Q is the shear modulus

The QCM measurements were conducted using a custom designed QCM microbalance shown in Figure 22. The QCM was operated at 5 MHz based on the Maxtex quartz crystal substrate used for the experiment.
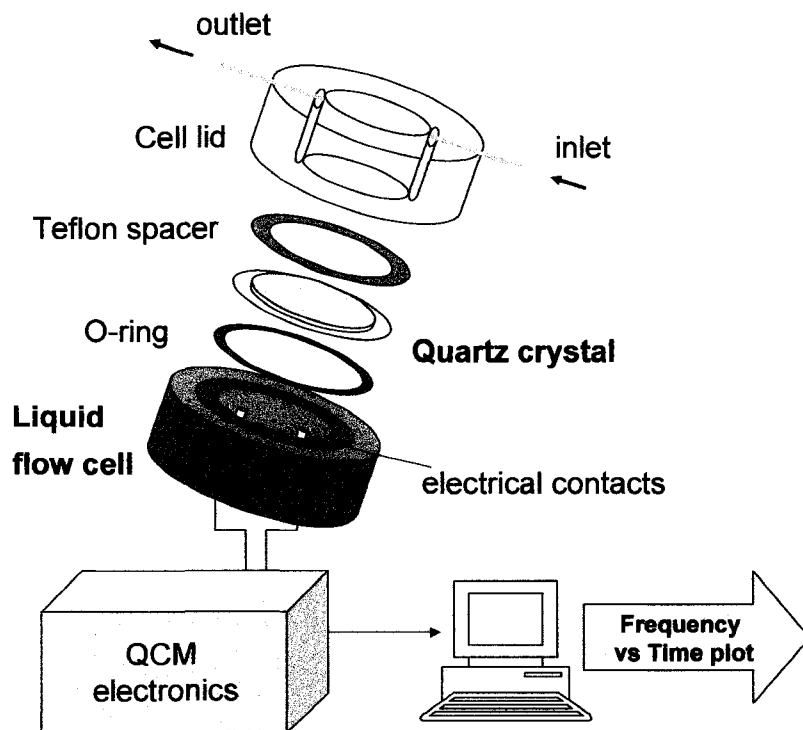
Figure 22. QCM schematic and set-up at IBM Almaden Research Center with the in-house flow cell design tilted at 45 degrees.

The exploded image of the flow cell and the schematic of the QCM balance are shown in

Figure 22. The set-up includes: a QCM oscillator circuit and frequency counter, a flow

cell connected to a fluidic system identical to that used in the SPR set-up and a computer.

The whole flow cell was oriented at 45 ^{0} tilt to push out air bubbles in the system. The

solution fills up the flow cell which contacts the surface of the quartz crystal that is held

by a vacuum chuck. The QCM oscillator is connected to the electrodes of the flow cell to

drive the oscillation of the quartz crystal. The quartz crystal is in contact with the

electrodes of the flow cell allowing detection of frequency changes due to deposition of

material on the surface. The signals from the QCM electronics box were received by a

computer to record the frequency response of the crystal over time.

4.3.3   Atomic Force Microscopy (AFM)

A Digital Instruments 3100 atomic force microscope (AFM) with lateral

resolution of 10 nm was used to acquire images. The AFM was operated under ambient

conditions, and intermittent contact mode at 1 Hz scan rate using silicon nitride

cantilevers with a spring constant of approximately 1 N/m. AFM images provided data

on the single layer coverage of the star polymer films on a substrate and also on the

multilayer star polymers. AFM was also used to determine the temporal stability of the

films over time by monitoring dipped sample surface quality at three times following

dipping: 20 hours, 8 days, and 15 days.

4.3.4 Grazing Attenuated Total Reflectance Infrared (GATR IR) Spectroscopy

A Grazing Attenuated Total Reflectance IR (GATR IR) spectroscope with a germanium crystal was used to study the IR spectra of the star polymers. PS-COOH polymer either in solution or as a film should show the carboxyl functional group in the IR spectra [47]. Upon interaction with PS-NH$_2$, PS-COOH would form a carboxylate anion and amine salt also identified by the IR spectra [47]. The IR data confirmed the reaction of PS-NH$_2$ and PS-COOH polymers mixed in solution through the spectra.

A star polymer thin film sample on the GATR IR accessory was prepared by the dipping method used for this study. The two samples were analyzed using the GATR IR: a star polymer thin film of PS-COOH and a thin film of mixed PS-COOH and PS-NH$_2$. A spectrum for each sample was obtained by placing the substrate in contact with the clean ATR crystal of the tool. The spectra were collected over 32 scans using MCT/A detector.

4.4   Data Analysis

The analytical tools in this study were: SPR, QCM, AFM, and IR spectroscopy.

As the data from these analytical tools were processed, the objectives were met. Table 4

summarizes the data that was collected to attain the objectives of the study.

Table 4. Summary of the analytical data obtained during the study and objectives
achieved through the analysis.

Experiment #	Method of analysis	Data	Attained Objectives
1, 2 and 3	SPR	• Plots of angle of reflectance versus intensity • Plots of time versus intensity	• Fitted SPR shifts from the THF baseline of each layer gave *relative thickness* • Undetected film formation of two consecutive deposition of star polymers indicating only a *specific electrostatic interactions* forms a monolayer
1	QCM	• Time versus frequency	• The change in frequency with absorbed mass for each deposited layer confirmed the *uniformity of layers*
5 and 6	AFM	• Images of surface morphology	• The type of coverage and *stability in terms of de-wetting* were obtained by images of *surface morphology* of star polymers layers
4	IR spectra	• Spectra of PS-COOH before and after interacting with PS-NH$_2$ layer	• Spectra determined the presence of carboxylate anion in the IR spectra verifying the *interaction of PS-COOH with PS-NH$_2$*

4.4.1 Mathematical Fitting for the SPR Angular Shifts

In order to determine the angular shifts of the SPR curves *in situ* LBL self-assembly, the exact location of the plasmon angle minimum was determined. The SPR curves were fitted to a theoretical curve derived from a mathematical model, the KNS function [19]. Although other fitting techniques were available, the shape of the SPR curves with one side of the minimum being steeper is not fit well by a parabola or other polynomial function, the KNS function was used to fit the SPR curves. The KNS function is an analytical model derived to fit SPR curves as shown in Equation 9 [19] and Equation 10 [19].

$$R\ (\theta) = A\ \{1 - [B + C\ (\theta - D)]/[(\theta - D)^2] + E^2\}$$ Equation 9

$$\theta_0 = D + \{-B + \sqrt{(B^2 + C^2 E^2)}\}/C$$ Equation 10

Where: A, B, C, D and E are real value parameters
θ_0 is the angle of minimum reflectance

This function was incorporated in a Matlab program written by Dr. William Risk of IBM Almaden Research Center specifically for the purpose of SPR data fitting. The real value parameters in this function were determined by the iterations in Matlab Program thereby obtaining the θ_0 as the angle of the SPR curve minimum.

In the KNSFit Matlab program, the raw data of the SPR curve were imported to the Matlab Program. Once imported, a new curve was plotted. With the plot, the range of data of the SPR curve under consideration was chosen by clicking the extreme left and

right ends of the SPR curve. These served as the limits for the set of coefficients that had

the least square error between the KNS function and the raw data [48]. Once the

calculation was done, a new plot of the original data with the best fit KNS function curve

was obtained as shown in Figure 23. By obtaining the location of the reflectance

minimum of the SPR curves, the angular shifts per layer were than calculated.
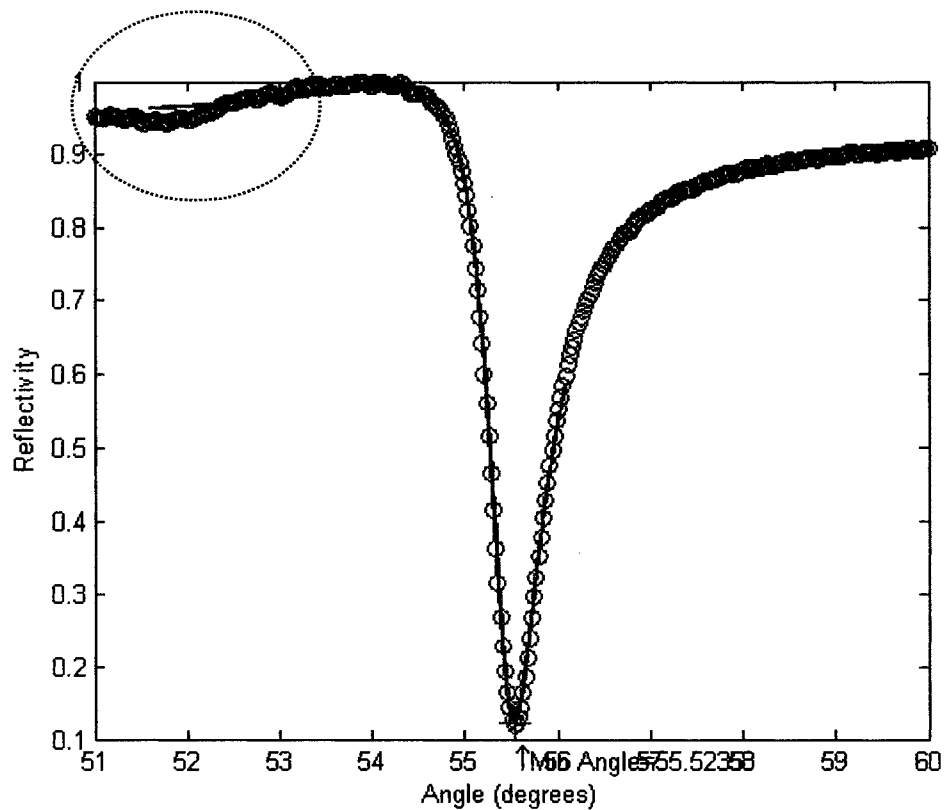
Figure 23. Replotted SPR curve fitted using the KNS function with the original data in black circles and best fit KNS curve as solid red line. SPR curve minimum angle location calculated at 55.524 degrees. The encircled part of the SPR curve reflected the total internal reflection (TIR) curve.

The slope at the left end of the SPR curve, marked in Figure 23, shows the total

internal reflection (TIR) curve. A well-defined TIR in the SPR curve was found to be

indicative of a good transition of light allowing total internal reflection. It was found that a shift in angular position of the TIR curve was indicative of a poor interface between the prism and the substrate surface possibly due to a dewetted index matching fluid or vibrations in the SPR set-up. In this case, either the substrate's surface was replaced with a new drop of index matching fluid or the TIR curve was adjusted with that of an initial SPR curve obtained.

CHAPTER FIVE
RESULTS AND DISCUSSION

The formation of multilayer thin films by electrostatic LBL self-assembly of PS-

NH_2 and PS-COOH star polymers was investigated using the different analytical tools

described: Atomic Force Microscope (AFM), Infrared Spectroscopy (IR), Surface

Plasmon Resonance (SPR), and Quartz Crystal Microbalance (QCM). In this chapter, the

results of the study regarding the thin film formation of the star polymer films on the

silicon dioxide surface and polymer films on polymer films as illustrated in Figure 24

will be discussed.
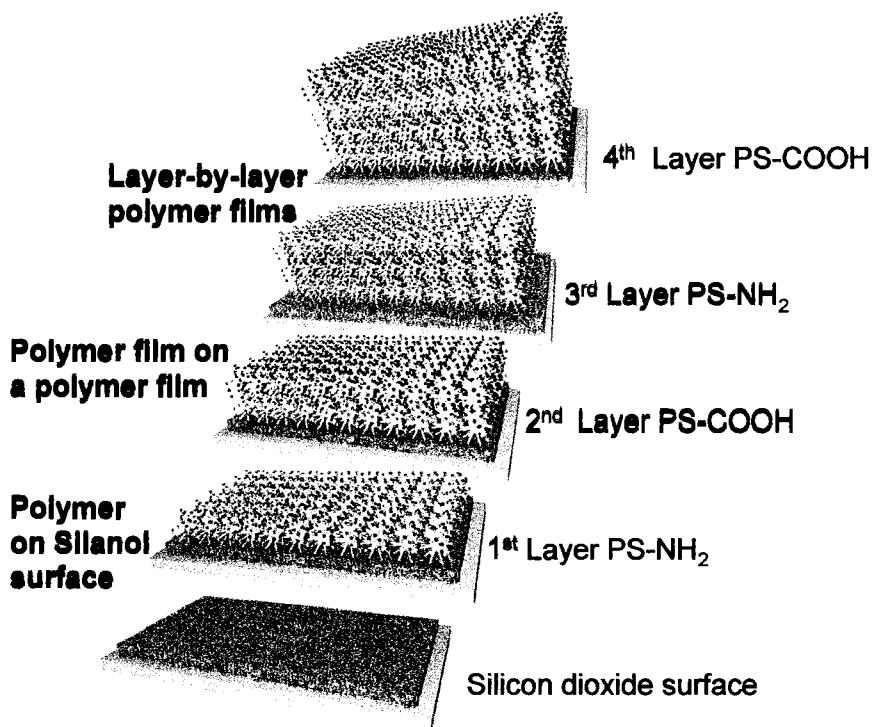
Figure 24. Functionalized star polymers (PS-NH_2 and PS-COOH) self-assembled on a silicon dioxide surface initially and ultimately on other polymer layers are shown schematically.

The self-assembly of polymer multilayers by acid-base interactions is not trivial. During the course of this study, issues such as having strong foundation layer for the multilayer polymeric structure and optimum conditions for deposition were addressed. Other issues such as the cleanliness of the initial silicon dioxide surface of the substrate, choice of solvent, and wash conditions were explored.

The optimum conditions for the multilayer self-assembly of star polymers by electrostatic interaction on a silanol surface were determined by several analytical techniques (*e.g.,* AFM, IR, SPR, and QCM). The characteristics of the star polymer films alone and the multilayer polymeric structures were studied. For example, the film coverage, surface roughness, and film stability over time were determined by AFM analysis. The information from the characterization of the star polymer films alone was valuable for studying the multilayer polymeric structures. The electrostatic self-assembly of PS-NH$_2$ and PS-COOH star polymers were also investigated by IR and SPR. The SPR data provided information on the uniformity and relative layer thicknesses of the star polymer films within the multilayer structure. This was further verified by the QCM experiment that provided complimentary results to the SPR.

5.1   Self-assembly of the First Layer of PS-NH$_2$ on Clean Silicon Dioxide

It is imperative to have a strong initial (foundation) layer for the multilayer polymeric structure. The investigation of self-assembly of the star polymers began by looking at the PS-NH$_2$ layer on the silicon dioxide surface as the foundation layer of the multilayer polymer structure. The success of the self-assembly of the PS-NH$_2$ star polymers on the silicon dioxide substrate is important as it determines the stability of the resulting multilayer structure and the realization of LBL self-assembly. It was therefore desired to have a smooth PS-NH$_2$ monolayer film that fully covers a clean silicon dioxide surface.

5.1.1   Preparation of the Surface of the Silicon Dioxide Substrate

Proper cleaning of the substrate surface is of utmost importance to the self-assembly of the star polymers. For the purpose of this study, the cleaning procedure for both the silicon wafers and SF 11 substrates utilized 20 minutes UV ozone treatment, Millipore water flush and filtered nitrogen gas drying. It was found by GATR IR studies that 20 minutes UV ozone treatment increased the concentration of SiOH on the surface and at the same time eliminated the unwanted organic contaminants. Although the most common cleaning step for oxide surfaces is wet processing using Piranha solution [24,25,38,40], UV ozone was effective and produced a strong surface interaction with the PS-NH$_2$ layer. This was verified by the homogeneity and film stability of the first layer of PS-NH$_2$ determined by AFM analysis. In addition, the integrity of the metal

(chromium-gold) stack deposited on the SF 11 substrates was preserved using the dry clean conditions which was questionable for the Piranha etching conditions.

5.1.2 AFM Analysis as Criterion for Solvent Choice

The choice of solvent for the LBL assembly process was based on the quality of deposited films as observed by AFM analysis. Different solvents (toluene, tetrahydrofuran (THF), chloroform ($CHCl_3$) and dichloromethane (CH_2Cl_2)) were tested as solvents for the self-assembly of the star polymers. The solvents were chosen based high solubility of star polymers . For the purpose of determining an appropriate solvent for the self-assembly of star polymers, the films were prepared by the dipping technique. The deposited PS-NH$_2$ film on the substrate surface was characterized by AFM. The films were characterized in terms of coverage, stability, and smoothness of film surface. Stable films were characterized and defined as continuous coatings with no detectible dewetting. Dewetted films exhibited holes that formed during evaporation of the solvent from the metastable polymer-solvent system. Typical dewetting features had round edges or lips as shown Figure 25a and d. Examples of satisfactory full coverage films together with unsatisfactory dewetted films are shown in the AFM images in Figure 25.

a.) Chloroform

b.) Toluene

c.) THF

d.) Dichloromethane
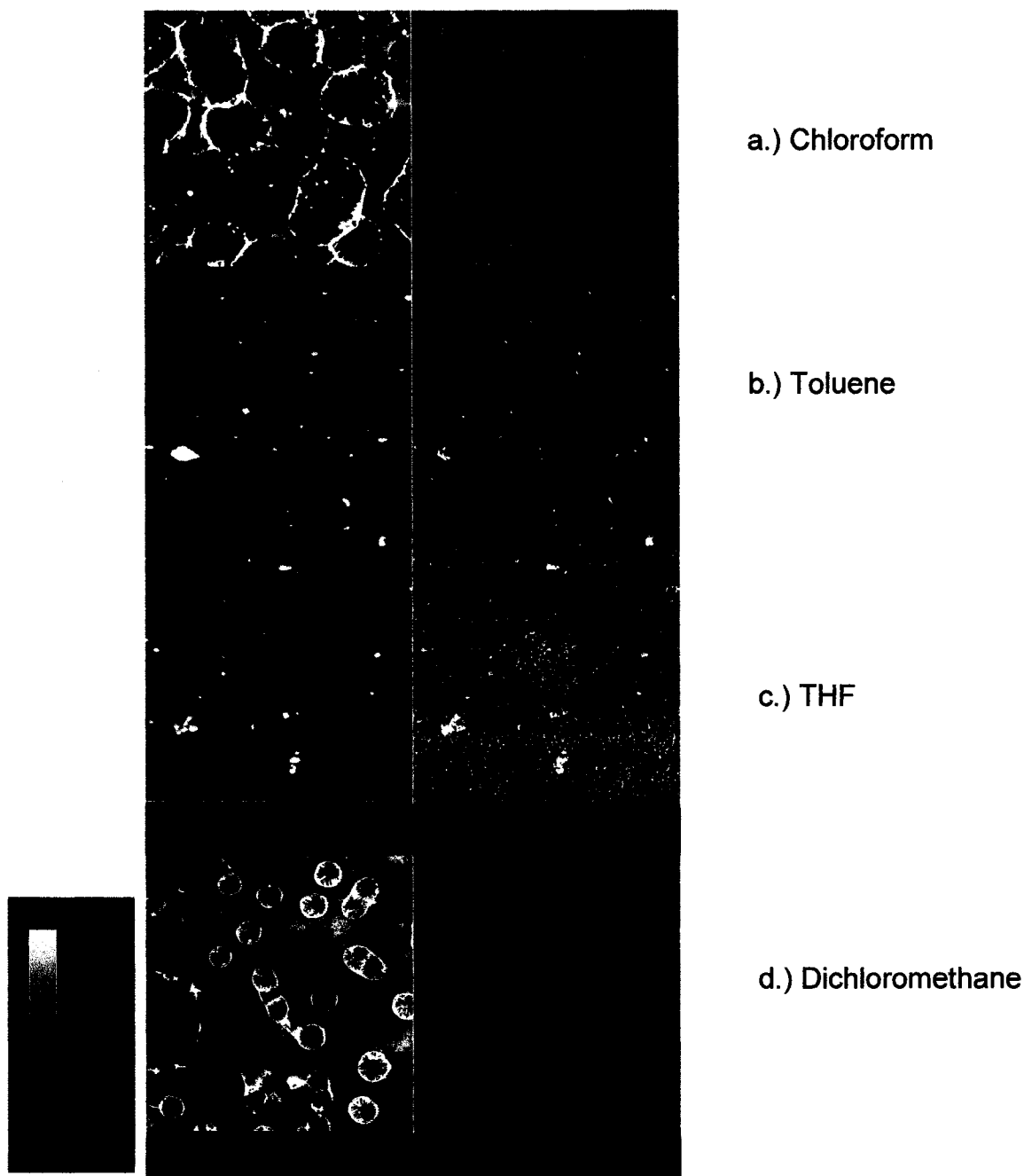
Figure 25. AFM images (5 μm x 5 μm) of single layer PS-NH$_2$ film on silicon wafer substrates. Films deposited from b) toluene and c) THF show continuous coverage with occasional defects of superficial artifacts; films from a) chloroform show dewetting. Bottom images (10 μm x 10 μm): Film deposited from d) dichloromethane, wider view showing the extent of dewetting. Left images: topography at z = 10 nm; Right images: phase images.

Comparison of AFM images of films of the PS-NH$_2$ star polymer on the clean surface of a silicon wafer deposited from a range of solvents indicated that the most stable films were produced from toluene or THF while the PS-NH$_2$ film dewetted when cast from CH$_2$Cl$_2$ or CHCl$_3$. With chloroform and dichloromethane, dewetting occurred shortly after dipping, and was observed in films studied within 4 hours after deposition. Films derived from THF and toluene were analyzed at least 20 hours after deposition due to slower drying rates; *e.g.*, attempts to image films from THF and toluene after 4 hours by AFM yielded blurry images indicating a wet surface. After 20 hours, these films showed no signs of dewetting.

Some superficial artifacts were observed on the surface of the films prepared from THF, toluene and chloroform, which result from the dipping process used to deposit the films. These artifacts contributed to the overall roughness of the films. The roughness of a surface can be quantified by RMS (root mean square) roughness analysis from the AFM software. The RMS numbers are only mathematical values based on the z-values from all of the x,y-data points of the image and so visual inspection is still necessary. Because of the poor quality of the dewetted films, only films deposited from THF and toluene are presented in Table 5 roughness data.

Table 5. Summary of RMS values from the AFM data of the 5 μm x 5 μm area, film surfaces from THF and toluene in Figure 25 compared to the silanol surface. Values were produced by AFM (Digital Instrument) roughness analysis software.

	RMS Roughness in nm
Surface (Si wafer)	0.6 nm + 0.1 nm
PS-NH$_2$ on substrate surface in THF	0.7 nm + 0.1 nm
PS-NH$_2$ on substrate surface in toluene	0.7 nm + 0.1 nm

Although the RMS values of deposited PS-NH$_2$ films using THF and toluene were

the same from Table 5, visual inspection suggests that the surface of THF film is rougher

than the toluene film as shown in Figure 25. The toluene film appeared to be smoother

compared to the more grainy surface from the THF deposited film. In this case, the

visual inspections of the film surface were taken as the absolute determinant of the

surface roughness of the films. In Table 6, the characteristics of the films produced from

the range of solvents determined from AFM analysis are summarized.

Table 6. Summary of AFM characterization on PS-NH$_2$ film deposited on silicon dioxide substrate using different solvents (THF, toluene, dichloromethane, and chloroform).

	Stability	Roughness by visual observation	Presence of surface artifacts
THF	Continuous film	Rough	Present
Toluene	Continuous film	Smooth	Present
Chloroform	Dewetted	NA*	Present
Dichloromethane	Dewetted	NA*	None

*NA- The roughness was not determined due to the highly pitted surface

By considering the AFM results and further experimentation using different

solvents and solvent combinations, a protocol was established for producing continuous

thin films and is summarized as follows. Surface artifacts were minimized with

dichloromethane as a dipping solvent. However, a second wash solvent was needed to

stabilize the films against dewetting. Based on tests of several solvent combinations, THF seemed to stabilize the films and prevent dewetting. Hence, LBL self-assembly of star polymers from dichloromethane followed by dry THF solvent wash was the optimum solvent combination used throughout this study.

5.1.3   Deposition Conditions

The initial AFM images from the dipping experiment showed some particles on the surface, seen as white artifacts on the AFM images as in Figure 26a. These particles are believed to be from the polymer solution or dust from the air. The presence of particles on the dipped samples required an appropriate washing technique to obtain cleaner film surfaces for both dipping and SPR *in situ* experiments. A flow set-up was designed with the aim of preventing and/or removing formation of the surface artifacts from the deposited films. Figure 26 shows the comparison of two films deposited by the dipping and flow techniques.
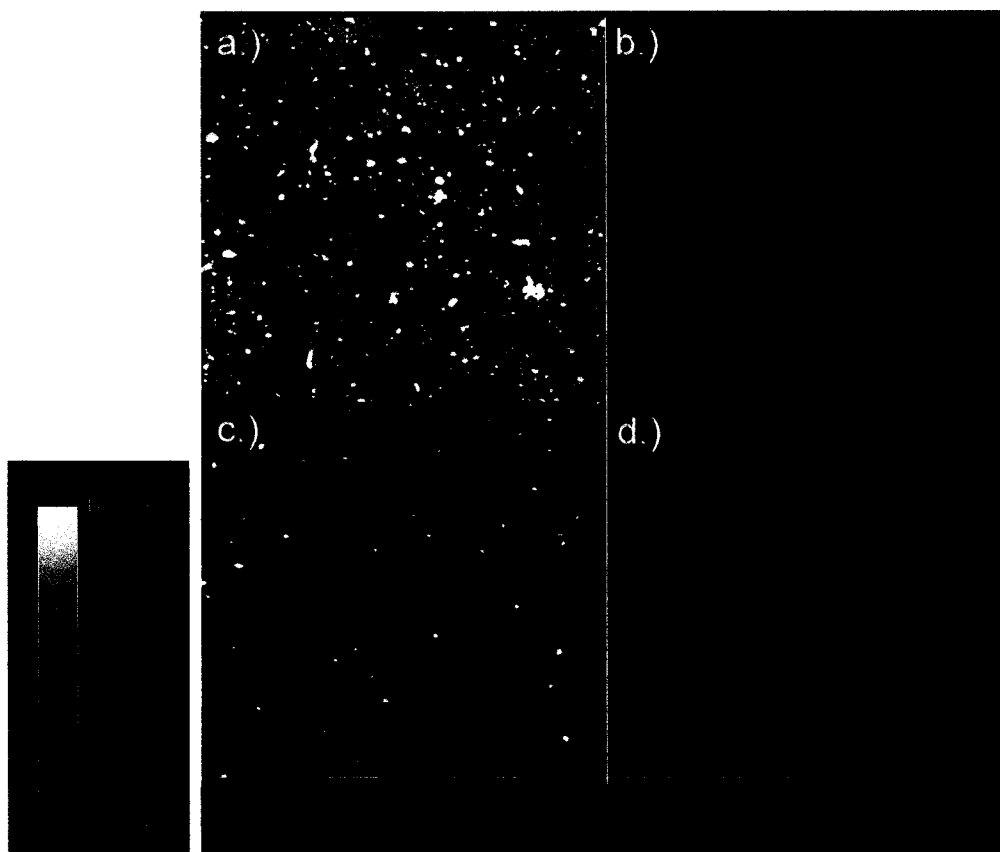
Figure 26. AFM, topography (a and c, z-range = 10 nm) and phase (b and d, arbitrary units) 5 μm x 5 μm images comparing surfaces from two techniques for depositing a single PS-NH$_2$ layer onto the silicon dioxide surface of a silicon substrate. Images a) and b): dipping into CH$_2$Cl$_2$/THF mixture (9 mL/3 mL); images c) and d): flow technique, CH$_2$Cl$_2$/THF mixture (9 mL/1 mL) at 2 mL/min.

To compare the two methods of deposition, the first layer of PS-NH$_2$ on the clean substrate surface was deposited by either dipping or flow techniques. The top images (Figure 26a and b) are from a film produced by the dipping method. The dipping method used 3 separate dichloromethane dipping wash solvents followed by a final washing with THF. Contaminants such as dust particles can be easily introduced with the transfer of the substrate from one solvent to another using this method. On the other hand, in the flow technique, the substrate was in position with the solvents contained and pumped

69

through the solvent lines to the flow cell. The flow set-up consists of a flow cell that has inlet and outlet ports for the solutions and a plate that holds a wafer under vacuum. The flow experiment eliminated the formation of the surface artifacts, shown in Figure 26c and d, in contrast to the dipping method.

The flow system produced cleaner films, illustrated by the two films shown in Figure 27 that were deposited under different flow conditions. Exposing the surface to a large volume of solvent (*e.g.,* 18 mL CHCl$_2$ and 18 mL THF) produced a clean film surface as shown in Figure 27c, d. The surface in this case was washed 6 times each with 3 mL CH$_2$Cl$_2$ and 3 mL THF washes at 1 mL/min. However, it was observed that a rougher film (Figure 27c, d) was produced using a large amount of solvent and longer deposition time of 1 mL/min of each solvent. Further experimentation showed that an exposure to 9 mL of CH$_2$Cl$_2$ followed by 1 mL of THF at the rate of 2 mL/min washed off the non-adsorbed artifacts on the surface producing the smoother film surfaces shown in Figure 27a, b. The 9:1 proportion of dichloromethane and THF was found to produce films which were stable over time.
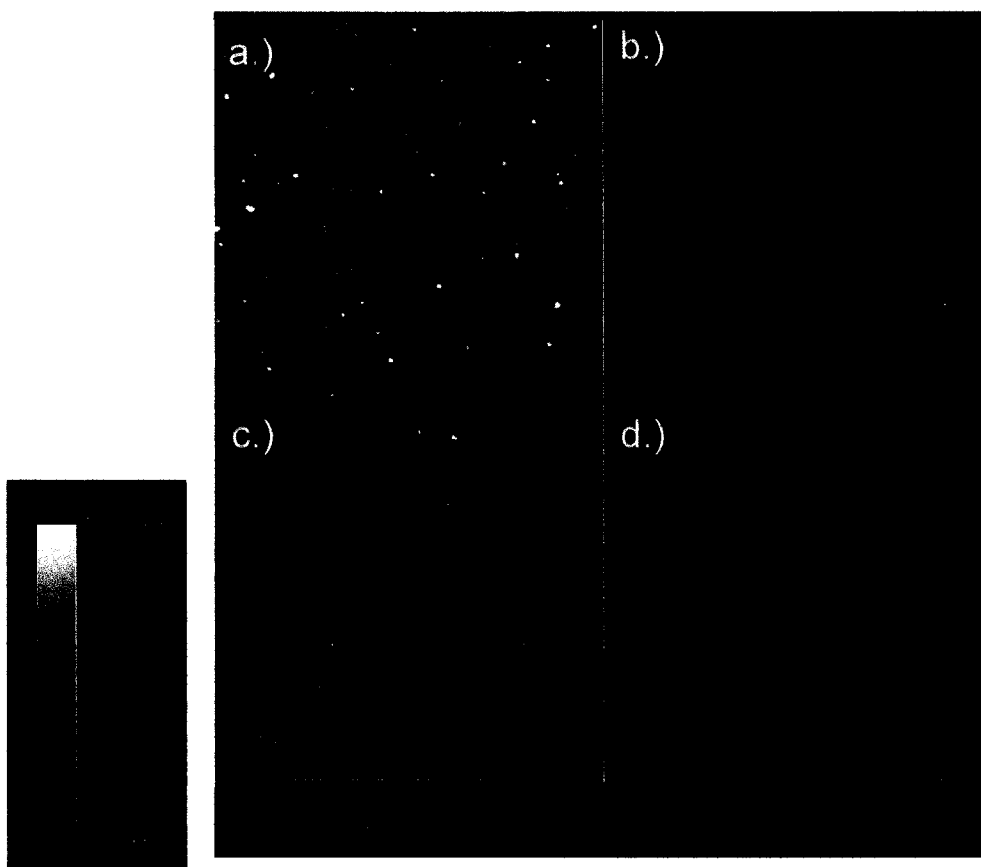
Figure 27. Comparison of the AFM images, topography (a and c, z-range = 10 nm) and phase (b and d, arbitrary units) of the PS-NH₂ film deposited by flow technique using different volumes and rates. Images a) and b): CH₂Cl₂/THF mixture (9 mL/1 mL) at 2 mL/min; images c) and d): CH₂Cl₂/THF mixture (18 mL/18 mL) at 1 mL/min.

5.1.4   Nature of Star Polymer Interactions

Previous studies showed that PS-NH₂ on silicon dioxide surface results in a strong

interaction where in the amine and residual silanol complex remained stable [49].

Among the available types of functionalized star polymers, the morphology of PS-NH₂

was studied by AFM and compared to PS-COOH and other functionalized star polymers

interaction on the surface. Table 7 summarizes the typical strength of these interactions

for each type of star polymers.

Table 7. Summary of the typical estimated strengths of bonding interactions of the different type of star polymers on silanol surface.

Star polymers	Type of Interaction	Strength, units
PS-NH$_2$ on silanol surface	Electrostatic	100-350 KJ per mol
PS-COOH on silanol surface	Hydrogen bonding	4-120 KJ per mol
Unfunctionalized PS on silanol surface	Van der Waals	5-50 KJ per mol

The AFM images in Figure 28 show the topography of the different type of star polymers on the silicon dioxide surface. It can be observed that the PS-COOH surface in Figure 28c and d is coated with droplet like features, possibly indicating an uncoated, dewetted surface. The functionalized/unreactive PS-treated surface in Figure 28e and f is relatively featureless, possibly even showing predominantly uncoated substrate surface. On the other hand, PS-NH$_2$ formed a contiguous film on the surface as shown in Figure 28a and b.
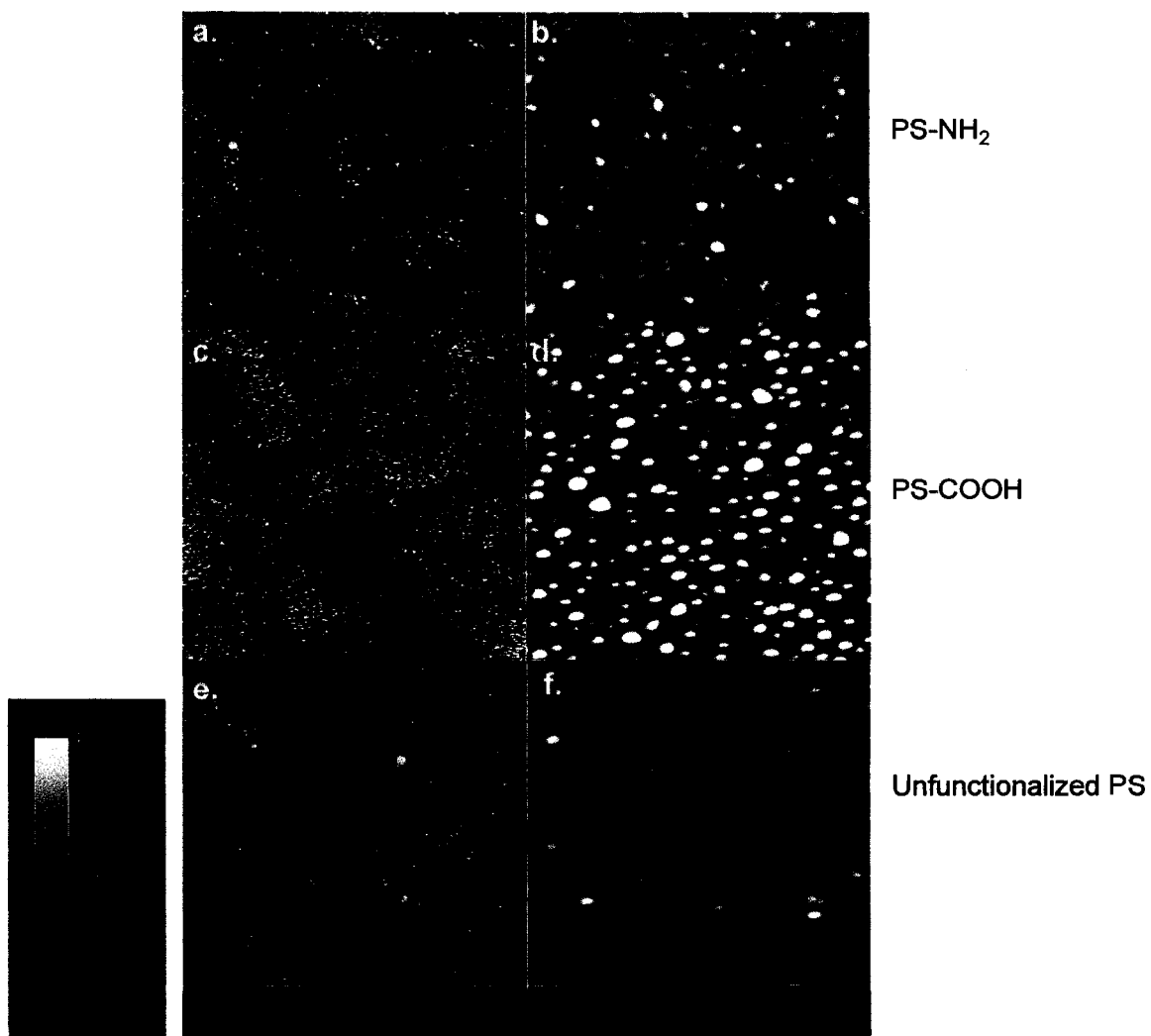
Figure 28. AFM topography images of a) and b) PS-NH₂; c) and d) PS-COOH; and e) and f) functionalized/unreactive PS stars on the silicon dioxide surface of a silicon wafer. Samples were prepared by dipping. Left and right images: 5 μm x 5μm (a,c and e) and 1 μm x 1 μm (b,d and f), respectively.

The details how the polymers are adsorbed on the surface regarding spreading or flattening are related to the type of polymer-surface interaction. An amine interacting with the acidic silanol surface forms a strong electrostatic interaction while carboxylic acid and silanol groups form a weaker hydrogen bonded and Van der Waals interaction. Because of the strong bond formed by electrostatic interaction of the amine and the

silanol groups on the substrate, the particles spread out covering most of the silanol surface as seen in Figure 28 a and b. Weaker interactions would result in islands instead of flat compact films. It can be observed from the 5 μm images of Figure 28a that PS-NH$_2$ fully covers the silicon dioxide surface compared to PS-COOH and unfunctionalized PS which do not. It is evident that the PS-COOH films in Figure 28c and d form a non-uniform coating. For this reason PS-NH$_2$ is chosen as first layer of the LBL star polymer multilayer structure. The importance of a stable first layer of PS-NH$_2$ in the realization of the LBL self-assembly was demonstrated in the SPR experiments which will be discussed later.

5.1.5 Film Thickness

The analysis of the AFM micrograph was used to estimate the thickness of the film after drying for 20 hours. With the layer thickness information, the state of compression of the first layer on the surface in its dry state was estimated. Film artifacts such as holes can also be used as shown in Figure 29b for thickness measurements by getting a peak-to-valley height difference. The hole shown in Figure 29b with a flat surface at the bottom was found to extend to the silicon substrate. The thickness measurements showed occasional depressions on the film as shown in Figure 29a. The two red markers on the cross-sectional line correspond to the two red markers in the topography image below. From the placement of these markers, peak-to-valley heights were found to be 3.4 nm and 6.3 nm + 0.1 nm for Figure 29a and b, respectively. The

images shown in Figure 29a and b were correlated to estimate the range for the film

thickness of the PS-NH₂ film on the silicon dioxide surface. Figure 29a provided the

surface background which can be subtracted from Figure 29b to give an estimated value

of film thickness of 2.9 + 0.1 nm.
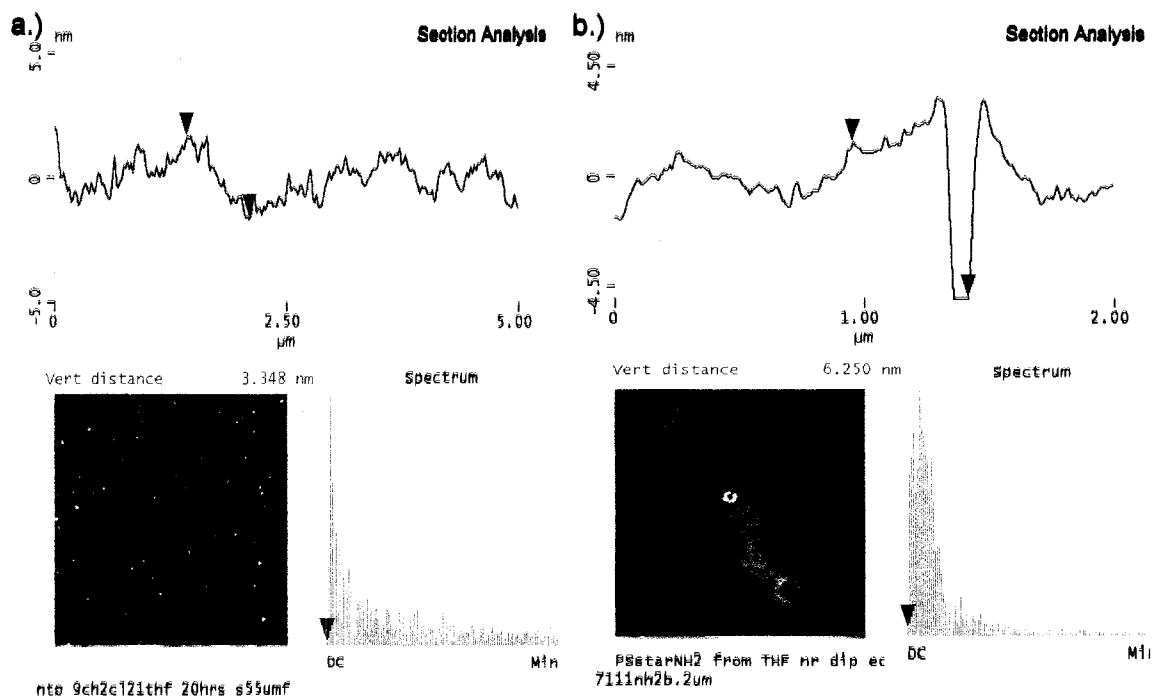
Figure 29. Cross sectional analysis of a) (5 μm x 5 μm) and b) (2 μm x 2 μm) AFM images of a PS-NH₂ film on a silicon dioxide surface. In image b), a hole, which was a film defect, was found during AFM imaging and used for thickness analysis. Notice that the right image shows a flat point on the film which appears to be the silicon substrate.

The value from the AFM section analysis was compared to the actual

hydrodynamic radius of the star polymers in solution. The average hydrodynamic radius

of the PS-NH₂ was found to be 4.5 nm (9.0 nm in diameter) [50]. The decrease from 9.0

nm to 2.9 nm indicated that the PS-NH₂ polymer was highly compressed normal to the

surface when dry as shown in Figure 30. The compression of star polymers was

anticipated since dendrimer counterparts collapse on a silica surface as well [36]. The

strong compression of the polymer on the silanol surface in Figure 30 can be explained

by the strong interactions of the amine functional groups with the acidic SiOH groups of

the silanol surface. As the PS-NH$_2$ was deposited on the surface, the components flatten

and spread out creating a homogenous and contiguous film.
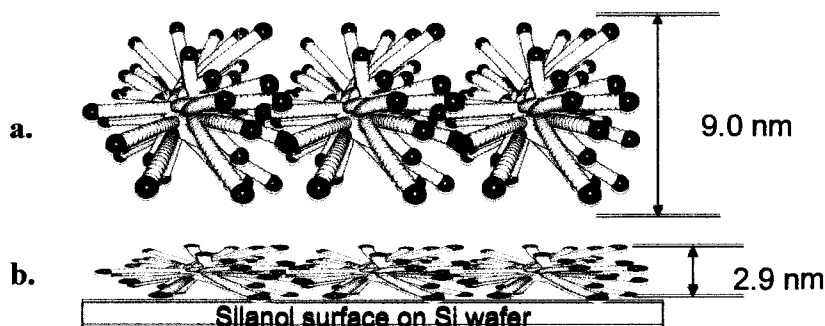
Figure 30. Comparison of the hydrodynamic diameter a) and dry state diameter b) of PS-NH$_2$ as it interacts with the silanol surface on the silicon substrate.

5.1.6   Summary for the Self-assembly of the First Layer of PS-NH2

The self-assembly of the first layer of PS-NH$_2$ star polymer on the oxide surface

of a silicon substrate was investigated. Intensive experimentation was conducted to

identify the optimum choice of solvent and deposition conditions.

Even with a clean surface prepared by UV ozone treatment, some surface

artifacts from the dipped samples were initially observed under the AFM examination.

Although the dipping experiments sufficed to produce films for AFM analysis, a flow

experiment was designed to obtain clean, self-assembled star polymer surfaces. The

force from the flowing solvent presumably removes the weakly absorbed materials on the

surface of the film. Optimal wash conditions of 9 mL dichloromethane/1 mL THF at 2 mL/min resulted in clean and smooth thin film surfaces.

With a clean surface, PS-NH$_2$ in dichloromethane with THF as the last wash solvent was found to produce stable and contiguous thin films. The investigation for the first layer of the multilayer polymeric structure confirmed that the PS-NH$_2$ star polymer was the appropriate foundation layer for the electrostatic LBL star polymer self-assembly. By AFM analysis, the PS-NH$_2$ was found to be the best foundation layer for the multilayer polymeric structure with the self-assembled films yielding the best film coverage and the most stable films. The PS-NH$_2$ on the silanol surface had the best coverage when compared to either PS-COOH or the unfunctionalized PS star polymers. Also, the PS-NH$_2$ on the surface in the dry state was a highly compressed polymer along the normal surface of the silanol.

5.2 Electrostatic Self-assembly of PS-COOH on PS-NH$_2$

With a strong foundation layer of PS-NH$_2$ on the silicon dioxide surface, optimum conditions that result in a strong PS-NH$_2$ to PS-COOH star polymer interaction were developed. Understanding the behavior of PS-COOH on PS-NH$_2$ and vice versa was necessary to build multilayer polymeric star polymer structures. The electrostatic interaction/reaction between PS-NH$_2$ and PS-COOH was demonstrated by IR spectroscopy. In addition, AFM analysis provided valuable information on film characteristics including coverage, roughness, and stability for the representative layers of the multilayer structure.

The first two layers will be discussed in detail since the PS-NH$_2$/PS-COOH interactions are critical to the formation of subsequent layers of the multilayer polymeric structure. To better understand and analyze the PS-NH$_2$/PS-COOH interactions/reactions, a representative sample of each layer (Layer 1-4) of the multilayer structure of the star polymers were prepared. The film characteristics and stability of the representative layers (Layer 1-4) of PS-NH$_2$ and PS-COOH in the multilayer polymeric structure were investigated by AFM. The coverage and surface roughness of the films were examined for comparison.

5.2.1 Confirmation of PS-NH$_2$ and PS-COOH Interaction/Reaction by GATR IR

Infrared spectroscopy is a technique used to identify molecules which absorb IR and is widely utilized [47]. GATR IR is a sensitive attenuated total reflection (ATR) technique especially used for very thin films. This technique was useful for the

identifying the nature of the PS-NH$_2$ and PS-COOH star polymers interactions. The particular signatures relevant to the confirmation of the PS-NH$_2$ and PS-COOH electrostatic interaction were the carbonyl stretch from the PS-COOH and the formation of ammonium carboxylates by the reaction of PS-NH$_2$ and PS-COOH.

The original goal was to use GATR IR analysis to verify the interaction of PS-COOH and PS-NH$_2$ in assembled star polymer thin films. This technique had inadequate sensitivity for self-assembled star polymer films since the films were so thin and the relevant signals were very weak. To find the relevant IR signals from the PS-NH$_2$ and PS-COOH interaction, concentrated solutions of the PS-NH$_2$ and PS-COOH were first mixed and then spun into film. The disappearance of the carboxylate signal and the appearance of a carboxylate anion signal was confirmed on these films.

The spectra for PS-COOH identified the presence of the carboxylic acid group frequency with an absorption at 1736 cm^{-1} as shown in Figure 31A. This absorption is absent in the combined PS-COOH and PS-NH$_2$ films for which a new absorbance was observed at 1652 cm^{-1} as shown in Figure 31B. These analyses were done on two separate film samples prepared by spin coating. This band confirmed the carboxylate anion formation, an electrostatic type interaction, resulting from the reaction of the amine with the carboxylic acid functionalities. The interaction of the amine and carboxylic acid in the IR is confirmatory of the anion formation expected in the 1650-1550 cm^{-1} range [47]. Because majority of the polymer was comprised of polystyrene with functionality only at the chain ends, the other major peaks identified in Figure 31 A and B were markers for polystyrene.
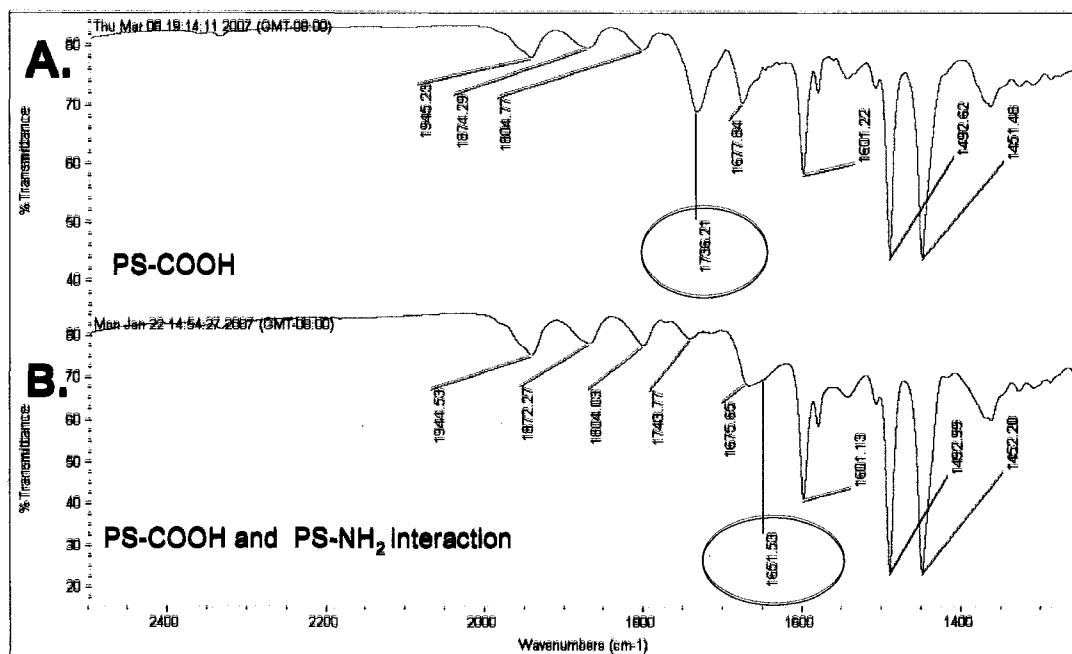
Figure 31. IR spectra of PS-COOH solution (A) and spun film of PS-NH₂ and PS-COOH (B) concentrated solutions.

To confirm that the PS-NH₂ and PS-COOH reaction occurs, an initial spectra of PS-COOH was recorded. The NH_2 group of the PS-NH₂ star polymer was difficult to characterize by IR due to the stronger signal from the C-H stretching that obscures the 3000 cm^{-1} peak N-H stretching of the amine. The initial PS-COOH spectrum was then compared to the mixed PS-NH₂ and PS-COOH star polymer film (samples mixed and cast).

5.2.2 Film Stability Study by AFM

The flow and dipping experiments indicated stable films are produced using both dichloromethane and THF solvent systems. To further qualify and quantify films

stability, representative dipped samples of alternating layers of PS-NH$_2$ and PS-COOH (Layers 1,2, 3, and 4) were characterized using AFM after periods of 20 hours, 8 days, and 15 days. The objective was to study the coverage and stability of each layer as a model for behavior in the multilayer polymeric structure.

The results for characterization of the first PS-NH$_2$ layer formed in a flow set-up for the multilayer polymer assembly were discussed earlier in this section. This same flow technique was used to examine PS-COOH deposited on PS-NH$_2$ as second layer of the multilayer structure. By AFM characterization, the strong interaction of the PS-COOH on the PS-NH$_2$ can be visually qualified in terms of coverage. As shown in the phase image in Figure 32d, the PS-COOH layer fully covered the initial PS-NH$_2$ surface unlike the results obtained for the PS-COOH on oxide. Although some non-absorbed particles were observed in the height image in Figure 32c, the PS-COOH completely interacted with the previously deposited PS-NH$_2$ layer and formed a contiguous film. The height image on the left did not show any indication of dewetting over 20 hours after deposition.
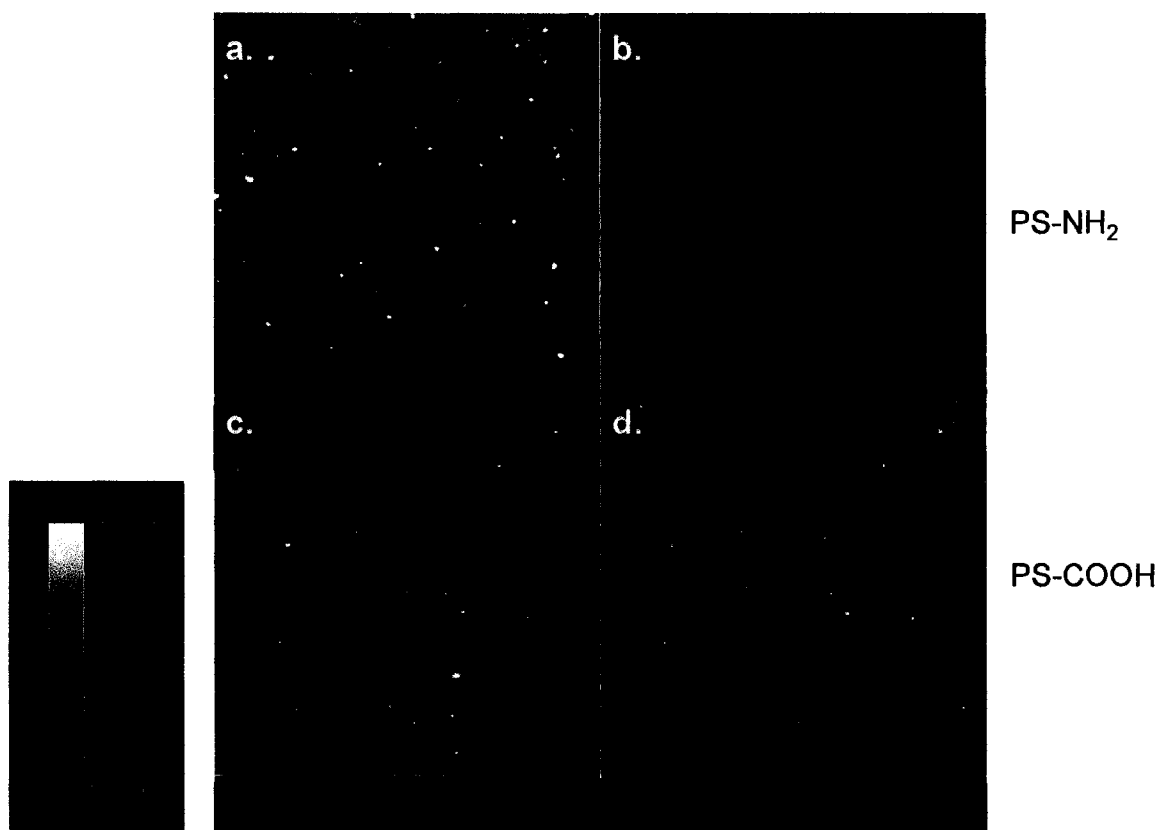
Figure 32. AFM image of the second layer, PS-COOH on PS-NH₂ (c and d), compared to the first layer of PS- NH₂ (a and b) after 20 hours following flow deposition. 5 μm x 5 μm images a and c: topography images with z = 10 nm; c and d: phase images.

On comparison with the foundation layer of PS-NH₂ (Figure 32 a and b) the second layer of PS-COOH (Figure 32 c and d), showed no major differences between the film surfaces as observed. Thin films of star polymers were expected to be rough since only the functional groups at the chain ends of the star polymers interact with the surface. The non-interacting parts of the star polymer are exposed creating the uneven surface with its macromolecular structure. The surface roughness of the star polymer films was analyzed and the roughness of silicon substrate and initial PS-NH₂ layer were compared with the surface produced by the addition of the second layer. The roughness of the films

was assessed by both visual observation and measured RMS values from the AFM

software. Because RMS values are mathematical calculations based on the z-values from

all of the x,y-data points of the image, concurrent image inspection is imperative.

The images in Figure 33 directly relate to the RMS values measured for the films

summarized in Table 8. Figure 33 represents 3D renderings of the AFM images,

highlighting the topography of the surface. The lightest shade of the peaks indicates

topographic heights of 10 nm. Based on the images in Figure 33, it was apparent that

there was not much difference in surface roughness between the substrate, first $PS-NH_2$

layer and the second PS-COOH layer. The RMS values obtained for the three samples in

Table 8 can be qualified as smooth since the roughness of the oxide surface is similar to

that of the deposited films. These smooth film surfaces suggest that the wash conditions

are optimized for the process.
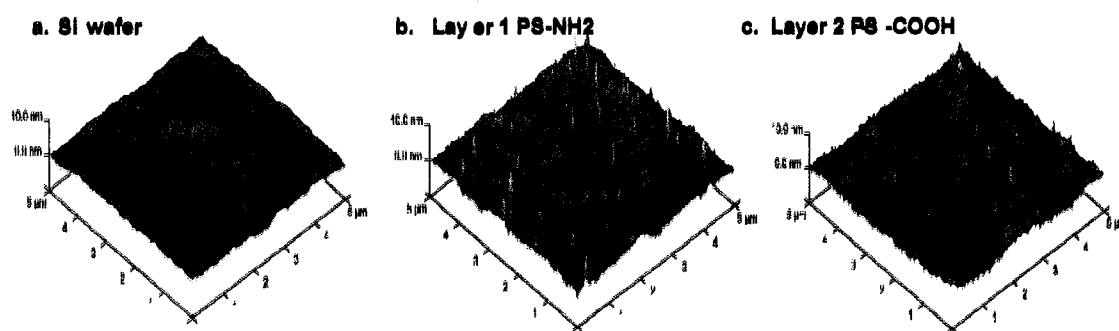
Figure 33. Surface profiles from 3D rendering of the AFM images with z = 10 nm of the
a) Si substrate, b) $PS-NH_2$ on Si, and c) PS-COOH deposited on the $PS-NH_2$.

Table 8. Summary of RMS values derived from the AFM data using a 5 μm x 5 μm area on the three surfaces in Figure 33: a) oxide surface (Si wafer), b) PS-NH$_2$ on oxide surface, and c) PS-COOH on PS-NH$_2$/oxide surface,. Values produced by AFM (Digital Instrument) roughness analysis software.

	RMS (Rough Mean Square) in nm
Oxide surface (Si wafer)	0.6 nm + 0.1 nm
PS-NH$_2$ on oxide surface*	0.8 nm + 0.1 nm
PS-COOH on PS-NH$_2$/oxide surface*	0.8 nm + 0.1 nm

*Polymer sample air dried after at least 20 hours.

A detailed analysis of the film stability was done by imaging each layer of the multilayer polymeric structure over time. Representative samples of the first, second, third and fourth layers were prepared by the dipping method. These four samples were imaged by AFM after drying for 20 hours (Figure 34A), 8 days (Figure 34B), and 15 days (Figure 34C) in air. The drying time was determined based on the AFM imaging experience during the course of this study. It was found that better imaging was achieved when the films were air dried at least 20 hours after deposition. With wet films, the AFM tip tended to drag material across the surface which ends up as surface artifact. Also, blurry images were produced due to poor tip-surface interaction. By observing the four samples over time under the AFM, the films were found to be stable with no traces of dewetting as shown in Figure 34. The PS-NH$_2$ and PS-COOH interactions between layers were intact as evidenced by the formation of contiguous films from each sample. Neither PS-NH$_2$ (Layers 1 and 3) nor PS-COOH (Layers 2 and 4) films deteriorated upon drying.
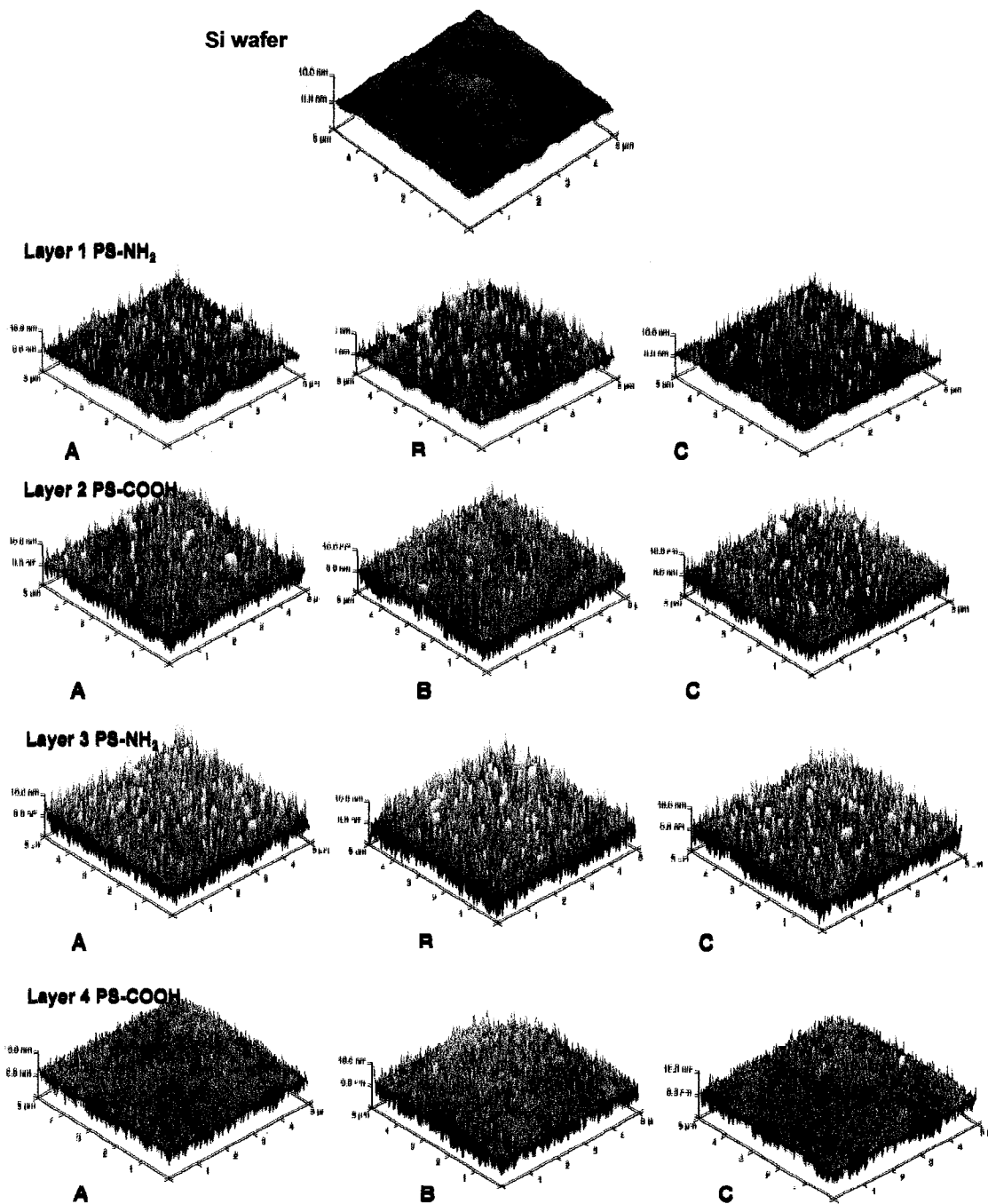
Figure 34. 3D renditions of the AFM data (z = 10 nm) of the layers 1,2,3 and 4 over time (A) 20 hours, (B) 8 days, and (C) 15 days after film deposition by dipping.

The surface roughness for the four samples was determined from the AFM images in Figure 34, and are given in Table 9. Surface artifacts were observed on the surface of Layers 2 and 3, contributing to higher surface roughness values than for layers 1 and 4. Visually, smoother films were obtained over time (left to right) in Figure 34. It was also observed that when the films dry over time, a better tip-surface interaction results in better images of smoother films. As mentioned earlier in the previous section, imaging wet films is problematic. The problems in imaging due to poor tip and surface interaction can be due to the solvent or to inherent characteristics of the polymer such as roughness. By looking at the images in Figure 34, it can be concluded that there was an overall smoothing of the film with deposition of more layers (top to bottom). As an example, the smooth surface of Layer 4 correlated to the RMS values in Table 9.

Table 9. Corresponding RMS (root mean square) + 0.1 nm values of the AFM (5 μm x 5 μm) images from Figure 34.

	(A) At least 20 hours	(B) 8 days	(C)15 days
Oxide surface	0.6 nm		
Layer 1 PS-NH$_2$	1.8	1.8	1.6
Layer 2 PS-COOH	2.7	3.0	3.0
Layer 3 PS-NH$_2$	3.6	3.5	3.3
Layer 4 PS-COOH	2.0	2.4	1.9

5.2.3 Summary for the Electrostatic Self-assembly of PS-COOH on PS-NH2

The PS-NH$_2$ and PS-COOH star polymer interactions were investigated by IR spectroscopy and AFM analysis. The interaction of PS-NH$_2$ and PS-COOH was proven by IR analysis. The presence of carboxylate anion in the mixture validated the proposed electrostatic interaction between the two star polymers.

The stability study of the films over time was designed to discover the appropriate conditions (solvent system and deposition conditions) for layer formation of each layer in the multilayer polymeric structure. The interaction of PS-NH$_2$ with the substrate and PS-COOH with the first polymer layer is crucial since it will be transferred to the subsequent layers of the polymeric structure. Based on the AFM analysis, homogenous films of PS-COOH on PS-NH$_2$ with good coverage were produced indicating a strong electrostatic interaction of the star polymers. The representative samples of the first, second, third and fourth layers were stable after 20 hours, 8 days, and 15 days after deposition. The films were all intact and no dewetting was observed. The morphology of the surfaces was characterized in terms of roughness as well. The surface roughness of the films was analyzed by visual inspection of the AFM images and by calculation of RMS roughness values from the data. The films were smooth with small differences in the RMS value from the starting silicon substrate indicating an optimized flow process. The same observations apply to the samples of the representative layers (Layer 1, 2, 3 and 4). The time dependence of the measured surface roughness was rationalized as a result of a better AFM tip and surface interaction for the drier films.

5.3 LBL Self-assembly of the Star Polymers as Monitored by Surface Plasmon Resonance (SPR)

Using the optimized deposition conditions established in Section 5.1, the LBL deposition of self-assembled alternating monolayer thin films of PS-NH$_2$ and PS-COOH was investigated using Surface Plasmon Resonance (SPR). SPR was chosen because of its advantages it offers as an optical detector in terms of its sensitivity, real-time and label-free data analysis. The film characteristics in terms of rate of film formation, film stability, and relative thickness can be derived from the SPR data analysis.

5.3.1 SPR Self-Assembly of PS-NH$_2$ on Clean Oxide Surface

The SPR experiments were conducted in two modes: scan and kinetics mode. Real-time data were obtained in both modes which were valuable for the investigation of the LBL self-assembly process of the star polymers by electrostatic interaction. The first step in the SPR *in situ* experiment was to perform a baseline scan of the surface plasmon resonance versus angle with the THF filling the cell. This was an important step of the *in situ* experiment since the angular shifts of the plasmon resonance will be based on this initial baseline. Then, the polymer solution was injected for the LBL self-assembly of the star polymers on the SF 11 substrate. Two sets of rinses were done with dichloromethane and THF, respectively. The kinetic and scanning modes were sequentially studied during the experiment. Initially, the layer deposition was monitored in the kinetics mode. The kinetics mode showed the change in intensity as a solvent (THF or dichloromethane) or polymer solution was injected in the flow cell. The equivalent plasmon shift

88

corresponding to the change in intensity in the kinetics mode is detected in the scan mode.

In the SPR *in situ* experiment, the SPR baseline of THF in the scan mode was obtained, showing the angle of the reflectance minimum to be 54.68 degrees. To monitor the layer deposition in the in the kinetics mode, the angle was set to 54.63 degrees, 0.05 degrees less than the resonance angle. In the kinetics mode, the change in intensity was monitored over time as shown in Figure 35.
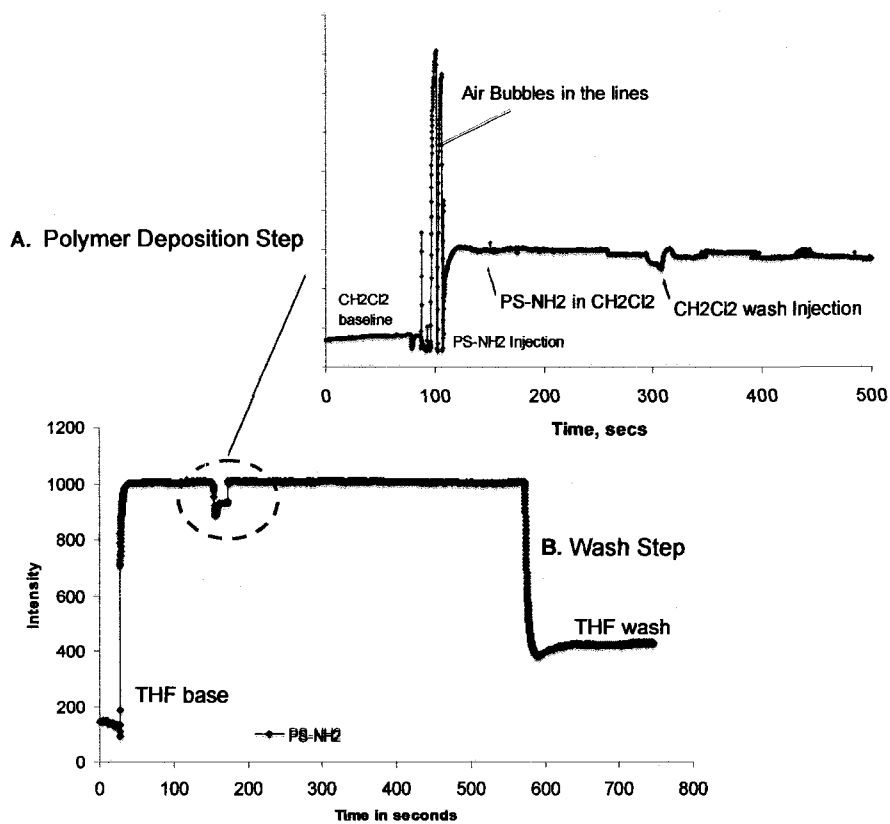
Figure 35. Kinetic mode plots for the polymer deposition (A) and wash steps (B) of PS-NH$_2$ on the oxide of gold coated SF 11 substrate. The set-up was sensitive to a pressure change during solution injection which is reflected as a dip in the plot.

In Figure 35B, an intensity of 100 was recorded as the THF solvent was injected to the SPR flow cell. This served as the THF solvent baseline in the kinetics mode. Dichloromethane was then injected to prepare the substrate surface for the deposition of the PS-NH$_2$ star polymer dissolved in dichloromethane as shown in Figure 35A. An abrupt rise in the intensity in Figure 35B was a result of solvent exchange between THF and dichloromethane in the system. As the THF was injected in the wash step, the reflected intensity decreased until it reached a constant intensity of 400. At this final intensity after the THF wash, a plasmon resonance angle of 54.88 degrees was recorded in the scan mode. It is expected for the THF and dichloromethane will result different intensities since each solvent has a different refractive index. Based on the observations from Figure 35B, the relative thickness of the layer formed can be estimated by the difference in intensities of the baseline and the final THF wash step, reflected intensity change of 300 in this case. This change in intensity of 300 in the kinetics mode was equivalent to a 0.194 degree shift of the plasmon angle in the scan mode.

In the polymer deposition step of Figure 35A, there was an observed stabilization of the reflected intensity from the polymer injection indicating the completion of film deposition. The completion of a layer deposition was rapid with the required time approximately18 seconds. The PS-NH$_2$ star polymer deposition sequence in Figure 35A started from the polymer injection resulting in an abrupt rise in intensity after 108 seconds until a steady state was reached at 120 seconds. During the PS-NH$_2$ layer deposition, after the dichloromethane was injected to wash the excess polymer on the surface, there was no observed change in the intensity. This could have two causes:

either the dichloromethane was not able to remove any excess polymers or non-adsorbed particles or there were no excess polymers or adsorbed particles to remove. Because there was no new material of different refractive index detected on the PS-NH$_2$ film surface, there was no change in intensity observed. From the deposition and wash processes, it can be concluded that the deposited first layer of PS-NH$_2$ on the SF11 substrate was stable to large amounts of dichloromethane and during the THF washes (6 mL in total).

5.3.2   SPR Mathematical Fitting

In order to interpret the angular shifts, a mathematical treatment of these data was done to determine certain star polymer thin film properties such as the film thickness and the specificity of the electrostatic type of interaction derived from SPR data. Each plot was fitted to exactly determine the location of the SPR minimum. The mathematical model used for fitting was based on a mathematical function that would express the angle at which the minimum reflectance occurs [48].

After monitoring the SPR *in situ* layer deposition in the kinetics mode, the position of the plasmon angle was identified in the SPR scanning mode. As explained in the beginning of this study, SPR responds to the refractive index change at the interface. In this case, the LBL self-assembly of the star polymers was monitored by the angular shift of the SPR signal for each layer deposited. The SPR instrument in the scanning mode was set to output a plot and table of reflected intensity versus angle after each scan.

The obtained angular shift not only provides a relative refractive index but also thickness of the deposited film.

The plots in the scan mode were recorded as qualitative data. The curves were mathematically fitted to get the exact location of the SPR reflectance minima. The SPR curve for the first PS-NH$_2$ layer SPR curve was fitted as shown in Figure 36. The figure shows a good fit of the measured (open circle) with the calculated (line) plasmon curves with the minimum at 54.878 $\pm$ 0.002 degrees.
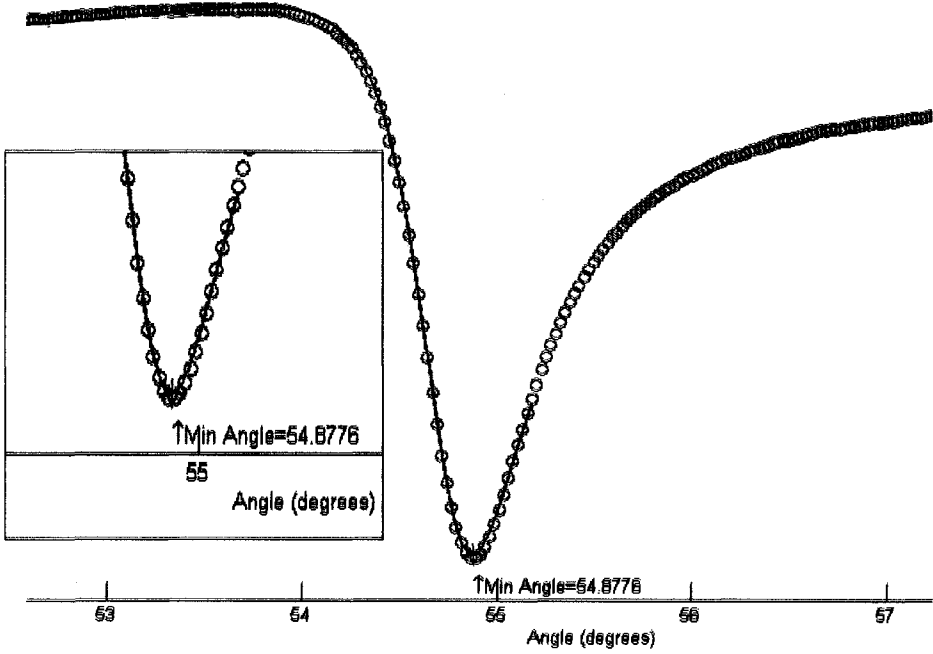
Figure 36. SPR of first PS-NH$_2$ layer fitted using the KNS Matlab program. The solid red line is the fitted curve of the experimental SPR curve.

By using the mathematical modeling, an estimated thickness of the thin film deposited was obtained. The mathematical model was based on the Fresnel equation that relates refractive index, thickness, wavelength, and angle of incidence [51]. Because the

angular shift is a function of both thickness and refractive index, the refractive index was assumed to solve for thickness. In this case, the refractive index of the star polymers was assumed to be that of polystyrene since the star polymer structure was composed of mostly polystyrene. During the LBL *in situ* experiments, the monolayer comprises the star polymers immersed in THF. It was also important to have a correct approximation of the volume of the star polymers in the monolayer to get the correct film thickness. For this reason, the packing of the star polymers in the monolayer is a major consideration. The deposited thin film on the multilayer polymeric structure was assumed to be polystyrene hard sphere monolayer hexagonally-packed with THF interpenetrating the interstitial space [51]. This model generates a film composition of polystyrene (60.5%) and THF (39.5%) as shown in Figure 37. Two comparisons of a monolayer with polystyrene taking up either 100% (solid) or 60.5% of the volume of the solvated monolayer were done to calculate the layer thickness as summarized in Table 10. Using the calculated effective refractive index using Maxwell-Garnet Theory based on the solvated monolayer model, a measured average shift of 0.15 degrees correlated to a film thickness of 4.5 nm [51]. See Appendix A for the assumptions and derivation of the monolayer film thickness (*calculated*) in the dry and solvated states.
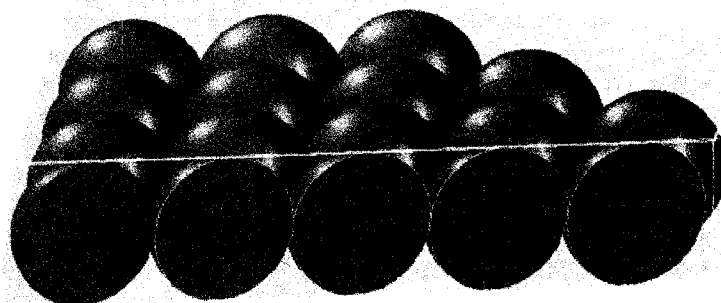
Figure 37. Hexagonally-packed with THF interpenetrating of the polystyrene hard sphere monolayer model assumed for the self-assembled star polymer thin films in the multilayer polymeric structure [51] (reprinted with permission from W. Risk)..

Table 10. Comparison of measured and calculated film thickness of the self-assembled star polymers via electrostatic interactions at its different states.

	Thickness in nm
Solid uniform monolayer, *calculated*	2.6 nm
60.5% solvated monolayer, *calculated*	4.5 nm
Dry state monolayer, *AFM analysis*	2.9 nm

Hydrodynamic diameter of star polymers is equal to 9.0 nm

Because the angular shift in the SPR is a function of both refractive index and thickness, the assumptions of the model and calculated thickness were analyzed. The assumptions of the monolayer model and calculated values can predict the SPR shift and if indeed monolayer thick films were obtained in the LBL *in situ* experiment. The thickness of the monolayer obtained through the mathematical analysis can be compared to the hydrodynamic diameter of the star polymers and thickness of the films in different states. First, the calculated solvated thickness of the film in the SPR experiment as 4.5 nm can be correlated to the hydrodynamic diameter of the star polymers of 9 nm [50].

94

The hydrodynamic diameter served as the maximum value of a fully solvated monolayer that can form in solution. The calculated 4.5 nm thickness suggests that a somewhat compressed monolayer was formed on the surface. The difference between 9 nm and 4.5 nm would mean 50% compression of the star polymers as they absorb to a surface. Because the star polymers are believed to be compressed, the classical hard sphere assumption earlier should not be valid. However, the approximation of the monolayer film composition (60.5% polystyrene) at the solvated state still holds. The compression of the star polymers is expected as it has been observed with dendrimers from previous studies [36].

In the dry state, the star polymer films are expected to be more compressed compared to the solvated state by virtue of the solvent surrounding the star polymers making the films swell. In this case, the value in the dry state of 2.9 nm by AFM analysis seems reasonable compared to the 4.5 nm solvated state thickness. In addition, the calculated solid monolayer film thickness of 2.6 nm corresponds reasonably well to the 2.9 nm measured by AFM. From this analysis, it seems that a monolayer thick film was deposited based on the measured angular shift of 0.15 degrees in the SPR.

5.3.3 Specific Electrostatic Interactions for Layer Formation in the SPR

The behavior of the PS-NH$_2$ star polymers interacting with the same PS-NH$_2$ stars and PS-COOH stars interacting with the same PS-COOH star polymer were investigated. This experiment aimed to look at the effect of possible types of interactions in the LBL

self-assembly of PS-NH$_2$ and PS-COOH. The objective of the experiment was to distinguish the specific electrostatic interactions that will generate a stable and self-limiting layer. The experiment was designed to have two consecutive depositions of each polymer type.

The two consecutive depositions of PS-COOH were done first followed by the two consecutive depositions of PS-NH$_2$. For the two sets of experiments, the procedure followed the same SPR *in situ* deposition and wash protocol described earlier. For the purpose of investigating the definitive electrostatic interactions of PS-COOH (1) and PS-COOH (2), the initial layer of PS-COOH 1 had a measured plasmon angle of 56.14 degrees. As the next layer of PS-COOH (2) was deposited, the plasmon angle actually decreased to 56.13 degrees as shown in Figure 38. The next set of depositions using PS-NH$_2$ was then studied. An initial layer of PS-NH$_2$ thin film (PS-NH$_2$ (1)) was deposited with a plasmon resonance angle of 56.29 degrees as shown in Figure 38. Another layer of PS-NH$_2$ (2) was the deposited and the plasmon resonance angle of 56.33 degrees measured. The angular shifts in the SPR for the two sets of experiments were summarized in Table 11.
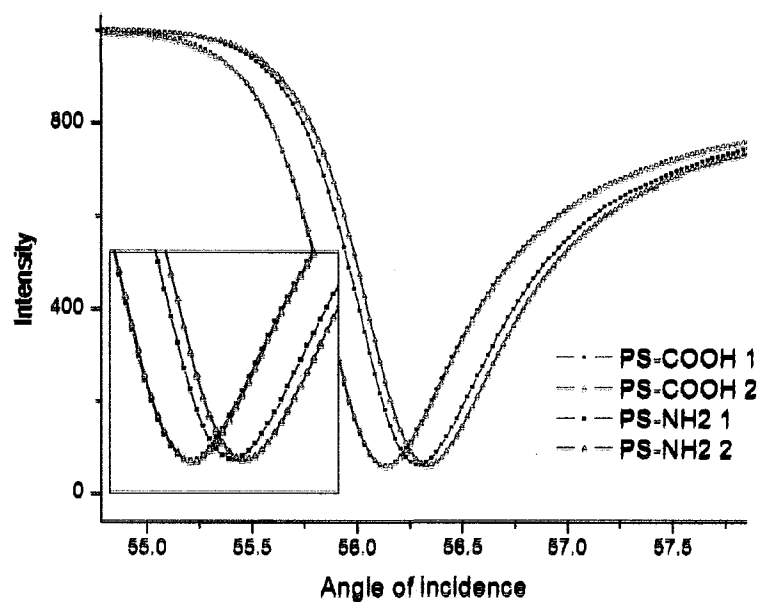
Figure 38. Angular shifts from two consecutive deposition of PS-COOH on PS-COOH and PS-NH$_2$ on PS-NH$_2$. No angular shift was observed for the PS-COOH on PS-COOH deposition while a 0.043 degrees shift was observed for PS-NH$_2$ on PS-NH$_2$.

Table 11. Summary of detected angular shift of two consecutive depositions of star polymers in the SPR.

	Run 2
PS-COOH 2 on PS-COOH 1	-0.007 $\pm$ 0.002 degrees
PS-NH$_2$ 2 on PS-NH$_2$ 1	0.043 $\pm$ 0.002 degrees

The two consecutive depositions of PS-COOH on PS-COOH resulted in a very small angular shift of -0.007 degrees. This suggested no second layer was deposited. It can be inferred that PS-COOH interacting with PS-COOH does not induce formation of another monolayer. The kinetics mode profile obtained from the deposition of PS-COOH 2 on PS-COOH 1 is shown in Figure 39. This was the kinetic data from the deposition of

PS-COOH 2 on PS-COOH 1 which initially resulted in a -0.007 angular shift in the scan

mode measured by SPR. It can be observed that the THF wash baseline was inline with

the starting THF baseline. And so, independent of predictions of the layer thickness, the

behavior of the initial and final THF intensities in the kinetics mode was indicative of the

success or failure of layer depositions. Thus, being able to monitor layer deposition in

real-time kinetics mode with SPR was valuable.
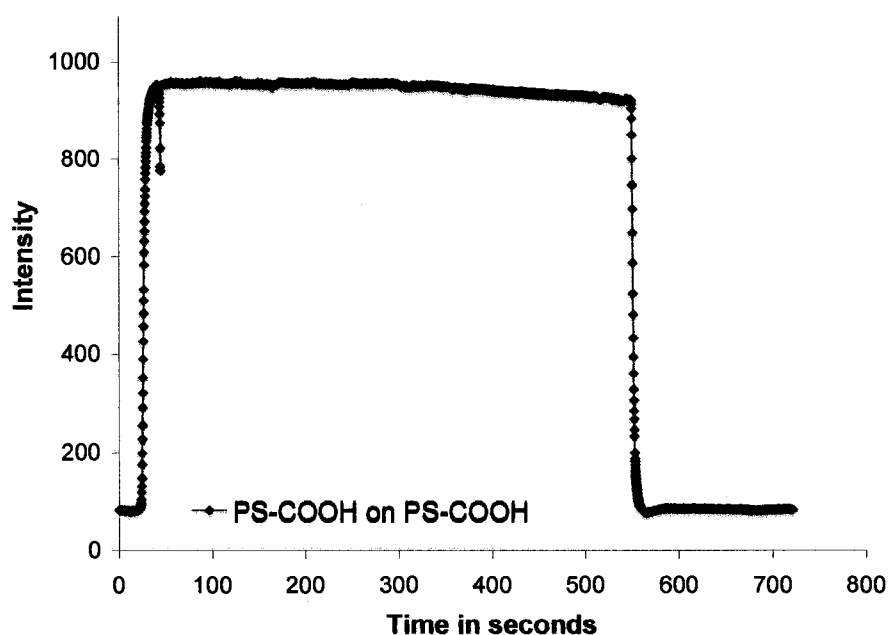
Figure 39. Kinetics mode plot of an unsuccessful layer deposition of PS-COOH on PS-COOH. A -0.007 angular shift was observed in the SPR scan mode. Observe that the initial dichloromethane and THF intensities are the same.

On the other hand, the two consecutive depositions of PS-NH$_2$ on PS-NH$_2$

showed a difference of angular shift calculated to be 0.043 degrees. To determine the

significance of this shift from the PS-NH$_2$ layer, the 95% confidence limit of the data

fitting program was calculated and found to be 0.002 degrees. In this case, the observed

0.043 degree shift from the deposition of 2 consecutive layers of PS-NH$_2$ was significant.

If compared to a deposited monolayer of PS-NH$_2$ with an average angular shift of 0.164

degrees, 0.043 would constitute only ¼ of a full monolayer. Therefore, it would seem

that the layer formed with the 0.043 degrees angular shift was non-uniform or patchy

possibly due to incomplete removal of excess polymer or non-adsorbed particles on the

surface. With this result, the importance of the optimal deposition conditions in terms of

wash steps was re-emphasized. PS-NH$_2$ and PS-COOH interaction is the only specific

type of electrostatic interaction that will form a monolayer thin film

For uncharged particles, a strong, specific interaction such as electrostatic is

necessary to form well ordered multilayers. Before the LBL self-assembly of multilayer

polymeric structures was investigated, the self-assembly of the base layer on oxide (PS-

NH$_2$) and the second PS-COOH layer was monitored in the *in situ* SPR experiment. This

was to verify and complement the results from the AFM studies using flow-through

technique.

As reported earlier, the first layer deposition of PS-NH$_2$ on the silanol-rich oxide

surface produced an angular shift of 0.194 degrees in the reflectance minimum from the

THF baseline by the *in situ* SPR experiment. The reflection intensity and equivalent

plasmon resonance angle of the first layer of PS-NH$_2$ were recorded as 400 and 54.88

degrees, respectively. For the deposition of the second layer composed of PS-COOH, the

first layer of PS-NH$_2$ was considered the new baseline. Just as in the kinetics mode for

monitoring the first layer of PS-NH$_2$, the angle was set to 54.83 degrees. The PS-NH$_2$

thin film surface was prepared for the next deposition layer by a dichloromethane wash

which caused another abrupt rise in intensity as shown in Figure 40A. The PS-COOH in

dichloromethane was then injected in the flow cell followed by wash cycles of

dichloromethane and THF. The intensity in THF after the rinse was measured as 200. In

the scan mode, the plasmon resonance angle for the deposition of the second layer of PS-

COOH on PS-NH₂ shifted and was located at 54.96 degrees as shown in Figure 40B.
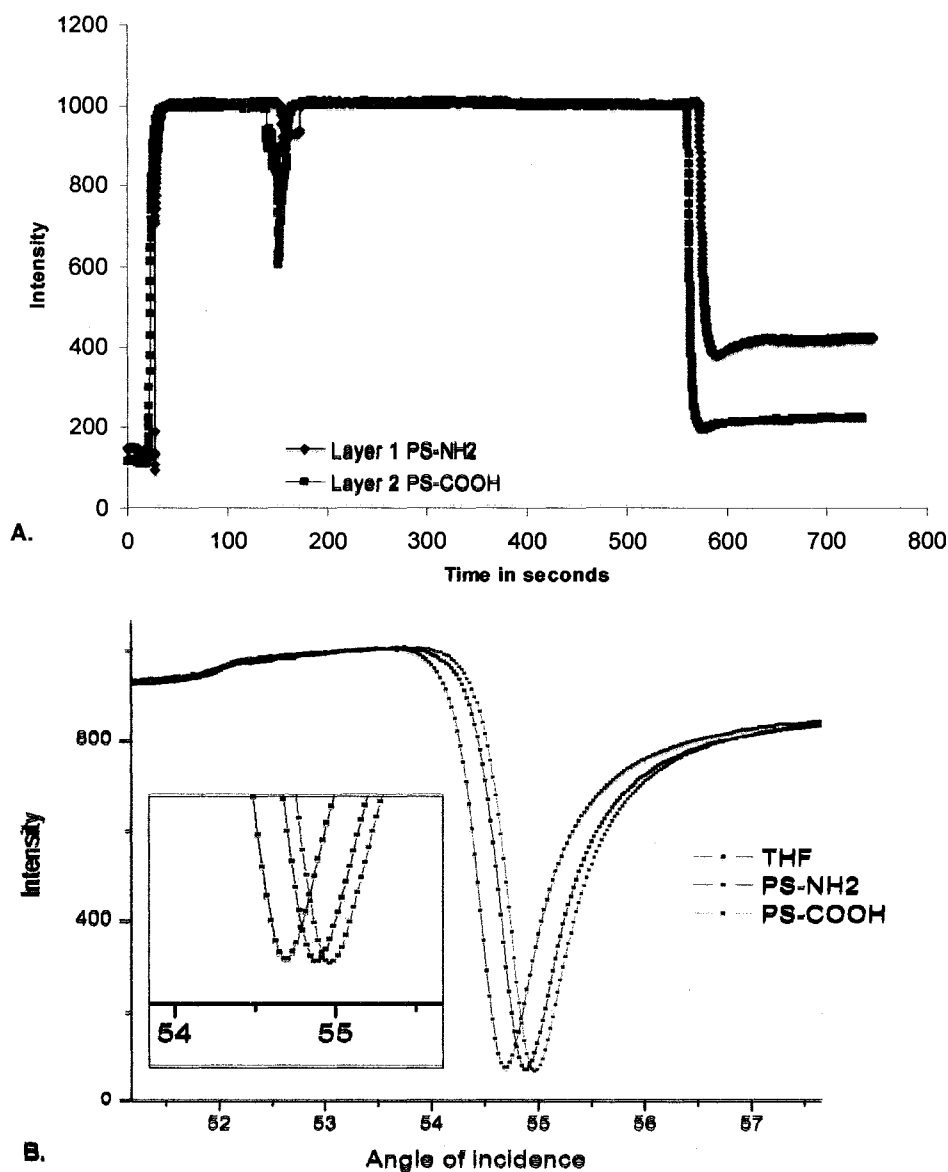
Figure 40. SPR kinetics (A) and scan mode (B) of LBL self-assembly of foundation
layer PS-NH₂ and second layer PS-COOH.

100

By looking at the kinetics mode plot in Figure 40A, the difference in reflection intensity for the second PS-COOH layer on $PS-NH_2$ of 100 compared to 200 for the first layer of $PS-NH_2$ was indicative of relative thickness of the two films. These intensities corresponded to angular shifts of 0.085 and 0.194 degrees for the second PS-COOH and first $PS-NH_2$ layers, respectively relative to pure THF. Because the angular shift in the SPR is directly related to refractive index and thickness of the layer as described by the Fresnel equations, it can be tentatively concluded that the initial $PS-NH_2$ layer was thicker than the second PS-COOH layer. Also, it is apparent that a good foundation layer was formed on the oxide coated substrate. A good foundation layer is important for the formation of stable multilayer structures.

5.3.4   SPR LBL Self-assembly of $PS-NH_2$ and PS-COOH

Having obtained a good foundation layer and established the efficacy of the interactions between $PS-NH_2$ and PS-COOH, further LBL self-assembly of the star polymers was studied. The objective of building a multilayer polymeric structure of uniform and stable polymer layers was monitored by the SPR technique.

The LBL multilayer self-assembly of star polymers by the alternating deposition, $PS-NH_2$ then PS-COOH, was monitored in the SPR. For each layer deposited, the polymer deposition and wash protocol were maintained and layer formation studied by the kinetics and scan modes of the SPR. The order of measurement for each monolayer was: measuring a plasmon resonance angle with THF; monitoring the polymer deposition

and wash cycles in the kinetics mode; and finally measuring another plasmon resonance angle in the scan mode. The plasmon resonance angle from the last step became the new the baseline for the next layer. These steps were repeated for alternating layer depositions of PS-NH$_2$ and PS-COOH. Figure 41 and Figure 42 demonstrated a successful LBL self-assembly of PS-NH$_2$ and PS-COOH structures up to 10 layers.

The relative thickness of each polymer, PS-NH$_2$ or PS-COOH, can be inferred by the difference in the resonance angular shift observed as the star polymers were deposited. This observed relative thicknesses of the PS-NH$_2$ and PS-COOH layers, also corresponded to the kinetic mode plots as shown in Figure 42. As mentioned earlier, the difference between the initial and final THF baselines is related to the relative thickness of the film deposited. Based on Figure 42, the average thicknesses of PS-NH$_2$ layers was somewhat greater than that of the PS-COOH layers with a larger difference in intensity than the PS-COOH layers. Also based on the scan plot, the angular shifts of the plasmons resonances were uniform for each bilayer indicating uniform deposition.
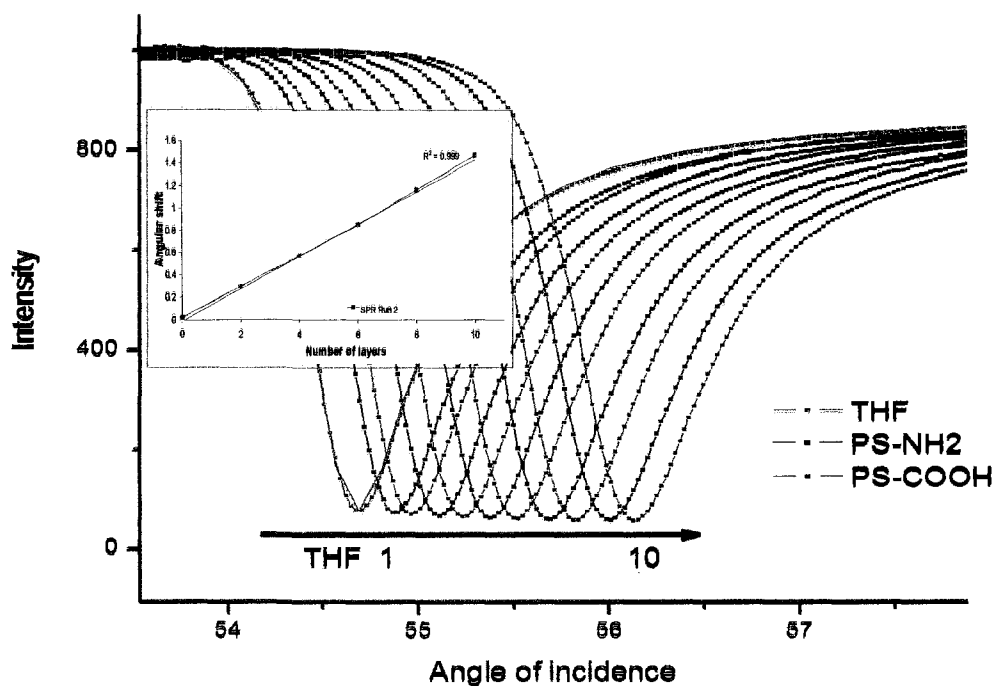
Figure 41. SPR (in scan mode) plot of LBL self-assembly of PS-NH₂ and PS-COOH via electrostatic interactions. Inset plot (Angular shift vs. Layer number) showing the uniform bilayer LBL self-assembly, $R^2 = 0.999$.
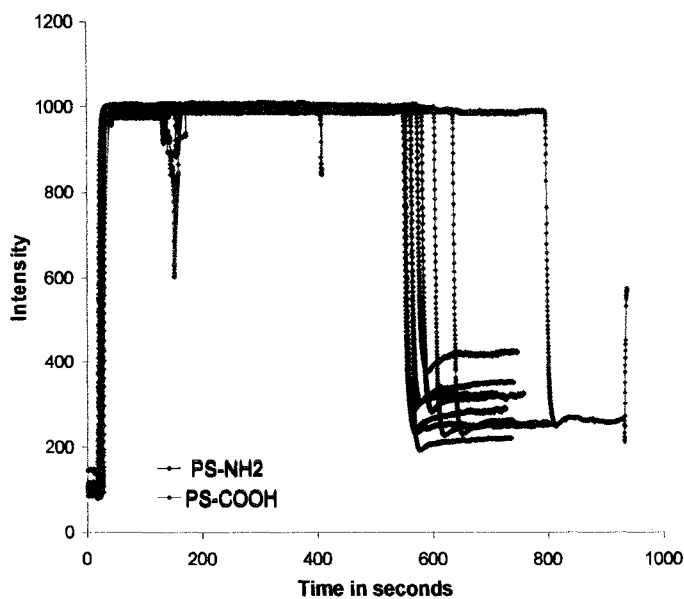
Figure 42. Kinetics mode plot of Run 2 of the LBL self-assembly of PS-NH₂ and PS-COOH via electrostatic interactions. SPR instrument set at initial fixed angle of 54.83 degrees.

The results indicated that the optimal conditions for LBL self-assembly,

determined by the AFM and initial SPR studies, were achieved. The sample from the

deposition of the 10 layers of alternating PS-NH$_2$ and PS-COOH star polymers was

characterized under the AFM and the images are shown in Figure 43. The 10th layer (PS-

COOH) of the multilayer polymeric structure built by the *in situ* SPR LBL self-assembly

had a smooth and contiguous surface as shown in Figure 43a, c. The film was stable and

no dewetting observed even 2 weeks after the deposition.
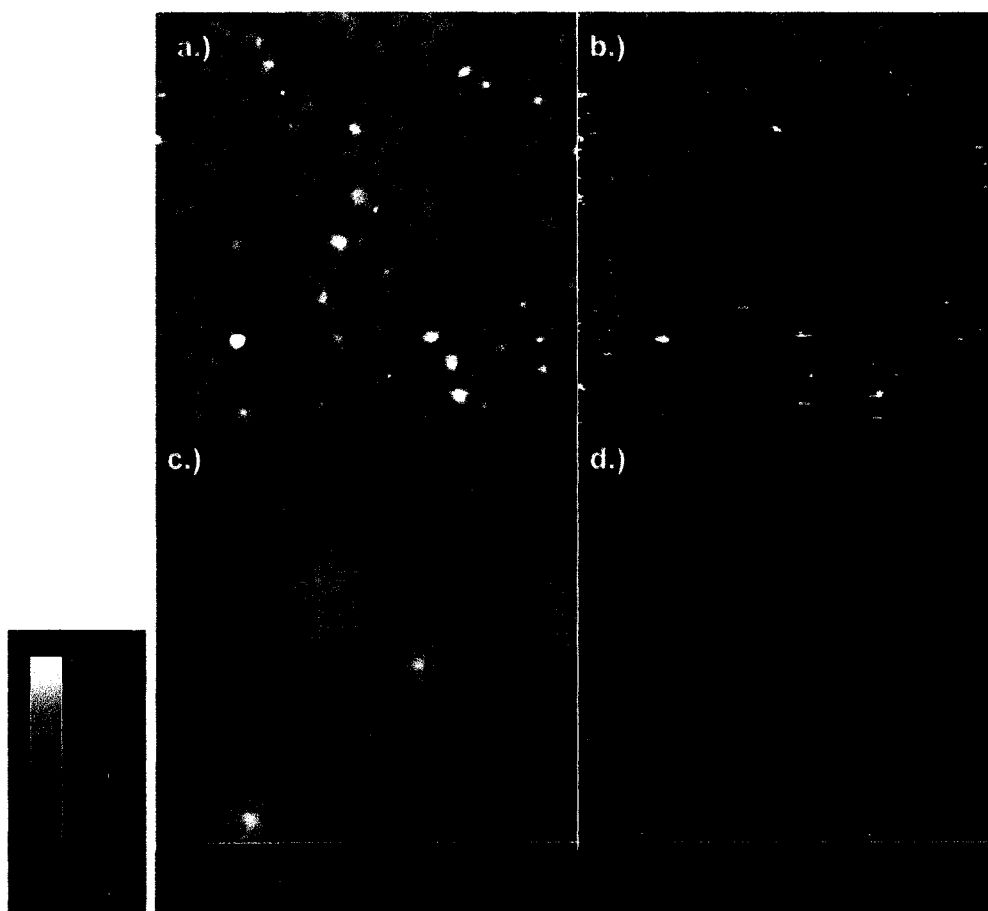
Figure 43. AFM topography (a and c, z = 15 nm) and phase (b and d) images of the 10th
layer from of SPR *in situ* LBL self-assembly of alternating PS-NH$_2$ and PS-COOH
layers. a and b: 5 μm x 5 μm image shows few superficial surface artifacts; c and d: 1 μm
x 1 μm image.

The angular shifts of the 10 layers deposited were fitted using the mathematical model described previously. The angular shifts were based on the initial THF baseline and the previously deposited layer and are shown in Table 12. This was done to eliminate any run-to-run discrepancies in the solvents and polymer refractive indices.

Table 12. Angular location of SPR minimum fitted in the KNS Program and corresponding angular shift for PS-NH$_2$ and PS-COOH layers deposited in Run 2.

Layer	Angle $\pm$ 0.002 ^{0} (fitted)	Angular shift per layer, $\pm$ 0.002^0	Angular shift, bilayer, $\pm$ 0.002^0
THF baseline	54.684	0.000	
Layer 1 PS-NH$_2$	54.878	0.194	
Layer 2 PS-COOH	54.962	0.085	0.278
Layer 3 PS-NH$_2$	55.107	0.144	
Layer 4 PS-COOH	55.233	0.126	0.271
Layer 5 PS-NH$_2$	55.376	0.143	
Layer 6 PS-COOH	55.512	0.136	0.280
Layer 7 PS-NH$_2$	55.688	0.176	
Layer 8 PS-COOH	55.824	0.136	0.312
Layer 9 PS-NH$_2$	56.002	0.178	
Layer 10 PS-COOH	56.136	0.134	0.312
Average PS-NH$_2$	0.164 $\pm$ 0.002	Average Bilayer	0.290
Average PS-COOH	0.123 $\pm$ 0.002	Average per layer	0.145

The fitted data also suggest thicker PS-NH$_2$ layers (average of 0.164 $\pm$ 0.002 degrees shift) than PS-COOH layers (average of 0.123 $\pm$ 0.002 degrees shift) in agreement with the kinetics and scan mode raw data. Three runs were performed to verify the repeatability of the experiment. Figure 44 shows the uniformity and repeatability of the LBL self-assembly in this study. A linear behavior was observed for

all three runs as shown in Figure 44. These SPR results indicated that the LBL self-assembly was a repeatable, uniform, and orderly deposition.
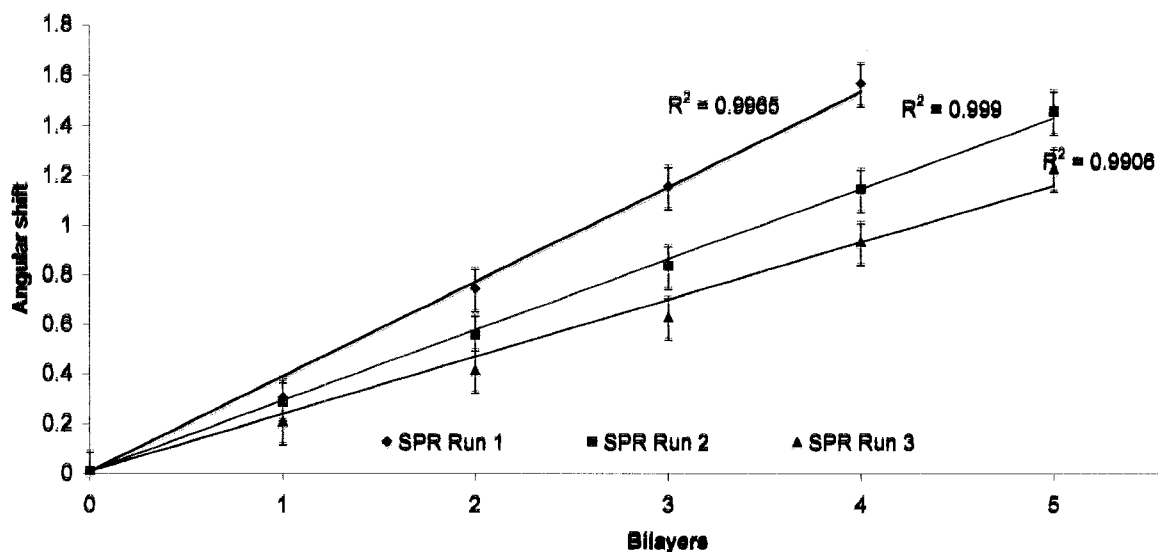
Figure 44. Cumulative bilayer angular shifts in three SPR runs. Variations between the three runs based on a standard error of 0.085 degrees based on five THF fitted SPR baselines from different days and runs.

The results of the three runs were repeatable, however some variability between them is evident in Figure 44. The variability within runs was due to the different substrates and some difference in the dry THF baselines. Because all of the SPR angular shifts obtained were relative to the THF baseline, a 0.085 degrees standard error for the fitted THF SPR shifts (5 different runs on different days) was obtained. Although the deposition conditions were constant, there was an expected difference in the batches of the substrates since the metal stack (chromium and gold) was deposited in different days. The variability with the THF was possibly caused by its high affinity for water. Although

"dry" THF was used during the runs, exposure to air during the measurement was inevitable.

5.3.5 SPR Analysis for the Choice of Solvent

Among the solvents used for the star polymer solutions, THF and toluene were the most viable for the electrostatic LBL deposition of $PS-NH_2$ and PS-COOH films. However, polymer-solvent interactions were considered. Although one solvent would work well for $PS-NH_2$, the behavior of PS-COOH in the solvent of choice was also a major consideration. Such was the case for THF as solvent. The initial SPR results, shown in Figure 45, using BK7 prism-substrate system verified that THF was not suitable for LBL self- assembly due to the different PS-COOH/THF interactions. From Figure 45, no angular shift was observed from the initial $PS-NH_2$ resonance angle of 73.92 degrees resulted from the deposition of the second layer of PS-COOH. Again for the deposition of the fourth layer (PS-COOH) no angular shift from 73.96 degrees was observed as well. This suggested that the THF effected the deposition of PS-COOH layer.
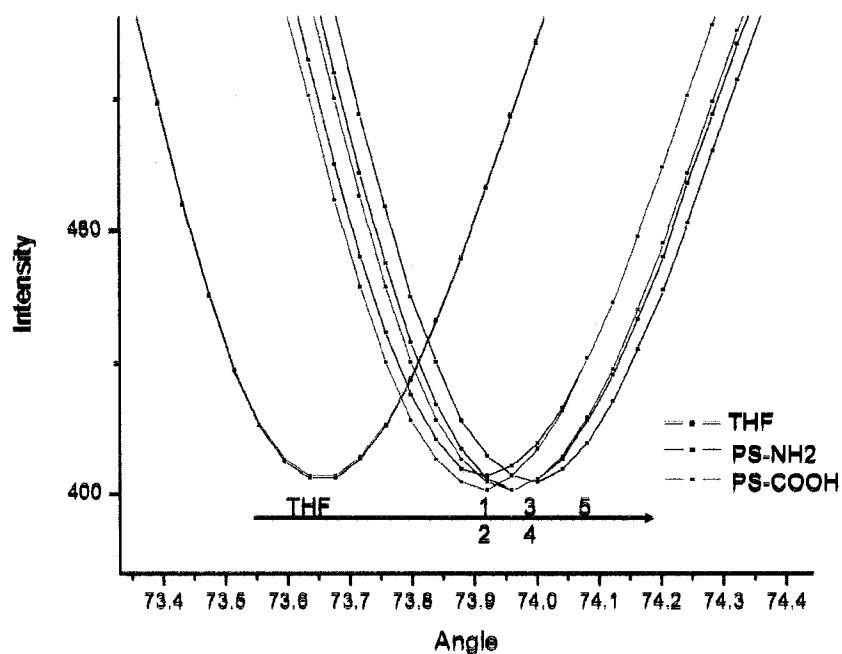
Figure 45. SPR study using dry THF in deposition for the electrostatic LBL self-assembly of PS-NH2 and PS-COOH.

Although the PS-NH$_2$ in THF on oxide surface produced contiguous films as judged by subsequent AFM characterization, THF was not used for multilayer formation since it was an unsuitable solvent for the PS-COOH star polymer deposition. It is known that the pKa of acid functional groups such as carboxylic acids (approximate COOH) changes in THF in the presence of water [39]. THF has a high affinity for water and controlling the amount of water during the LBL self-assembly experiments is difficult.

In the case of toluene, initial SPR studies showed that it too was an ineffective solvent for the LBL self-assembly. SPR results using toluene for LBL deposition are shown in Figure 46. Although for each of the first few layers was deposited, the plasmon dip shifted by a similar amount, erratic angular shifts were observed after the sixth layer as shown.
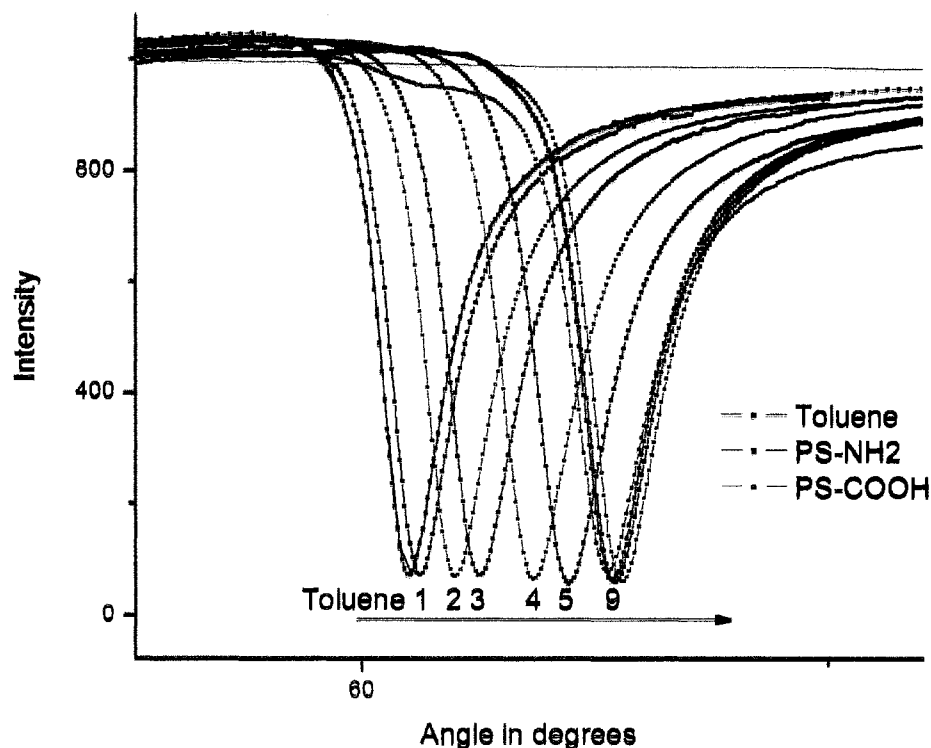
Figure 46. SPR study using toluene as solvent for electrostatic LBL self-assembly of PS-NH$_2$ and PS-COOH.

From the SPR analysis, it was obvious that some of the deposited layers were more than a monolayer thick layer causing the system to reach the limits of layer formation by LBL self-assembly. After the ninth layer, no additional layers were added. These results indicated that inferior layers were formed, as indicated by non-uniformity in angular shifts detected by the SPR analysis. The termination of LBL self-assembly can be due to the excess polymer or non-adsorbed artifacts that were not washed off by toluene. In practice, the deposition surface is exposed to excessive concentrations of the polymer during deposition which is normally washed off leaving a monolayer thick film. The change from an initial angular shift of 0.15 degrees to approximately 0.5 degrees

suggested that thicker layers were ultimately formed due to incomplete rinsing of excess polymers or adsorbed artifacts from the surface. The layer formation in a LBL self-assembly can be limited by poor surface interactions between layers. For toluene, it can be inferred that poor layers were formed characterized by non-uniformity in the angular shifts detected by the SPR.

As in the toluene experiment, uniform layers were deposited initially using chloroform as shown in Figure 47. However by the sixth layer, the angular shift became progressively smaller and layer deposition stopped after the ninth layer. The LBL self-assembly of the star polymer may have ceased because of the unstable foundation of dewetted PS-NH$_2$ films observed by AFM for the chloroform deposition. The inconsistent angular shifts can also be explained by the polymer filling the resulting holes from the previous layer each deposition.
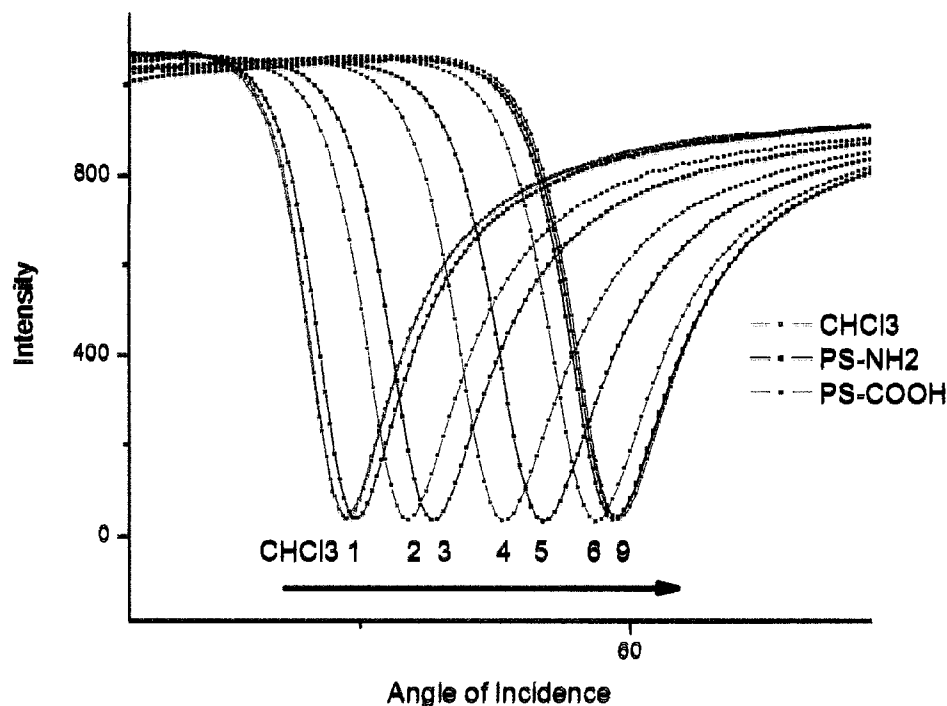
Figure 47. SPR study using chloroform as solvent for electrostatic LBL self-assembly of PS-NH₂ and PS-COOH.

Even though stable films were formed using THF based on the AFM, the LBL films of star polymers in this solvent were unstable. THF is known to have high affinity for water. Because the PS-NH₂ and PS-COOH self-assembly is an acid-base interaction, the reaction was inhibited by the presence of water in THF as shown by previous studies in polyelectrolyte LBL self-assemblies [38,39]. Due to the unknown water concentrations in THF as it was exposed to air during preparation of solutions and runs, SPR runs were unrepeatable although "dry" THF was used. The *in situ* SPR experiment using dichloromethane demonstrated the importance of having a stable foundation of PS-NH₂ for the realization of LBL multilayer self-assembly of star polymers.

Based on the studies using the kinetics mode of *in situ* SPR run, THF was found to wash-off the excess star polymers deposited using dichloromethane. Because of the limitations of each solvent studied (toluene, dichloromethane, and THF) investigated in this study, the choice of appropriate solvent system was based on the efficacy of the solvent to wash-off the excess polymer on the surface. It was found that the combination of dichloromethane-THF for deposition and wash, not only facilitates electrostatic self-assembly of the star polymers, but also produces stable films.

5.3.6   Summary for the LBL Self-Assembly of the Star Polymers as Monitored by SPR

The objective of building a multilayer polymeric structure by LBL self-assembly of star polymers via electrostatic interaction was achieved and monitored by SPR. The data showed that the PS-NH$_2$ and PS-COOH star polymer thin films were deposited and anchored as uniform monolayer films that were stable to solvent washes even in the multilayer polymeric structure. By using dichloromethane for deposition and THF for washing, the LBL self-assembly of PS-NH$_2$ and PS-COOH was successfully and reproducibly demonstrated as monitored by SPR analysis.

Real-time analysis by SPR showed that self-assembly of a monolayer of star polymer on a surface takes place in about 18 seconds. The SPR in kinetics mode provided valuable information about the dynamics of self-assembly of the star polymers. These studies not only confirmed the layer formation but it also gave qualitative information on the thickness of the layer formed. The SPR technique also provided a

real-time data showing removal of excess polymer or surface artifacts by THF washing after each deposition.

The mathematical fitting analysis provided an accurate plasmon resonance angle location of within 0.002 degrees at 95% confidence level which was crucial in determining layer properties, *e.g.*, thickness. Because the average angular shift obtained in the SPR experiment was 0.15 degrees, several additional studies were done to verify if indeed a monolayer thick polymer film was deposited. The maximum thickness assumed for these star polymer thin films was based on the measured hydrodynamic diameter of 9.0 nm. The assumption of a hard polystyrene spheres model was not appropriate for the star polymer thin films since they were expected to be somewhat compressed on the surface both in the dry and solvated states as observed for dendrimers. An amount of solvation (60.5% in THF) was found consistent with a 4.5 nm thick solvated film suggesting approximately 50% compression of the star polymer during deposition. The calculated thickness of 2.6 nm for a solid monolayer of polystyrene validated the initial AFM thickness measurements of 2.9 nm at its dried state. It was concluded based on these data that each self-assembled star polymer layer was monolayer thick. The self-assembly by electrostatic interaction was found to be specific only for the $PS-NH_2$ and $PS-COOH$ interaction. The results of two consecutive depositions of $PS-NH_2$ showed a significant angular shift which was indicative of needed improvement in the wash cycles of the *in situ* experiment.

When studied by the SPR, the process of LBL self-assembly of the star polymers was reproducibly uniform with a linear relationship of angular shifts versus bilayers

113

deposited. The process of LBL self-assembly of the star polymer by electrostatic interaction was repeatable from run to run but showed some variations. In multiple runs, a 0.085 degrees standard error was obtained from 5 THF SPR baselines on different days using different substrates. Due to the tendency of THF to absorb water, some variability was observed in the runs. The initial results from the AFM analysis provided information on the proper choice of solvent and deposition conditions. The kinetics mode of the SPR showed why THF was needed for the self-assembly of the star polymers multilayers and how the other solvents caused cessation of the LBL self-assembly. It was observed that the final THF wash stabilizes the films and prevents dewetting of the films upon drying.

5.4 LBL Self-Assembly of the Star Polymers Monitored by Quartz Crystal Microgravimetry (QCM)

The QCM experiments were conducted to measure the LBL deposition of star polymer thin films over time by recording the changes in resonance frequency of the QCM quartz crystal. The QCM detection depends on a change in frequency of a resonating quartz crystal as material is deposited on (or is removed from) the crystal. This frequency is related by physical properties such as density and viscosity of the film in contact with the surface to the mass of the material detected on the surface. These parameters are additive but can be evaluated separately. A decrease in frequency indicates an increase in mass detected on the surface during the layer deposition. Likewise, a difference in the frequencies during processing was indicative of layer deposition or removal of excess polymer or superficial surface artifacts.

The objective of the QCM experiment was to confirm the LBL self-assembly of the star polymers via electrostatic interaction using a different analytical technique to verify the uniformity of layer deposition. Because of the larger surface area of the QCM crystal compared to the SPR, the deposition conditions for the QCM were designed to use larger solvent volumes and polymer solution volumes to deposit the film. Just like the other analytical techniques, solvent is important and must be optimized for the QCM experiments.

During the course of the QCM studies, some erratic frequency changes were encountered during the PS-NH$_2$ or PS-COOH polymer deposition. These erratic changes can be due to the sensitivity of the QCM set-up. As with the SPR, the QCM was also

sensitive to pressure changes due to solvent injection. Since the detection in the QCM is based on electromechanical response, the apparatus is sensitive to small intrinsic vibrations. Another source of the erratic data was from air bubbles in the system or the fluid lines. Although the QCM crystal was oriented at 45^0 to minimized bubble formation, the bubbles were not fully eliminated and are obvious in some of the plots in the following sections. Other measures were taken to prevent bubble formation as well. Cleaning the flow cell with the same solvent (dichloromethane) before the run provided smooth flow as the solvent was injected.

5.4.1   QCM Self-assembly of PS-NH$_2$ on Silanol-rich Oxide Surfaces

Using the optimal solvent conditions established in the previous sections, the study of the LBL self-assembly by QCM was initiated. The *in situ* QCM experiment started with a frequency baseline recorded in air. This is the intrinsic frequency crystal oscillation in air. THF was then injected to obtain a solvent baseline. Because the polymers were used in dichloromethane solution, a solvent exchange of THF by dichloromethane followed to prepare the surface for polymer deposition. After equilibration, the first layer of PS-NH$_2$ in dichloromethane was formed. Two consecutive washes with dichloromethane, and one with THF wash followed to remove excess polymers and non-adsorbed materials. To monitor the change in frequency, the baseline was allowed to stabilize after injection of the solutions. The beginning and end of the solution injection serve as the plateaus from which the average frequency change for that deposition interval was then calculated. An experimental run in the QCM showing the

deposition of PS-NH$_2$ on the oxide surface of a QCM substrate coated with silicon

dioxide is shown in Figure 48.
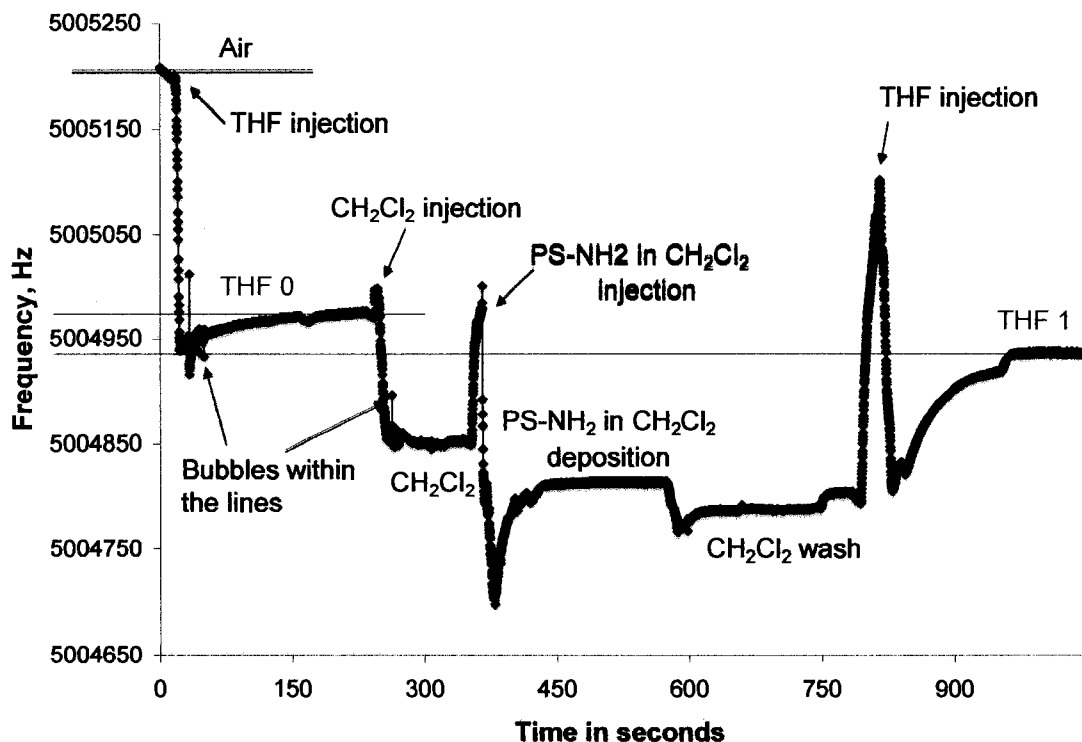
Figure 48. QCM plot showing the deposition steps in the QCM *in situ* experiment. The
baselines for the deposition step (THF, dichloromethane, polymer in dichloromethane,
dichloromethane and THF washes) were identified. The red lines labeled THF 0 and
THF 1 correspond to the frequency differences for the PS-NH$_2$ deposition. The artifacts
due to bubbles appear as spikes in the plot.

The starting frequency of the quartz crystal with air was recorded at 5005205 Hz

in Figure 48. As the THF was injected, the frequency stabilized lower at an average of

value 5004970 Hz. This was used as the THF baseline (THF 0) for the experiment from

which each successive layer deposited will be measured. A solvent exchange with a

dichloromethane wash followed and an abrupt change in frequency was observed. This

117

was an inherent characteristic of the system due to the different viscoelastic properties of THF and dichloromethane. The first layer of PS-NH$_2$ was then injected and a decrease in frequency was observed and the frequency monitored until it stabilized. The wash cycle was completed followed by re-introduction of THF for final comparison with the original baseline, THF 0. As the THF wash was injected, a decrease in the frequency was observed to an average value of 5004930 Hz. As shown in Figure 48, there was a 40 Hz change in frequency after the second wash of THF (THF 1) compared to its starting baseline (THF 0). The decreased frequency suggests that the initial layer of PS-NH$_2$ was successfully formed. The frequency change for the deposition of the first layer of PS-NH$_2$ is based on the difference of THF 1 and THF 0 baselines.

As in the SPR analysis, two sets of dichloromethane and THF washes were incorporated to remove excess polymers or superficial artifacts on the surface. It was observed previously that after the dichloromethane wash was injected there was no change in the reflected intensity from the SPR kinetics mode indicating complete formation of stable layers. The QCM wash cycles (dichloromethane and THF) verified the stability of the PS-NH$_2$ layer over the large surface area of the QCM crystal. Because the time response of the QCM monitor is sufficiently fast, the rate of layer formation can also be monitored just like in the SPR kinetics mode. For the first layer of PS-NH$_2$ deposition, the polymer deposition was complete in only 16 seconds. The deposition step in the QCM was started at time equal to 242 seconds. An abrupt increase in frequency was observed as soon as the polymer solution was injected until steady state was at 258 seconds as determined by the frequency stabilization. The observed layer formation over

118

16 seconds was consistent with that measured by SPR (18 seconds) even considering the

differences in active surface areas of the two techniques.

5.4.2   PS-NH$_2$ and PS-COOH Electrostatic Interaction for Layer Formation Monitored by QCM

Using the conditions established from the previous section to build the multilayer

polymeric structure, the deposition of PS-COOH on PS-NH$_2$ was then analyzed by QCM.

The deposition and wash cycles were conducted to first form a PS-NH$_2$ layer as shown in

Figure 49 as preparation for the deposition of PS-COOH. Figure 49 illustrates the

deposition cycles for the fifth and sixth layer with PS-COOH on PS-NH$_2$. The film

surface of the fifth layer composed of PS-NH$_2$, with a THF 5 crystal frequency of

5004839 Hz, was prepared by flowing dichloromethane through the cell. After which,

the sixth layer (PS-COOH) was injected and washed with dichloromethane and THF.

After the THF wash (THF 6) for the sixth layer of PS-COOH, a frequency of 5004789 Hz

was measured.
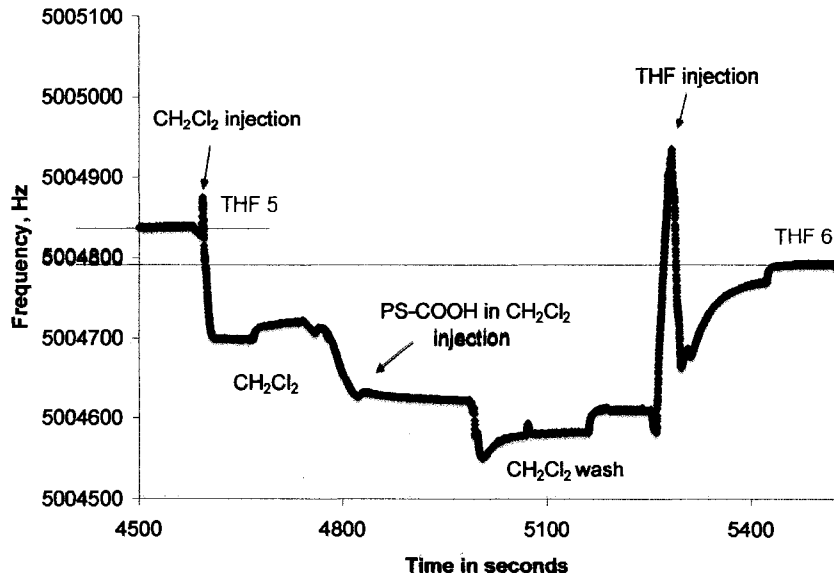
Figure 49. QCM plot of frequency versus time for the fifth layer (PS-NH₂) and sixth (PS-COOH) layers in the LBL self-assembly of star polymers using dichloromethane and THF.

In terms of frequency changes due to self-assembly of the fifth layer, addition of

the layer of PS-NH₂ caused a frequency shift of 31 Hz. This was the difference between

the initial and final THF (THF 5 in Figure 49) wash baselines. For the sixth layer (PS-

COOH), the difference between the THF (THF 5) baseline was based on that previously

determined for PS-NH₂ (5004839 Hz (THF 5)) and the final THF wash (5004789 Hz

(THF 6)). This sixth layer composed of PS-COOH produced a frequency shift of 50 Hz.

It is inferred that the larger frequency change observed from the PS-COOH deposition

(50 Hz) meant a larger mass was deposited relative to the 31 Hz change observed from

the previous PS-NH₂ layer. The difference in the amount of material applied by the PS-

NH₂ and PS-COOH in solution deposition can be due to the difference in compression of

the star polymers on the surface. To verify this observation, a trend for the amount of

material deposited each by PS-NH$_2$ and PS-COOH treatment was investigated in the LBL self-assembly of the star polymers.

5.4.3   QCM LBL Self-assembly of PS-NH$_2$ and PS-COOH

With a good base layer of PS-NH$_2$ on oxide and the strong interaction of PS-NH$_2$ and PS-COOH, the LBL self-assembly of star polymers was monitored by QCM. The *in situ* QCM experiment monitored the self-assembly of successive layers of PS-NH$_2$ and PS-COOH by the changes in the frequencies of the THF baselines for each deposition cycle. In this experiment, 10 layers of self-assembled star polymers were deposited as shown in Figure 50. Here, the THF baselines are highlighted with arrows and serve as the basis for the frequency changes calculated. The initial THF baseline frequency throughout the experiment was 5004970 Hz.
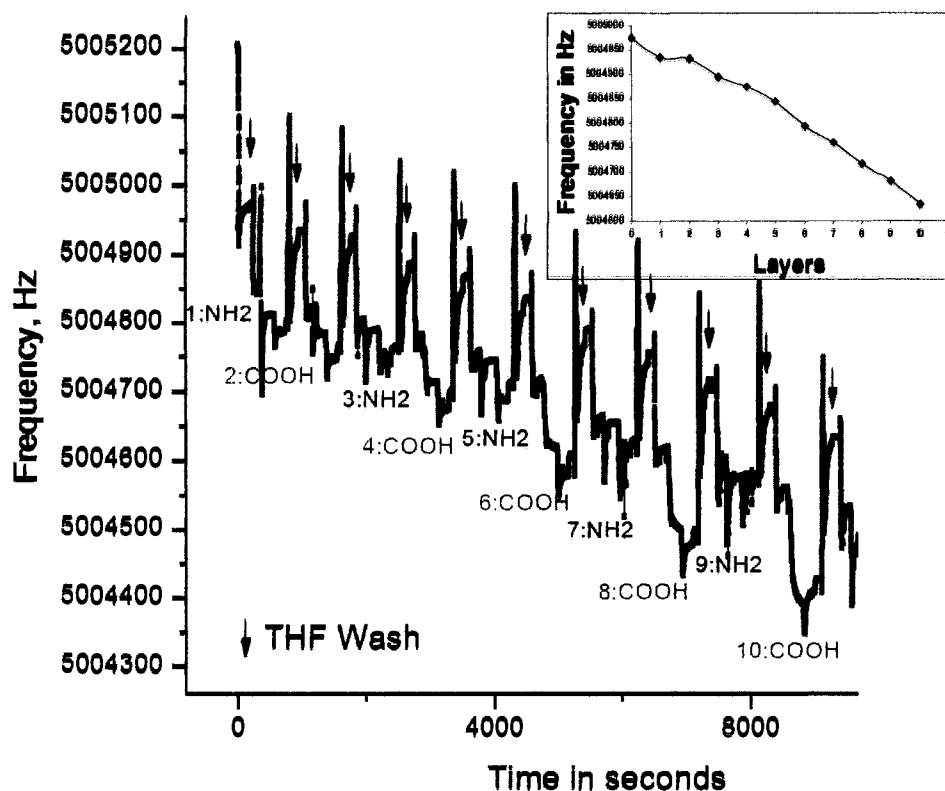
Figure 50. QCM of LBL self-assembly of PS-NH₂ and PS-COOH by electrostatic interaction. Inset is a plot of frequency versus layer numbers.

As described in the previous section, the polymer deposition and wash cycles

included the injection of dichloromethane for surface preparation, the polymer in

dichloromethane solution, and the two sets of washes with dichloromethane and THF.

Included in Figure 50 is an inset plot of the corresponding frequencies of the respective

THF baselines for each deposition cycle over 10 layers of self-assembly. As expected,

the frequency decreased each successive layer in a linear behavior. The frequency

changes observed for the QCM run in Figure 50 were processed. As mentioned earlier,

the average frequencies of the THF baselines were calculated and summarized in Table

13. Over the course of QCM studies, achieving consistency over the first few layers was

difficult. For this reason, a very small shift was obtained from the second layer deposition (PS-COOH) as shown in Table 13 and the inset plot of Figure 50. This data was neglected for the calculation of the average of the frequency change for PS-NH$_2$ and PS-COOH deposition.

Table 13. Summary of frequencies and frequency changes of the LBL self-assembled PS-NH$_2$ and PS-COOH by electrostatic interaction in the QCM.

Layer	Average Frequency, ± 1 Hz	Change in Average Frequency, ± 1 Hz per layer	Bilayer Frequency Change, ± 1 Hz
THF baseline	5004970	0	0
*Layer 1 PS-NH$_2$	5004930	40	
*Layer 2 PS-COOH	5004928	2	42
*Layer 3 PS-NH$_2$	5004887	39	
*Layer 4 PS-COOH	5004870	19	58
*Layer 5 PS-NH$_2$	5004839	31	
*Layer 6 PS-COOH	5004789	50	81
*Layer 7 PS-NH$_2$	5004755	34	
*Layer 8 PS-COOH	5004714	41	75
*Layer 9 PS-NH$_2$	5004679	35	
*Layer 10 PS-COOH	5004631	48	83
Average PS-NH$_2$	36 ± 1 Hz	*Average Bilayer*	68
Average PS-COOH	39 ± 1 Hz	*Average per Layer*	34

* THF baseline for one deposition cycle

The average frequency changes from the successive deposition of the PS-NH$_2$ and PS-COOH were 36 and 39 Hz, respectively. These values indicate that there was virtually no difference in the amount of material being deposited for PS-NH$_2$ and PS-COOH layers. Aside from this, it was observed that the frequency changes were slightly increasing as more layers were deposited based on the bilayer frequency changes.

The LBL QCM experiments were analyzed for reproducibility. A plot for three typical experiments is shown in Figure 51. The difficulty in the deposition for the first and second layer depositions was observed previously in Figure 50. In Figure 51, the change in frequencies for the first and second layers varied from run to run but eventually became constant as more layers were added.
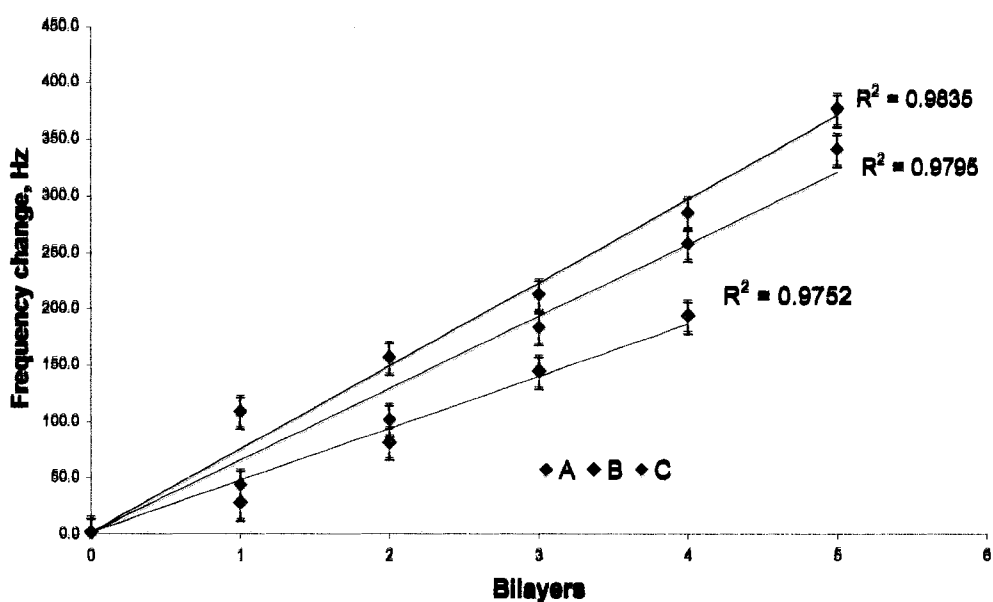
Figure 51. Uniform electrostatic LBL self-assembly of cumulative bilayers of PS-NH$_2$ and PS-COOH in the QCM. Standard error of 14 Hz was obtained from the THF frequency shifts from eight runs done on different days with different substrates.

In each case, a linear change in frequency for bilayers was observed in the LBL self-assembly of the star polymers. The uniform LBL self-assembly showed a high degree of reproducibility based on the three runs presented in the Figure 51. To assess different runs on different days, the THF baselines were evaluated. The variation between the runs maybe attributed to the different sources of THF solvent used.

124

This produced a standard error of 14 Hz. This standard error was obtained from 8 runs done on different days. As observed in the SPR experiments, although "dry" THF was used, the high affinity of THF for water made it difficult to control precisely the amount of water present in THF during the runs.

5.4.4   QCM Analysis to Determine the Choice of Solvent

The role of the solvent selection in producing uniform layers of star polymer thin films was studied using QCM. In the case of the SPR experiments, the LBL self-assembly sometimes eventually ceased after deposition of certain number of layers for certain solvents. The QCM results also showed the effect of incomplete removal of excess polymer and other surface artifacts. Because of the earlier problems in the choice of solvent and deposition conditions for SPR, the problems encountered in the QCM experiments were easily resolved.

By using the same *in situ* QCM procedure, THF was replaced by chloroform to wash off excess polymers on the surface. By looking at the frequencies in Figure 52, after the deposition of first layer of PS-NH$_2$, the frequency did not change as the chloroform was injected. Aside from these, it seems that the first three layers of deposition for the star polymers are characterized by a smaller frequency shift. As the layer deposition proceeded, the frequency change became larger. This indicated non-uniform deposition of the layers and incomplete rinsing of the film surface. These results correlated to initial AFM and SPR findings using the same solvent conditions.
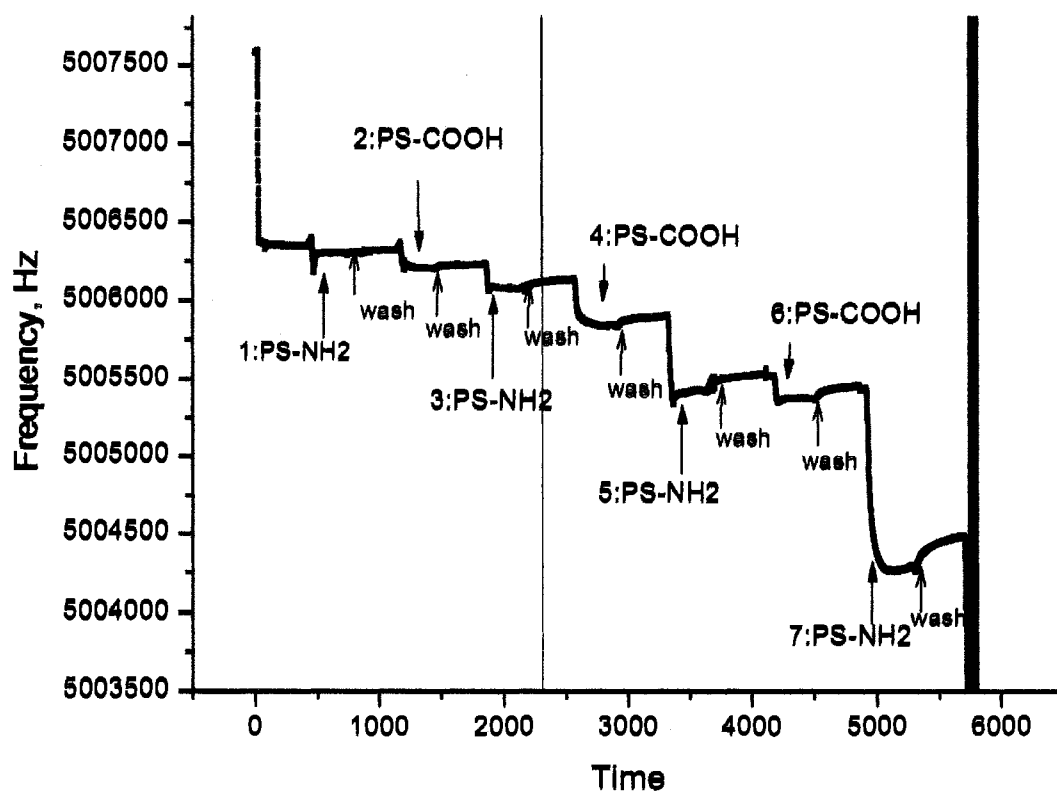
Figure 52. QCM LBL self-assembly of star polymers by electrostatic interaction in chloroform. The lines in the middle (at approximately 2400 seconds) and at the right of the image are uncontrollable oscillation of the driver circuit due to cessation of oscillation of the quartz crystal.

The increasingly large frequency changes resulting from the sequential layer depositions indicate that progressively larger masses were being deposited, presumably due to incomplete removal of excess polymer materials. The deposition of large amounts of material eventually caused the cessation of crystal oscillation. This is signified by the black vertical lines around 6000 seconds in the experiment as shown in Figure 52. This erratic frequency change was indicative of the non-oscillation of the crystal. This behavior is related to the thickness and the mechanical properties of the deposited film [46]. This often indicates excessively thick films have been deposited but because of the

126

gel-like properties of the star polymer thin films, the viscous energy loss is so great that the oscillator circuit can no longer drive the crystal oscillation [46].

5.4.5   Star Polymer Film Properties Derived from the QCM

The electromechanical response of the QCM made it possible to study mechanical properties of the star polymer films. Aside from the frequency shifts, the QCM set-up provides resistance (impedance) data. From the resistance data, mechanical properties such as viscosity and shear modulus of the films may be inferred. The question of the mechanical properties will be based on the analysis of the resistance obtained during layer deposition.

For the purpose of studying the mechanical properties of the LBL self-assembled star polymers, Figure 53 shows the relationship between frequency and resistance changes versus layer formation. A linear and an exponential relationship was observed respectively, for the frequency and resistance during bilayer deposition of the star polymer thin films. In both cases, as more bilayers were deposited, the frequency change and film resistance increased.
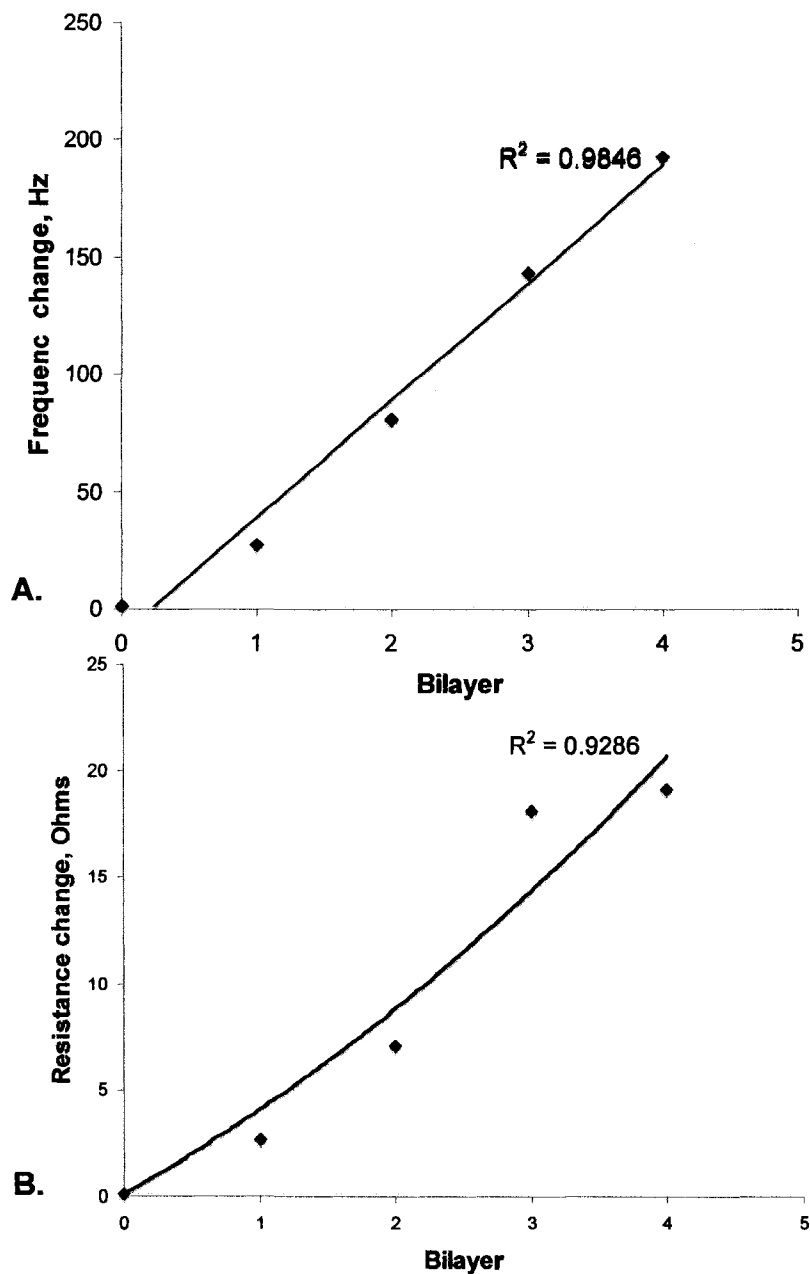
Figure 53. LBL self-assembly of PS-NH₂ and PS-COOH layers driven by electrostatic interaction. Plots of frequency change versus number of bilayers (A) and resistance change vs number of bilayers (B).

The non-linear behavior of the resistance versus the bilayer deposition suggests

that the behavior of end groups of the last deposited layer (PS-COOH in a bilayer) had an

effect on the mechanical properties of the star polymer thin films. It can be inferred that the star polymer thin films appear to behave as gel-like materials compared to the abrupt increase in resistance usually observed from other types of polymers [47]. This is consistent with our initial hypothesis based on SPR studies, that the monolayer thin films are highly solvated and contain in both polymer and solvent.

5.4.6   Summary for the LBL Self-Assembly of the Star Polymers Monitored by QCM

The analysis by QCM verified the uniformity of LBL self-assembly of the PS-NH$_2$ and PS-COOH shown first by SPR. While SPR techniques probe optical properties of the film, QCM provides information on the deposited mass and physical properties of the deposited layer. The rate of deposition of the star polymer thin films and stability of films were studied by QCM. The QCM results provided information on the layer formation over a larger surface areas than studied by SPR.

As mentioned, the QCM monitors the LBL deposition by frequency changes in oscillation over time. A rapid layer deposition (16 seconds) was observed based on the QCM results. This was comparable to that of 18 seconds for layer deposition determined during the SPR studies. The layer formation of star polymer thin films seems to be independent on the surface area for deposition in any environment, in this case polymer-rich, which is advantageous for future applications. Another similarity to the SPR results was the verification of the stability of the deposited films during solvent exposure. As observed by SPR, THF was observed to wash off only excess polymers or non-adsorbed materials from the QCM surface. In both cases, the choice of solvent and wash

conditions was important with dichloromethane and THF providing an effective solvent combination while chloroform was not.

The QCM results verified the uniform LBL self-assembly of PS-NH$_2$ and PS-COOH via electrostatic interactions. The bilayers of PS-NH$_2$ and PS-COOH were analyzed to obtain the relative contributions of each star polymer. By analyzing the bilayer formation by QCM, a relatively linear relationship of the frequency shift to the layer deposition was observed. The bilayer frequency shifts and those for each individual deposited layer of thin film were measured, indicating a behavior consistent with Sauerbrey analysis. The Sauerbrey relationship shows that the change in mass is proportional to the change in frequency [46]. Within these bilayers, the PS-COOH layer contributed a somewhat greater mass than the PS-NH$_2$ layer as indicated by its greater frequency change compared to the PS-NH$_2$. A possible explanation is that the difference may be due to differences in layer compression and the interaction of PS-NH$_2$ and PS-COOH. Similar results were observed in the LBL self-assembly of the star polymers in the SPR experiments.

5.5   Orthogonal Results of the SPR and QCM

The gel-like layer properties suggested by the QCM results is consistent with the initial modeling of the star polymers in its solvated state in the SPR experiments. In the section 5.3.2, a model of the films was presented which depicts the films as considerably solvated and assumes that the polymers occupy approximately 60.5% of the total volume.

In the SPR results, the angular shifts measured were due to the change both in refractive index and layer thickness. In this study, the refractive index and the relative volume occupied by the star polymer and solvent were assumed to result in a layer thickness . For a given shift, as the polymer ratio increases (*e.g.,* towards 100% solid) in this model, the film thickness decreases. Conversely, for a given thickness, as the polymer content increases (approximately 60.5% polymer), the angular shift decreases.

On the other hand, the QCM results which are based on crystal frequency shifts are related to the change in deposited mass. In this case, the overall effect of the detected mass of the star polymers and associated solvent within the film driven by the frequency shifts obtained. As the shift increases, the amount of mass deposited on the quartz crystal also increases.

By looking at the mathematical fitting data obtained from the SPR experiments, some properties of the QCM can be predicted. A 0.15 degree shift was measured in the SPR *in situ* studies and is associated with the formation of a monolayer. Using experimental procedures and deposition conditions similar to those used with the SPR, QCM LBL deposition yielded a monolayer causing a 34 Hz average frequency shift measured from the experiment. Table 14 shows the implications of the measured by SPR and QCM assuming a solvated monolayer of PS-NH$_2$ and PS-COOH.

131

Table 14. Considerations of the SPR and QCM results from the electrostatic LBL self-assembly of PS-NH$_2$ and PS-COOH.

Polymer	Angular shift, degree	Frequency shift, Hz
PS-NH$_2$	0.164	36
PS- COOH	0.123	39

The difference in SPR angular shift between the PS-NH$_2$ and PS- COOH layers could be attributed to a number of factors: a different refractive index between the two polymers, amount of material deposited, or unequal ratios of polymer to solvent. The first case is unlikely since the both PS-NH$_2$ and PS-COOH are composed largely of polystyrene, thus the refractive indices should be the same. Because the QCM results showed that there were no significant differences in mass deposited between PS-NH$_2$ and PS- COOH, these suggest that the differences observed in the SPR and QCM are due to differences in the ratio of the polymer to solvent. Because the SPR experiments only measures the average refractive index of a film, the ratio of the polymer to solvent can not be determined.

CHAPTER SIX
CONCLUSIONS

The overall objective of this work was to study the formation of LBL self-assembled functionalized star polymer thin films on oxide surfaces where assembly is driven by electrostatic interaction. This was accomplished using different analytical techniques including AFM, IR, SPR, and QCM. The successful LBL self-assembly required optimized deposition conditions and choice of solvent. By thorough experimentation, the efficacy of using dichloromethane and THF in tandem as solvent system was demonstrated.

Using AFM, the film coverage, roughness, stability, and uniformity of the self-assembled PS-NH$_2$ on the oxide surfaces, polymer films on polymer films and subsequent layers of the multilayer structure were probed. Also by AFM characterization, the efficacy of the electrostatic interactions from PS-NH$_2$ and oxide were validated with the formation of highly compressed, stable, and contiguous PS-NH$_2$ films suitable for a foundation layer for the multilayer polymeric structure. The interaction of PS-COOH with PS-NH$_2$ film was effective for assembly as proven by the controlled deposition and homogenous and smooth films obtained. The representative layers of PS-NH$_2$ and PS-COOH in the multilayer polymeric structure were stable with no dewetting observed up to 15 days after deposition. The optimized flow method produced pristine, stable, smooth, and contiguous thin films using dichloromethane for deposition and washing with THF as final rinse .

By IR analysis, the presence of carboxylate anion with absorbance of 1651.53

cm^{-1} was obtained. This was a signature product from the PS-NH$_2$ and PS-COOH star polymer reaction that confirmed the electrostatic interaction type interaction.

The LBL self-assembly of PS-NH$_2$ and PS-COOH by electrostatic interaction was demonstrated by SPR. The angular shifts from the LBL self-assembly were reproducibly uniform. The kinetics study by SPR showed a rapid monolayer formation within 18 seconds. The deposited star polymer thin films were stable during the wash cycle of *in situ* SPR LBL self-assembly.

In the QCM, the LBL self-assembly of the star polymer thin films were reproducibly uniform based on the frequency shifts measured from the bilayer deposition. Here, a rapid monolayer formation (16 seconds) was also observed. The PS-NH$_2$ and PS-COOH layers were stable to solvent exposure of the monolayer during the wash cycles in both the *in situ* QCM method and the SPR technique.

The intensive optimization studies on the choice of solvent and wash sequences in the AFM, SPR, and QCM studies was the key for the successful electrostatic LBL self-assembly of the star polymers. It was shown by SPR and QCM that the dichloromethane (deposition/wash) and THF wash solvent mixture effectively facilitates the LBL self-assembly of the star polymers. On the other hand, AFM imaging demonstrated the efficacy of the final THF wash in stabilizing the dichloromethane deposited films. This study proved that this LBL self-assembly is not a trivial process and is dependent on the specific polymer and solvent interactions as driving force for the self-assembly.

CHAPTER SEVEN
FUTURE WORK

The powerful technique of self-assembly provides an inspiration to new approaches to fabrication of nano-structures. This thesis work laid the preliminary work for further studies in applications of LBL self-assembly of star polymers. The controlled LBL self-assembly by electrostatic interactions makes it a viable technique for developing nanotechnologies for drug delivery and catalysis. In this case, the future work on the electrostatic LBL self-assembly of star polymers will begin with refinements of the process after which the long term studies shall be initiated. The LBL self-assembly of star polymers is predicted to be of great potential in industrial and commercial applications

The refinements of LBL self-assembly of the star polymer represent a short term effort for enhancement of the process. Modifications on some of the analytical tools will improve the LBL self-assembly process for the star polymers. An improvement in film preparation for the GATR IR analysis is needed to utilize the intrinsic sensitivity of the procedure. Fine tuning the QCM experiment to eliminate experimental artifacts will be beneficial for data analysis and interpretation. Since the properties of star polymer thin films are not well studied, obtaining the star polymer properties from SPR and QCM studies is valuable. Therefore, calculating the physical (thickness) and mechanical (viscosity and elastic modulus) parameters from the SPR and QCM data is required to obtain the star polymer properties.

A wide range future commercial and industrial applications are now accessible with the controlled LBL self-assembly of star polymers. Different functionalities on the star polymers provide validation of the star polymers as novel materials. As an example, functionalizing the star polymer with nanoparticles offers an alternative advanced particulate media which maybe useful for magnetic tape technology. The occlusion of hydrophobic materials in the star polymer core suggests potential delivery applications. Another application would be as recyclable/recoverable catalysts for industrial applications. The star polymers occluded with a catalytic metallic nanoparticle in the core could protect the catalyst and promote reuse. Another application for occluded reagents could be for the photodynamic therapy in cancer treatment. Here the dye could be both dissolved and stabilized by polymer coating. If occluded dye material is in a biodegradable star polymer, the cargo could be released to the body through hydrolytic/enzymatic degradation of the polymer.

REFERENCES

1. V. Uskokovic, *"Nanotechnologies: What we do not know,"* Technology in Society, **29**, 43-61 (2007).

2. Feynman, R.P. (1960). *Feynman's Talk: There's plenty of room at the bottom* [Online]. Available at http://www.zyvex.com/nanotech/feynman.html (Accessed April 8, 2007).

3. M. Boncheva and G.M. Whitesides, *"Making things by self-assembly,"* MRS Bull., **30**, pp. 736-741 (2005).

4. J-M Lehn, *"Toward self-organization and complex matter,"* Science, **295**, pp. 2400-2403 (2002).

5. G.M. Whitesides, M. Mammen and S-K.Choi, *"Polyvalent interactions in biological systems: Implications for design and use of multivalent ligands and inhibitors,"* Angew. Chem. Int. Ed., **37**, pp. 2754-2794.

6. T.O. Yeates and J.E. Padilla, *"Designing supramolecular protein assemblies,"* Current Opinion in Structural Biology, **4**, pp. 464-70 (2002).

7. O.N. Oliveira Jr., J.A. He, V. Zucolotto, S. Balasubramanian, L. Li, H.S. Nalwa, J. Kumar and S.K. Tripathy, *"Layer-by-layer polyelectrolyte-based thin films for electronic and photonic applications,"* in <u>Handbook of Polyelectrolytes and their Applications:Volume 1: Polyelectrolyte-based Multilayers, Self-assemblies and Nanostructures,</u> edited by S.K. Tripathy and J. Kumar (American Scientific Publishers, Stevenson Ranch, CA, 2002), pp 12-14.

8. H.S. Nalwa, *"Nanostructured materials, micelles and colloids,"* <u>Handbook of Surfaces and Interfaces of Materials,</u> **3** (Academic Press, San Diego, CA. 2001), pp. 170-171.

9. J.C. Dijit, Ph.D Thesis, Wagenningen University 1993.

10. J.W. Steed and J.L Atwood, <u>Supramolecular Chemistry,</u> (John Wiley and Sons Ltd., Chichester, 2000), pp.19-21.

11. A.K Ray and A.V Nabok, *"Composite polyelectrolyte self-assembled films for sensor applications,"* in <u>Handbook of Polyelectrolytes and their Applications: Volume 3: Applications of Polyelectrolyte and Theoretical Models,</u> edited by S.K. Tripathy and J. Kumar (American Scientific Publishers, Stevenson Ranch, CA, 2002), pp 293-297.

12. D.A. Tomalia and J.M.J Frechet, "*Discovery of dendrimers and dendritic polymers: A brief historical perspective,*" J. Polym. Sci., Part A: Polym. Chem., **40**, pp. 2719-2726 (2002).

13. Y.H. Kim, "*Hyperbranched polymers 10 years after,*" J. Polym. Sci., Part A: Polym. Chem., **36,** pp. 1685-1698 (1998).

14. J. Sly, V. Lee and R.D. Miller, "*Versatile polyvalent support architectures for nano-scale constructs,*" unpublished results, August 2006.

15. Helms and E.W. Meijer, "*Dendrimers at work,*" Science, **313**, pp 929-930 (2006).

16. D.R. Shankaran, K.V. Gobi, and N. Miura, "*Recent advancements in surface plasmon resonance immunosensors for detection of small molecules of biomedical, food and environmental interest,*" Sens. Actuators, B, **121,** pp. 158, 177 (2006).

17. Van der Merwe A.P., "*Surface plasmon resonance,*" [Online]. Available at http://users.path.ox.ac.uk/~vdmerwe/internal/spr.pdf (accessed 13 April 2006).

18. J. Himola, S.S. Yee and G. Gauglitz, "*Surface plasmon resonance sensors: Review,*" Sens. Actuators, B, **54,** pp. 3-15 (1999).

19. K. Kurihara, K. Nakamura, and K. Suzuki, "*Asymmetric SPR sensor response curve-fitting equation for the accurate determination of SPR resonance angle,*" Sens. Actuators, B, **86,** p. 49 (2002).

20. G. Decher, "*Fuzzy nanoassemblies toward layered polymeric multicomposites,*" Science, **277,** pp. 1232-1236 (1997).

21. S. Raleve, "*Langmuir Blodgett technology,*" [Online]. Available at http://www.fkp.tu-darmstadt.de/stuehn/equipment/LB.html (accessed 24 April 2007.

22. H. Kuhn and D. Mobius, "*Systems of monomolecular layers -assembling and physico-chemical behavior,*" Angew. Chem. Int.Ed., **10,** pp. 620-637 (1971).

23. R. K. Iler, "*Multilayers of colloidal particles,*" J. Colloid Interface Sci., **21,** pp. 569-594 (1966).

24. S. W. Keller, H. N. Kim, and T.E. Mallouk. "*Layer-by-layer assembly of intercalation compounds and heterostructures on surfaces: Toward molecular "beaker" epitaxy,*" J. Chem. Soc., **116,** pp. 8817-8818 (1994).

25. D. Yoo, S.S. Shiratori, and M.F. Rubner, *"Controlling bilayer composition and surface wetability of sequentially adsorbed multilayers of weak polyelectrolyte,"* Macromolecules, **31**, pp. 4309-4318 (1998).

26. M.C. Berg, L. Zhai, R.E. Cohen and M.F. Rubner, *"Controlled drug release from porous polyelectrolyte multilayers,"* Biomacromolecules, **7**, pp. 357, 364 (2006).

27. C. R. Yates and W. Hayes, *"Synthesis and applications of hyperbranched polymers,"* Eur. Polym. J., **40**, pp. 1257-1281 (2004).

28. J-G Zilliox, P. Rempp and J. Parrod, *"Preparation de macromoleculies a structure en etoile, par copolymerization anionique,"* J. Polym. Sci., Part C, **No. 22**, pp. 145-156 (1968).

29. D.M. Vriezema, M.C. Aragones, J.A.A.W. Elemans, J.J.L.M. Cornelissen, A.E. Rowan and R.J.M Nolte, *"Self-assembled nanoreactors,"* Chem. Rev., **105**, pp. 1473-1473 (2005).

30. S. Mecking, R. Thomann, H. Frey, and A. Sunder, *"Preparation of catalytically active palladium nanoclusters in compartments of amphiphilic hyperbranched polyglycerols,"* Macromolecules, **33**, pp. 3958-3960 (2000).

31. M.Q Slagt, S.-E. Striba, R.J.M. Kelin Gibbick, H. Kautz, H. Frey, and G. van Koten, *"Encapsulation of hydrophilic pincer-platinum(II) complexes in amphiphilic hyperbranched polyglycerol nanocapsules, "* Macromolecules, **35**, pp. 5734-5737 (2002).

32. A.W. Bosman, R. Vestberg, A. Heumann, J.M.J Frechet, and C.J. Hawker, *"A modular approach toward functionalized three-dimensional macromolecules: from synthetic concepts to practical applications,"* J. Chem. Soc., **125**, pp. 715-728 (2003).

33. T. Terashima, M. Kamigaito, K.-Y Baek, T. Ando, and M. Sawamoto, *"Polymer catalysts from polymerization catalysts: Direct encapsulation of metal catalyst into star polymer core during metal-catalyzed living radical polymerization,"* J.Chem. Soc., **125**, pp. 5288-5289 (2003).

34. B. Helms and E.W. Meijer, *"Dendrimers at work,"* Science, **313**, pp 929-930 (2006).

35. D. C. Tully and J.M.J. Frechet, *"Dendrimers at surfaces and interfaces: chemistry and applications,"* The Royal Society of Chemistry, pp. 1229-1239 (2001).

36. V.V. Tsukruk, F. Rinderspacher, and V. N. Bliznyuk, *"Self-Assembled multilayer films from dendrimers,"* Langmuir, **13**, pp. 2171-2176 (1997).

37. A.R. Hirst and D.k. Smith, " Solvent effects on supramolecular gel-phase materials: two component dendritic gel," Langmuir, **20,** pp. 10851-10857 (2004).

38. X. Tuo, D. Chen, and X. Wang, "Fabricating water-insoluble polyelectrolyte into multilayers with layer-by-layer self-assembly," Polym. Bull., **54,** pp. 427-433 (2005).

39. D. Barron, S. Buti, M. Ruiz, and J. Barbosa, " Preferential solvation in the THF-water mixtures. Dissociation constants of acid components of pH reference materials," Phys. Chem. Chem. Phys., **1,** pp. 295-298 (1999).

40. S.T. Dubas and J.B. Schlenoff, " Factors controlling the growth of polyelectrolyte multilayers, " Macromolecules, **32,** pp. 8153-8160 (1999).

41. B. Liedberg, C. Nylander and I. Lundstrom, "Biosensing with surface plasmon resonance- how it all started," Biosens. Bioelectron., **10,** pp. i-ix (1995).

42. J. Sly, J. D.J. Samuel, C.S. Bonifacio, L. Chang, V.Y. Lee, M. McNeil, W.P. Risk, C.M. Jefferson, and R. D. Miller, "Versatile layer-by-layer surface modification using functionalized star-polymers and epitaxial polyvalent self-assembly," American Chemical Society, unpublished results, March 2007.

43. S. Shrinivas, On-going Research, San Jose University, 2006.

44. W.P. Risk, IBM Almaden Research Center, private communication (October 2007).

45. J. Rickert, A. Brecht and W. Gopel, "Quartz crystal microbalances for quantitative biosensing and characterizing protein multilayer," Biosens. Bioelectron., **12,** pp. 567-575.

46. W. Hinsberg, F.A. Houle, S.-W. Lee and H. Ito, "Characterization of reactive dissolution and swelling of polymer films using a quartz crystal microbalance and visible infrared reflectance spectroscopy, " Macromolecules, **38,** pp. 1882-1898 (2005).

47. R.M. Silverstein, G.C. Bassler and T.C. Morrill, Spectrometric Identification of Organic Compounds , (John Wiley and Sons Ltd., New York,USA, 1991), pp. 117-118.

48. W. Risk, Matlab Data Fitting based on other fitting techniques, unpublished document, (March 2007).

49. R.F. Conley and M.K.Llyod, "Adsorption studies on kaolinites-II adsorption of amines, " Clay and Clay Minerals, **19,** pp. 273-282 (1971).

50. J. Sly, IBM Almaden Research Center, *private communication (December 2007).*

51. W.P. Risk, IBM Almaden Research Center, *private communication (October 2007).*

APPENDIX A: COMMUNICATION RECEIVED FROM DR. WILLIAM RISK
REGARDING THE SPR FILM THICKNESS DERIVATION AND CALCULATIONS.

Per request today, I calculated the shifts that would be expected by deposition of a uniform layer in a set-up using SF11 as the prism material and THF as the liquid. As usual, I had to assume a uniform layer of some thickness, and I had to make a guess about the refractive index of that layer.

First I assumed a uniform layer with a refractive index of bulk polystyrene.

Using the best values I could come up with:

nSF11 = 1.76196
nPS = 1.577
nTHF = 1.3992
nCr = 3.0318-i*2.5642
nAu = 0.1644 - 5.3512i
$nSiO_2$ = 1.4575
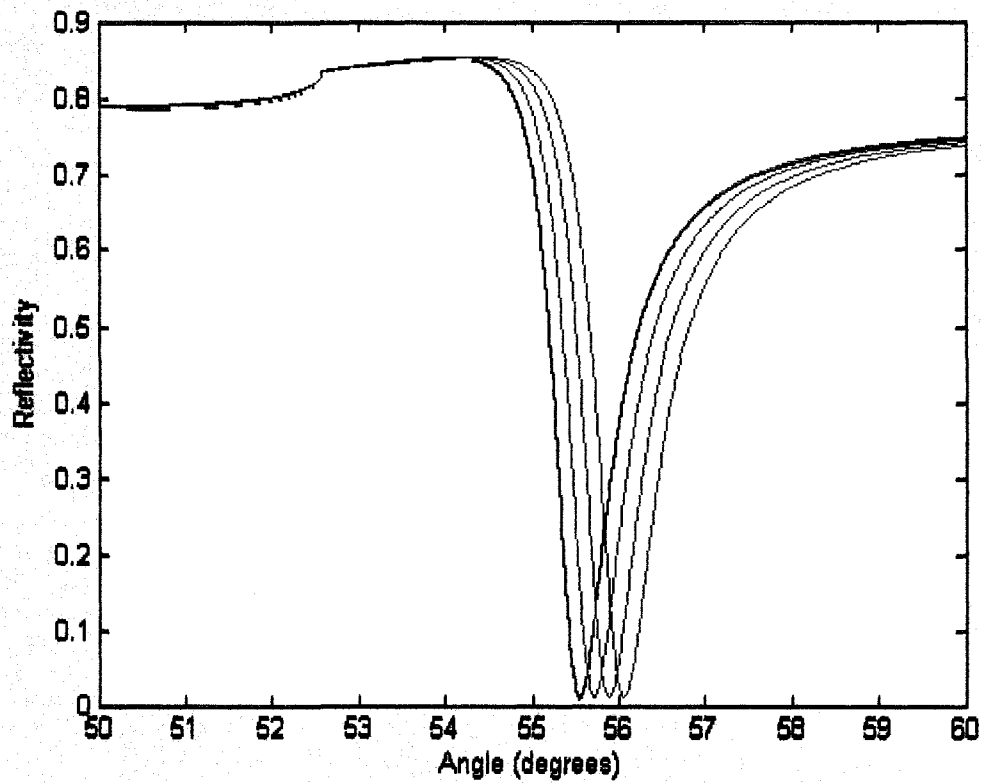
Starting stack: 3 nm Cr / 50 nm Au / 4 nm SiO_2

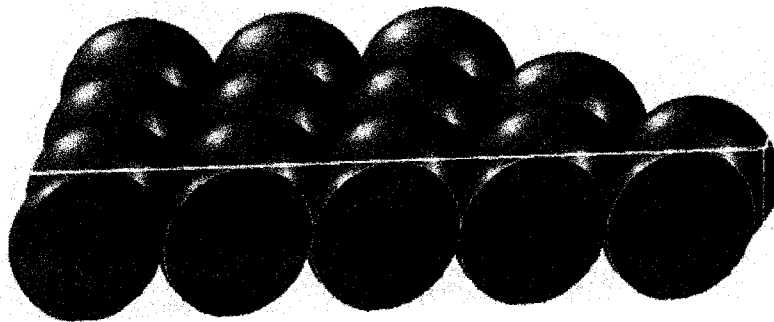I find the following shifts for different thicknesses of PS:

3 nm: 0.17 degrees
6 nm: 0.34 degrees
9 nm: 0.51 degrees

So a shift of *0.15 degrees would correspond to a thickness of about 2.6 nm.*

If we assume that the layer looks like a monolayer of hexagonally-packed hard PS spheres with THF interpenetrating (so that the PS occupies 60.5% of the volume of the monolayer):
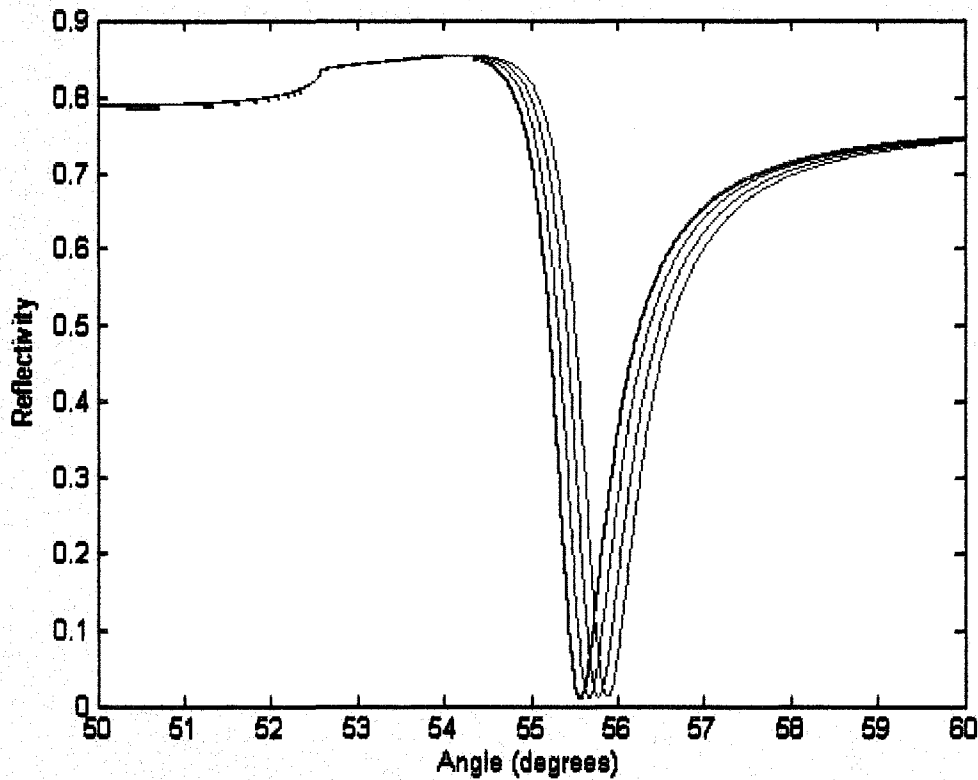

143

and use Maxwell-Garnet theory to calculate the effective refractive index of the layer, we get shifts of:

3 nm thick: 0.1 degrees
6 nm thick: 0.2 degrees
9 nm thick: 0.3 degrees

So a shift of *0.15 degrees would correspond to a thickness of about 4.5 nm*

William P. Risk
IBM Almaden Research Center
650 Harry Rd., MS K13/D2
San Jose, CA 95120
Ph.: 408-927-2467
Fax: 408-927-2100
risk@almaden.ibm.com

APPENDIX B: STANDARD ERROR COMPUTATIONS

To get the significance of a measured data in the SPR and QCM, the standard error was calculated based on the equations:

$$\text{Standard Error} = \frac{\text{Standard deviation}}{\sqrt{\text{number of samples}}}$$

$$\text{Standard deviation} = \sqrt{(1/N) \sum_{i=1}^{N} (x_i - \bar{x})^2}$$

where $\bar{x}$ is the average of measured values from $i = 1$ to N
x_i is the measured value
N is a real number

1. SPR standard error based on 5 THF angular locations on different days and samples data:

SPR THF baselines	Degrees
1	55.064
2	55.164
3	55.061
4	54.684
5	55.109
average	55.016
Standard deviation	0.190
Standard error	0.085 degrees

2. QCM standard error based on 8 frequency shifts of the bare crystal to THF injections

on different days and samples.

	Delta (Hz air - Hz THF)
1	332
2	232
3	276
4	228
5	306
6	325
7	266
8	285
Standard deviation	39
Standard error	14 Hz

3. QCM standard error based on 3 resistance shifts of the bare crystal to THF injections

on different days and samples.

	Delta (Ohms THF - Ohms air)
1	354
2	345
3	319
Standard deviation	18
Standard error	10 Ohms